Available online at www.sciencedirect.com
SCIENCE DIRECT®
Coordination Chemistry Reviews 249 (2005) 2787–2844
COORDINATION CHEMISTRY REVIEWS
www.elsevier.com/locate/ccr

Review

Lanthanides and actinides: Annual survey of their organometallic chemistry covering the year 2000

Ji-Young Hyeon, Jochen Gottfriedsen, Frank T. Edelmann *

Chemisches Institut, Otto-von-Guericke-Universität, Universistätsplatz 2, Geb. 16, D-39106 Magdeburg, Germany

Received 14 February 2005
Available online 20 April 2005

Contents

Keywords: Lanthanides; Actinides; Cyclopentadienyl complexes; Cyclooctatetraenyl complexes; Organometallic chemistry

1. Introduction

The review covers complexes of the lanthanides, actinides and also scandium and yttrium, which contain metal–carbon bonds as defined by Section 29 of Chemical Abstracts. Abstracts of papers presented at conferences, dissertations and patents have mostly been excluded.

* Corresponding author. Tel.: +49 391 6718327; fax: +49 391 6712933.
E-mail address: frank.edelmann@vst.uni-magdeburg.de (F.T. Edelmann).

doi:10.1016/j.ccr.2005.03.001

2. Lanthanides

Stanghellini et al. [1] investigated the values of *R*, the ratio of the overall C–H bending and C–H stretching IR intensities of the cyclopentadienyl ligand, and reported them for several organometallic complexes containing the Cp-M unit (Table 1). The parameter *R* is related to several properties of the complexes, such as the ionic charge, the nature of the metal and the ancillary ligands, the C–H bending force constant and to the solid-state structure.

2.1. Lanthanide complexes without supporting cyclopentadienyl and cyclopentadienyl-like ligands

2.1.1. Alkyl, alkynyl and arene complexes

Niemeyer [2] published the synthesis and characterization of the solvated ytterbium alkyl complex $(CH_2{}^tBu)_3Yb(THF)_2$. The complex was obtained in moderate yield from the reaction of ytterbium metal with neopentyl iodide (Scheme 1). The ruby-red air-sensitive crystals were characterized by melting point, elemental analysis, IR, NMR and UV/Vis spectroscopy and by X-ray crystallography (Fig. 1).

The ytterbium atom is located in the center of a trigonal bipyramid with the neopentyl groups and the THF ligands occupying the equatorial and axial positions, respectively.

Amberger and co-workers [3] investigated the electronic structure of organometallic σ-complexes of lanthanide elements. The linear dichroism spectrum of an oriented single crystal of tris[bis(trimethylsilyl)methyl]erbium was

Table 1
Values of the IR intensity ratio between the C–H stretching and bending modes

Complex	*R*
CpLi	38
CpNa	11
CpK	17
CpTl	22
Cp_3La	8.0
Cp_4U	12
Cp^*_2Fe	0.3
$[Cp^*_2Fe]^+$	1.2

$$3\,Yb + 3\,{}^tBuCH_2I \longrightarrow 3\,{}^tBuCH_2YbI$$
$$3\,{}^tBuCH_2YbI + 3\,{}^tBuCH_2I \longrightarrow 3\,{}^tBuCH_2YbI_2 + 3\,{}^\bullet CH_2{}^tBu$$
$$3\,{}^tBuCH_2YbI_2 \rightleftharpoons (CH_2{}^tBu)_3Yb(THF)_2 + 2\,YbI_3$$
$$2\,YbI_3 + Yb \longrightarrow 3\,YbI_2$$
$$4\,Yb + 6\,{}^tBuCH_2I \longrightarrow (CH_2{}^tBu)_3Yb(THF)_2 + 3\,YbI_2$$

Scheme 1. Successive formation of $(CH_2{}^tBu)_3Yb(THF)_2$.

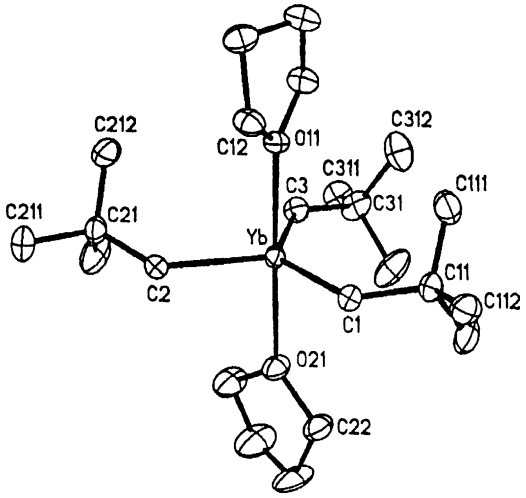

Fig. 1. ORTEP view of the complex $(CH_2{}^tBu)_3Yb(THF)_2$.

measured at room and low temperatures. From the spectra obtained, a truncated crystal field splitting pattern was derived and simulated by fitting the parameters of an empirical Hamiltonian. For 39 assignments, a reduced r.m.s. deviation of 20.4 cm^{-1} was achieved. The parameters derived allowed the estimation of the crystal field strength produced by the bis(trimethylsilyl)methyl ligand, the insertion of this ligand into truncated empirical nephelauxetic and relativistic nephelauxetic series, and the construction of experimentally based non-relativistic and relativistic molecular orbital schemes in the f range.

Gambarotta and co-workers [4,5] reported the synthesis of calix-tetrapyrrole-supported samarium alkyl and alkenyl complexes. The trivalent methyl and vinyl samarium derivatives supported by a calix-pyrrole ligand system (Et_8-calix-pyrrole)(R)Sm(μ^3-Cl)[Li(THF)]$_2$[$Li_2(THF)_3$] (R = Me, CH=CH_2) were prepared via reaction of (Et_8-calix-pyrrole)(Cl)Sm[$Li_2(THF)_3$] with the corresponding organolithium reagent. The dinuclear complex (Et_8-calix-pyrrole)$Sm_2\{(\mu\text{-Cl})_2[Li(THF)_2]\}_2$ was alkylated in diethyl ether resulting in the formation of the isostructural alkyl complex (Et_8-calix-pyrrole)$Sm_2\{(\mu\text{-}CH_3)_2[Li(THF)_2]\}_2$.

Takats and co-workers [6] reported the reaction of $(Tp^{Me,Me})_2Sm$ with $Hg(C{\equiv}CPh)_2$ in THF, which afforded the monomeric, base-free lanthanide alkynide complex $(Tp^{Me,Me})_2Sm(C{\equiv}CPh)$ (Fig. 2).

Roesky [7] published the first bridged aminotroponiminate complexes of lutetium and successfully synthesized these complexes by the reaction of dipotassium-1,3-bis[2-(isopropylamino)troponiminato]propane, $K_2[(^iPr)TP]$, with lutetium trichloride.

The complex was characterized by single-crystal X-ray crystallography. Roesky et al. also published a study of the reactivity with some selected derivatives such as alkyl, amide, η^5-cyclopentadienyl and η^3-borohydride (Scheme 2 and Fig. 3).

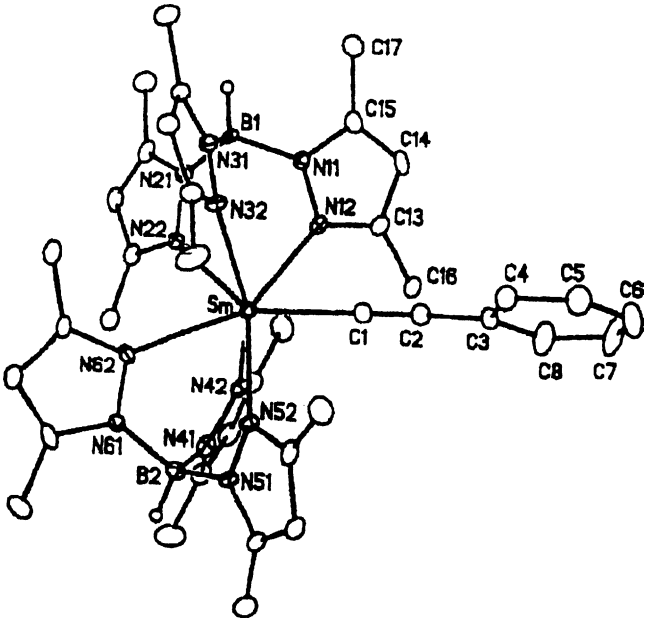

Fig. 2. ORTEP view of the complex $(Tp^{Me,Me})_2Sm(C{\equiv}CPh)$.

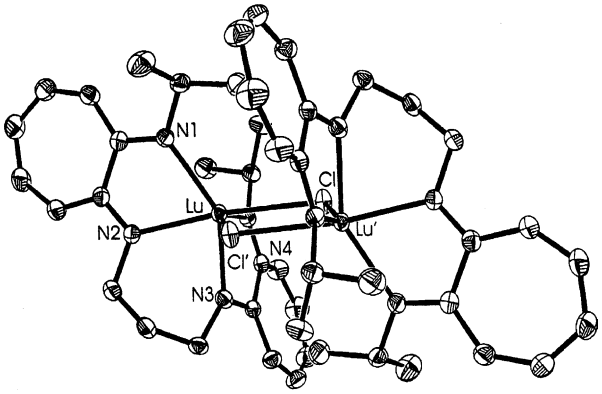

Fig. 3. ORTEP view of the molecular structure of $[\{(^{i}Pr)TP\}Lu(\mu\text{-}Cl)]_2$.

Gambarotta and co-workers [8] studied mixed samarium clusters supported by dipyrrolide ligands. Treatment of $SmI_2(THF)_2$ with the potassium salt of the methylphenyl dipyrromethanyl dianion in THF resulted in a rapid reaction with formation of $[\{[MePhC(C_4H_3N)_2]Sm\}_5(\mu\text{-}I)][K(THF)_6]$. Single-crystal X-ray determinations showed that the complex is formed by a pentanuclear anion consisting of five $\{[MePhC(C_4H_3N)_2]Sm\}_5$ units with the five

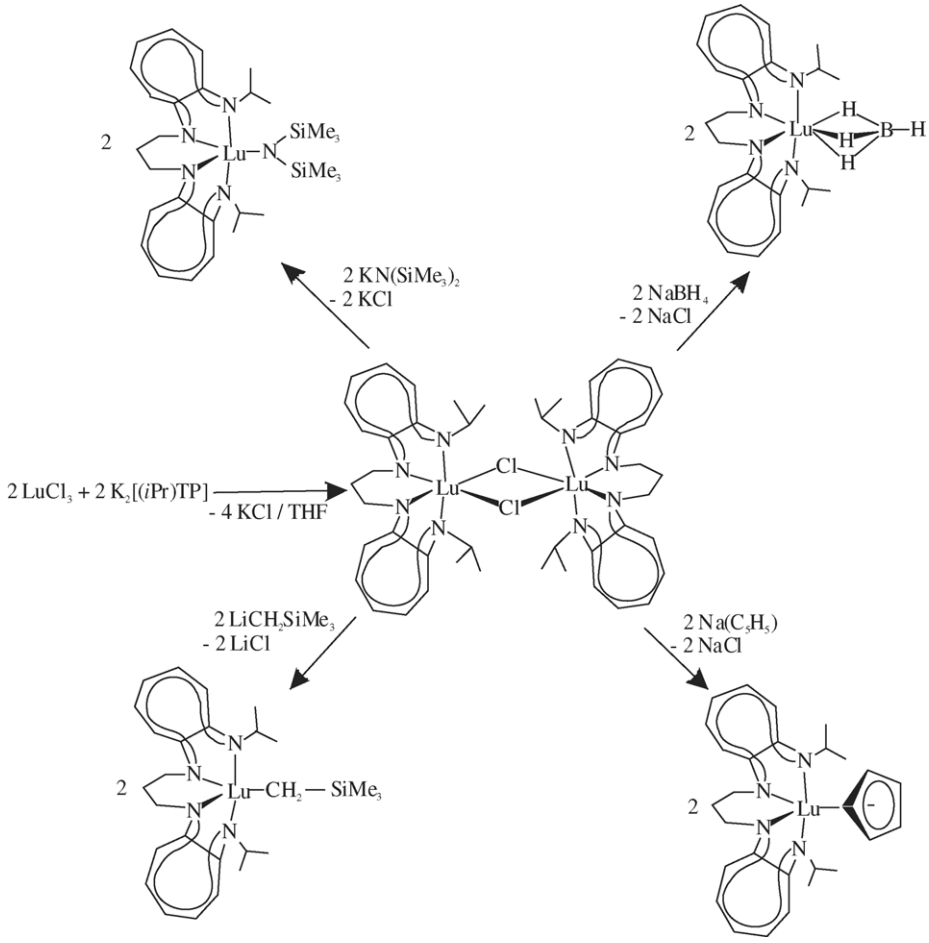

Scheme 2. Reactivity of the complex $[\{(^{i}Pr)TP\}Lu(\mu\text{-}Cl)]_2$.

samarium atoms pentagonally arranged around a central iodine atom. Each ligand bridges two samarium atoms with the pyrrole rings being in turn π-bonded to one samarium and σ-bonded to a second.

2.1.2. Metallacarborane complexes

Xie and co-workers [9] reported the synthesis of half- and full-sandwich lanthanacarboranes of the C_2B_9-carborane ligand. Treatment of $LnCl_3$ with 1 equiv. of Na_2[*nido*-7,8-$C_2B_9H_{11}$] in THF gave the half-sandwich lanthanacarborane chloride compounds (η^5-$C_2B_9H_{11}$)Ln(THF)$_2$(μ-Cl)$_2$Na(THF)$_2$ (Ln = Y, Er, Yb, Lu). Recrystallization of the yttrium and ytterbium complexes from a wet THF/toluene solution gave the ionic compounds [$LnCl_2$(THF)$_5$][*nido*-$C_2B_9H_{12}$] (Ln = Y, Yb). Reaction of (η^5-$C_2B_9H_{11}$)Ln(THF)$_2$(μ-Cl)$_2$Na(THF)$_2$ (Ln = Y, Yb) with Na_2[*nido*-7,8-$C_2B_9H_{11}$] in a molar ratio of 1:1 in THF afforded the full-sandwich lanthanacarboranes [(η^5-$C_2B_9H_{11}$)$_2$Ln(THF)$_2$][Na(THF)$_2$] (Ln = Y, Yb).

2.2. Cyclopentadienyl complexes

Evans et al. [10] investigated the utility of electrospray mass spectrometry for the characterization of air-sensitive organolanthanides and related species. They investigated a wide variety of lanthanide complexes, including divalent and trivalent compounds, neutral and cationic species and complexes with cyclopentadienyl as well as alternative ancillary ligands. The spectra are sensitive to the composition of the complex and the oxidation potential of the lanthanide ion. The [Cp^*_2Ln][BPh_4] (Ln = Nd, Sm, Y, Tm) complexes form the solvated parent ions [Cp^*_2Ln(MeCN)$_x$]$^+$, whereas [Zr_2(O^iPr)$_9$]LnCp (Ln = Sm, Yb) form the unsolvated parent ions {[Zr_2(O^iPr)$_9$]LnCp}$^+$. [Cp^*_2Ln(MeCN)$_x$]$^+$ ions are also observed in the spectra of Cp^*_2Ln(C_3H_5) (Ln = Sm, Y) and Cp^*_2Ln(THF)$_x$ (Ln = Sm, Eu, Yb). [Cp^*_2Ln(μ-I)(THF)$_2$]$_2$ (Ln = Sm, Yb, Eu) and LnI_2(THF)$_2$ (Ln = Sm, Yb, Eu) gave differing sets of ions, depending on the specific metal. The spectra of dinuclear compounds, [Cp^*_2Ln(THF)$_x$]$_2$(COT) (Ln = Sm, Yb), were also investigated.

2.2.1. Mono(cyclopentadienyl) complexes

Takats and co-workers [11] published the synthesis and characterization of mixed pyrazolylborate/cyclopentadienyl derivatives of divalent lanthanides. Reaction of [($Tp^{tBu,Me}$)YbH]$_2$ ($Tp^{tBu,Me}$ = hydrotris(3-*tert*-butyl-5-methylpyrazolyl)borate) with cyclopentadiene (C_5H_6) and trimethylsilylcyclopentadiene ($C_5H_5SiMe_3$) resulted in the formation of the corresponding mixed-ligand complexes ($Tp^{tBu,Me}$)Yb(C_5H_4R) (R = H, $SiMe_3$) in quantitative yield. The complexes were characterized by multinuclear NMR spectroscopy (Scheme 3).

The complex ($Tp^{tBu,Me}$)Yb($C_5H_4SiMe_3$) was characterized by single-crystal X-ray diffraction. This complex consists of well-separated monomeric units with a η^5-$C_5H_4SiMe_3$ ring, but the $Tp^{tBu,Me}$ ligands exhibit an unusual

$$[(Tp^{tBu,Me})YbH]_2 + 2\ C_5H_5R \xrightarrow[\text{toluene}]{\text{benzene or}} 2\ (Tp^{tBu,Me})Yb(C_5H_4R) + 2H_2$$

R = H, $SiMe_3$

Scheme 3. Synthetic route to mixed pyrazolyborate/cyclopentadienyl ytterbium(II) complexes.

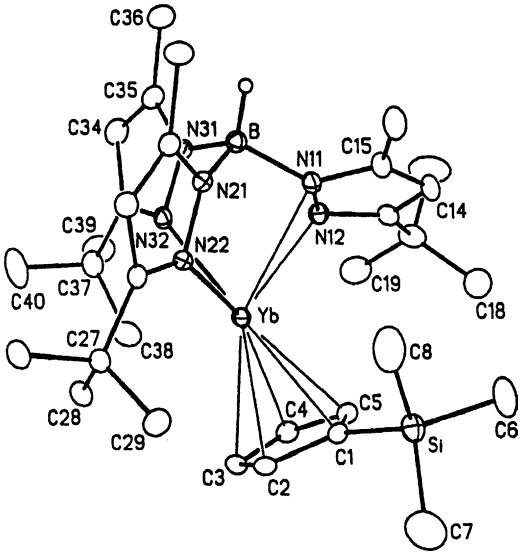

Fig. 4. Perspective view of ($Tp^{tBu,Me}$)Yb($C_5H_4SiMe_3$).

distortion (Fig. 4). One of the pyrazolyl rings is rotated in such a way as to bring both pyrazolyl nitrogens in bonding contact with ytterbium, while the other two pyrazolyl moieties interact in the normal way (lone-pair donation from 2-N). This is evidenced by the large Yb–N12–N11–B torsional angle, 75.3(3)°, compared with 14.9(3)° and 14.3(3)° for the other two pyrazolyl rings [11].

Barbier-Baudry et al. [12] reported the synthesis of the first half-metallocene bis(borohydrides) of lanthanides and actinides (Scheme 4). They also determined the first structures of half-metallocene bis(borohydrides) of the lanthanides. Reaction of the tetraisopropylcyclopentadienyl sodium salt $C_5H^iPr_4Na$ with Ln(BH$_4$)$_3$(THF)$_3$, Ln = Sm, Nd, at room temperature afforded the analytically pure monocyclopentadienyl complexes ($C_5H^iPr_4$)Sm(BH$_4$)$_2$(THF) and ($C_5H^iPr_4$)Nd(BH$_4$)$_2$(THF) in 50–60% yield (Figs. 5 and 6). These complexes are thermally stable and melt without decomposition around 170 °C.

The same authors also synthesized a new half-metallocene derivative of uranium, which is described in Section 3.1.1.

$$(C_5H^iPr_4)Na \xrightarrow{Ln(BH_4)_3(THF)_3} (C_5H^iPr_4)Ln(BH_4)_2(THF)$$

Ln = Sm, Nd

Scheme 4. Synthesis of the complexes ($C_5H^iPr_4$)Ln(BH$_4$)$_2$(THF).

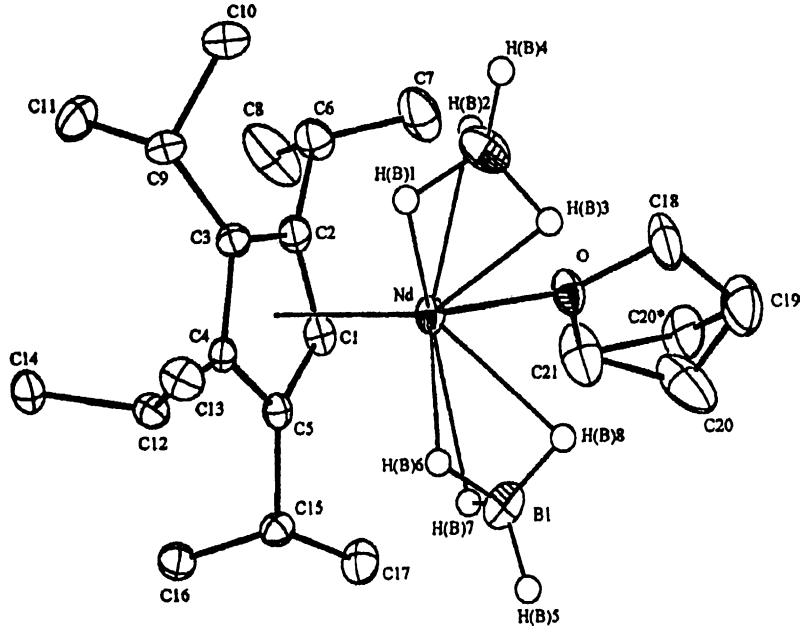

Fig. 5. ORTEP view of the complex $(C_5H^iPr_4)Sm(BH_4)_2(THF)$.

Xie and co-workers [13] synthesized the mono-, di- and trianion of the compound $Me_2C(C_5H_5)(C_2B_{10}H_{11})$ (Scheme 5): $[Me_2C(C_5H_4)(C_2B_{10}H_{11})]^-$, $[Me_2C(C_5H_4)(C_2B_{10}H_{10})]^{2-}$ and $[Me_2C(C_5H_4)(nido\text{-}C_2B_{10}H_{11})]^{3-}$.

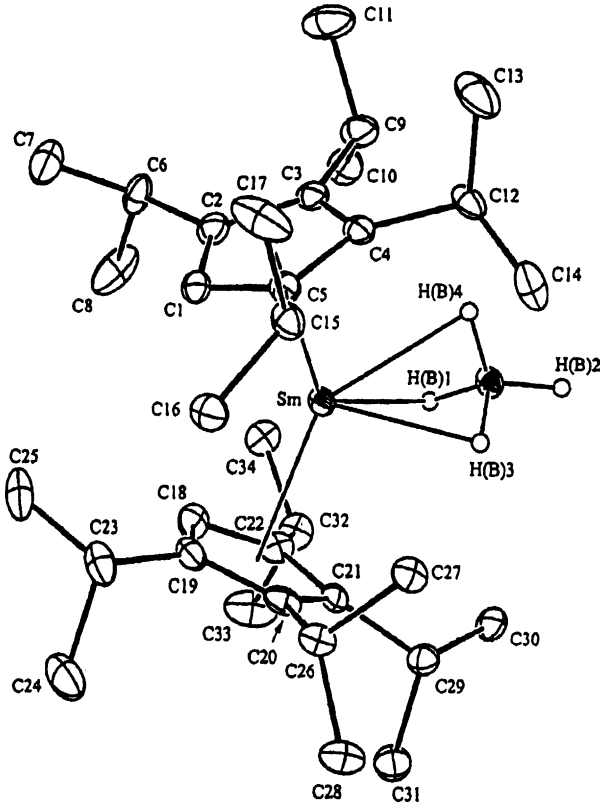

Fig. 6. ORTEP view of the complex $(C_5H^iPr_4)Nd(BH_4)_2(THF)$.

Reactions of $LnCl_3$ with the monoanion in molar ratios of 1:1, 1:2 and 1:3 generated the mono-, bis- and tris-ligated organolanthanide compounds $[\eta^5\text{-}Me_2C(C_5H_4)(C_2B_{10}H_{11})]LnCl_2(S)_n$, $((S)_n = (THF)_3$, Ln = Er, Sm, $(S)_n = (DME)_2$, Ln = Nd) $[\eta^5\text{-}Me_2C(C_5H_4)(C_2B_{10}H_{11})]_2SmCl(THF)_2$ and $[\eta^5\text{-}Me_2C(C_5H_4)(C_2B_{10}H_{11})]_3Sm{\cdot}0.5C_7H_8$, respectively (Scheme 6).

Reaction of $LnCl_3$ with 1 or 2 equiv. of the dianion gave the same compounds, $[\{\eta^5{:}\sigma\text{-}Me_2C(C_5H_4)(C_2B_{10}H_{10})\}_2Ln][Li(DME)_3]$, Ln = Sm, Yb.

Treatment of $[\eta^5{:}\eta^6\text{-}Me_2C(C_5H_4)(C_2B_{10}H_{11})]Er(THF)_2$ with excess Na metal gave the first organolanthanide compound containing an η^7-carboranyl ligand $[\{[\eta^5{:}\eta^7\text{-}Me_2C(C_5H_4)(C_2B_{10}H_{11})]Er\}_2\{Na_4(THF)_9\}]_n$ (Scheme 7). In the case of dysprosium, $[\{[\eta^5{:}\eta^7\text{-}Me_2C(C_5H_4)(C_2B_{10}H_{11})]Dy\}_2\{Na_4(THF)_9\}]_n$ was isolated in a "one-pot" reaction of $DyCl_3$ and the monoanion in the presence of excess Na metal. Treatment of $[\{[\eta^5{:}\eta^7\text{-}Me_2C(C_5H_4)(C_2B_{10}H_{11})]Er\}_2\{Na_4(THF)_9\}]_n$ with 2 equiv. of $ErCl_3$ in THF gave the novel tetranuclear cluster $[\{\eta^5{:}\eta^7\text{-}Me_2C(C_5H_4)(C_2B_{10}H_{11})\}Er_2(\mu\text{-}Cl)(THF)_3]_2$, in which the Er^{3+} ions replace all Na^+ ions in the complex.

All these compounds were fully characterized by various spectroscopic data, single-crystal X-ray analyses and elemental analyses (Figs. 7–11).

Shen and co-workers [14] successfully synthesized neutral heteroleptic diphenylamido complexes of ytterbium: $(MeC_5H_4)_2YbNPh_2(THF)$, $(^tBuC_5H_4)_2YbNPh_2(THF)$ and $Cp^*_2YbNPh_2$. The complexes were obtained by the reaction of ytterbocene chlorides with $NaNPh_2$ in THF or THF/toluene at 0 °C (Scheme 8).

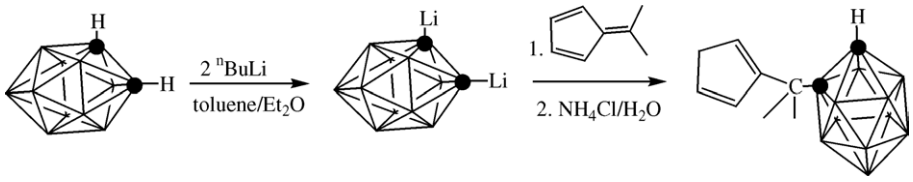

Scheme 5. Synthesis of the neutral ligand $Me_2C(C_5H_5)(C_2B_{10}H_{11})$.

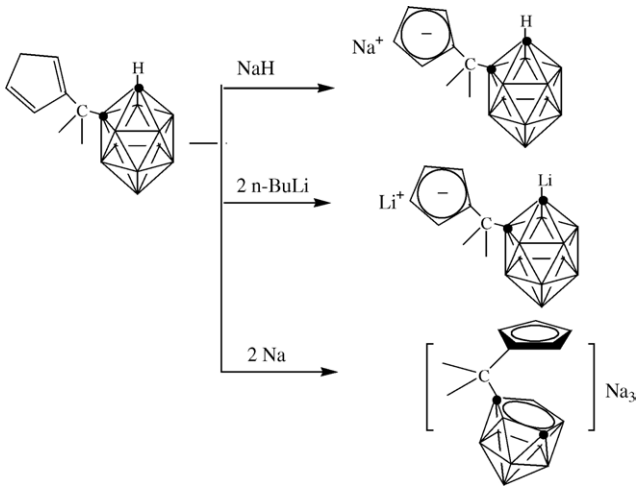

Scheme 6. Formation of $Na[Me_2C(C_5H_4)(C_2B_{10}H_{11})]Na$, $Li_2[Me_2C(C_5H_4)(C_2B_{10}H_{10})]$, and $Na_3[Me_2C(C_5H_4)(nido\text{-}C_2B_{10}H_{11})]$.

The crystal structures of $(MeC_5H_4)_2YbNPh_2(THF)$ and $Cp^*_2YbNPh_2$ were determined by X-ray diffraction analysis (Figs. 12 and 13, respectively). The complex $(MeC_5H_4)_2YbNPh_2(THF)$ has a distorted tetrahedral arrangement around ytterbium by two MeC_5H_4 groups, one oxygen atom and one nitrogen atom.

The crystal structure of the complex $Cp^*_2YbNPh_2$ is monoclinic (space group $P2_1/n$) and shows a triangular array of two Cp^*-ligands and one nitrogen atom surrounding ytterbium with additional intramolecular Yb–η^2-Ph chelate interactions.

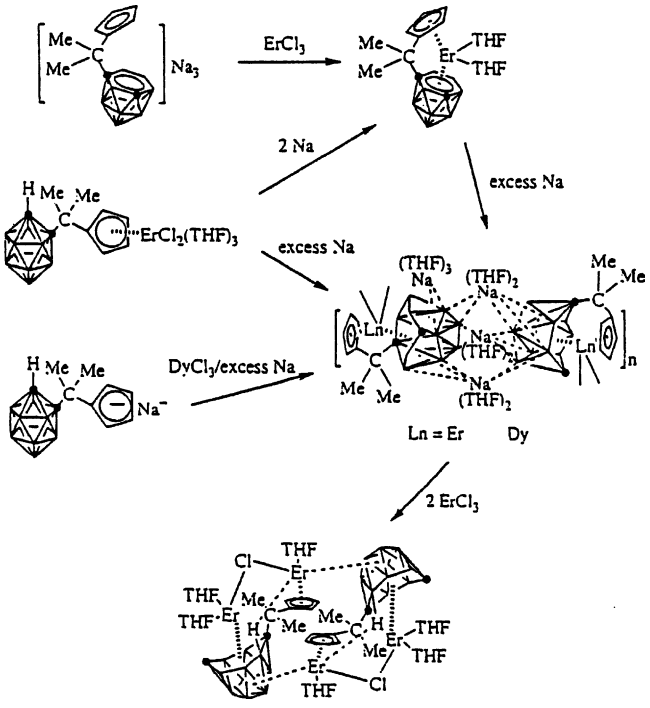

Scheme 7. Formation of the tetranuclear cluster $[\{[\eta^5{:}\eta^7\text{-}Me_2C(C_5H_4)(C_2B_{10}H_{11})]Er\}_2\{Na_4(THF)_9\}]_n$.

Yasuda and co-workers [15] published the synthesis and crystal structures of samarium complexes incorporating bridged Cp′-$SiMe_2$allenyl/propargyl ligands ($Cp' = (Me_3Si)_2(C_5H_2)$) (Scheme 9).

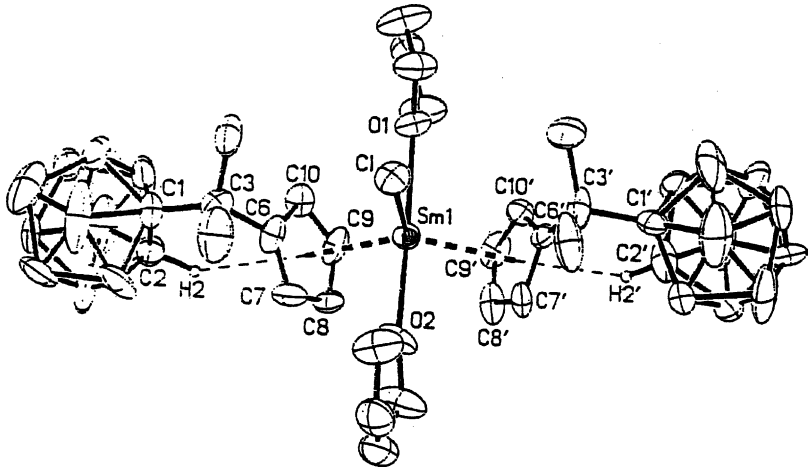

Fig. 7. Molecular structure of $[\eta^5\text{-}Me_2C(C_5H_4)(C_2B_{10}H_{11})]_2SmCl(THF)_2$.

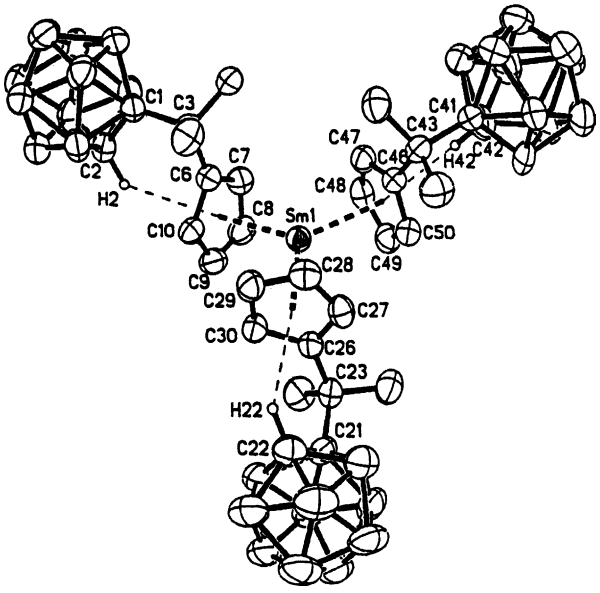

Fig. 8. Molecular structure of $[\eta^5\text{-}Me_2C(C_5H_4)(C_2B_{10}H_{11})]_3Sm\cdot 0.5(toluene)$.

The complex $\{[(Me_3Si)_2(C_5H_2)]SiMe_2(\eta^3\text{-}C{=}C{=}C[H]SiMe_3)\}SmCl_3Li_2(TMEDA)_2$ (TMEDA = *N*,*N*,*N*′,*N*′-tetramethylethylenediamine) was obtained by the reaction of a dilithium salt of $[(Me_3Si)_2(C_5H_3)]SiMe_2CH_2C{\equiv}CSiMe_3$ with $SmCl_3$ (Scheme 10).

An η^1-propargyl complex, $\{[(Me_3Si)_2(C_5H_2)]SiMe_2(\eta^1\text{-}CHC{\equiv}CSiPh_3)\}$Sm-(TMEDA)$[Cl_2Li(TMEDA)]$, was obtained by the reaction of the dilithium salt of the Ph_3Si substituted ligand $[(Me_3Si)_2(C_5H_3)]SiMe_2CH_2C{\equiv}CSiPh_3$ with $SmCl_3$ (Scheme 11).

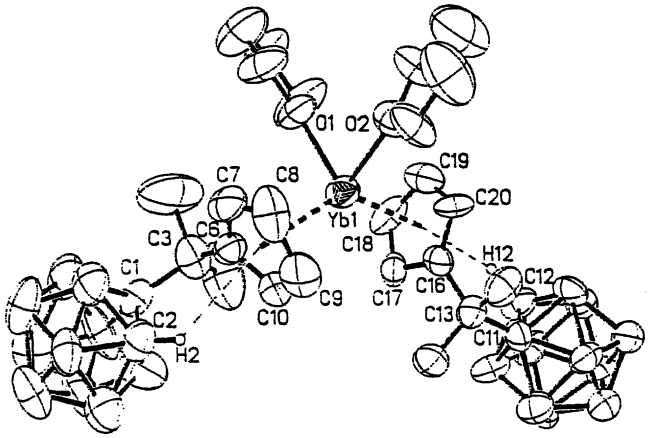

Fig. 9. Molecular structure of $[\eta^5\text{-}Me_2C(C_5H_4)(C_2B_{10}H_{11})_2Yb(THF)_2]$.

A conversion of the bonding mode from η^1-propargyl to η^3-allenyl was observed by removing the coordinated TMEDA molecule on the Sm center and exchanging two anions for two iodide anions in the complex $\{[(Me_3Si)_2(C_5H_2)]SiMe_2(\eta^1\text{-}CHC{\equiv}CSiPh_3)\}Sm(TMEDA)[Cl_2Li(TMEDA)]$ (Scheme 12 and Figs. 14 and 15).

Fedushkin et al. [16] published new half-sandwich complexes of lanthanum(III) and ytterbium(II). The ligand is a 1.5:1 mixture of isomeric 1,2- and 1,3-disubstituted with two dimethylaminoethyl side chains (Scheme 13).

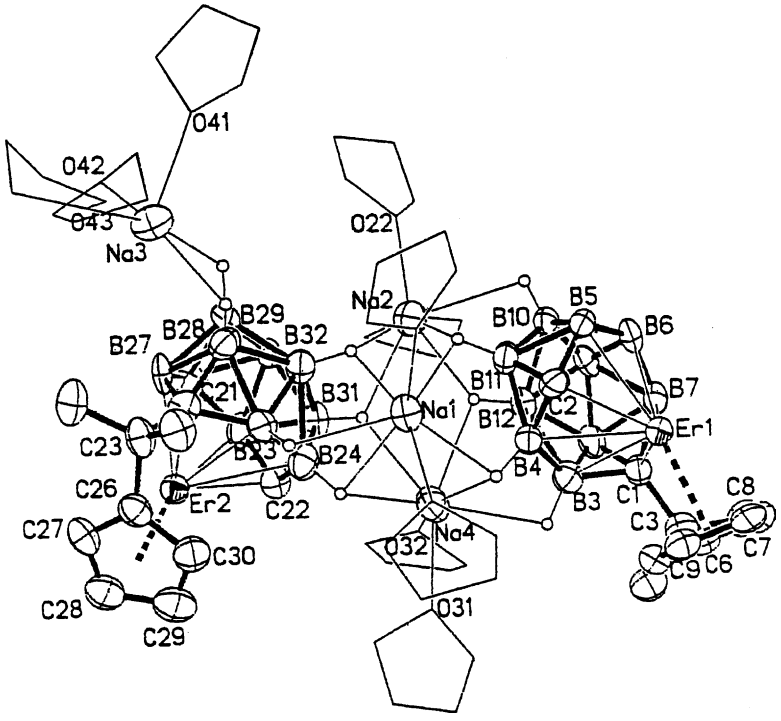

Fig. 10. Molecular structure of $[\{[\eta^5{:}\eta^7\text{-}Me_2C(C_5H_4)(C_2B_{10}H_{11})]Er\}_2\{Na_4(THF)_9\}]_n$.

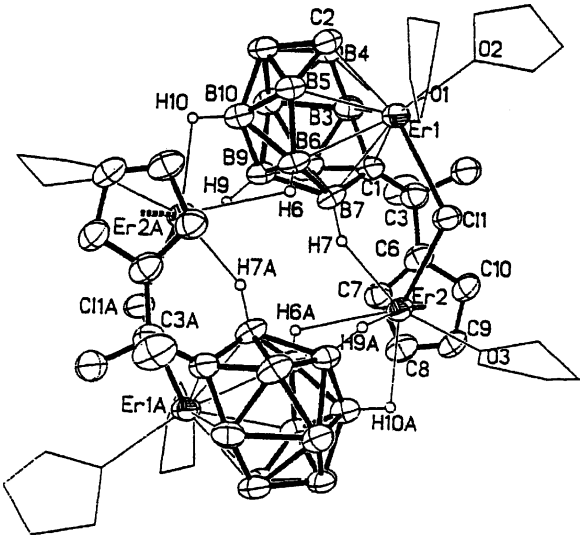

Fig. 11. Molecular structure of $[\{[\eta^5{:}\eta^7\text{-}Me_2C(C_5H_4)(C_2B_{10}H_{11})]\}Er_2(\mu\text{-}Cl)(THF)_3]_2$.

$$Cp'_2YbCl(THF) + NaNPh_2 \xrightarrow[0\ ^\circ C]{THF/toluene} Cp'_2YbNPh_2(THF)_n + NaCl$$

$Cp' = MeC_5H_4$, $^tBuC_5H_4$, n = 1

$Cp' = C_5Me_5$, n = 0

Scheme 8. Synthetic routes to the complexes $(MeC_5H_4)_2YbNPh_2(THF)$, $(^tBuC_5H_4)_2YbNPh_2(THF)$ and $Cp^*_2YbNPh_2$.

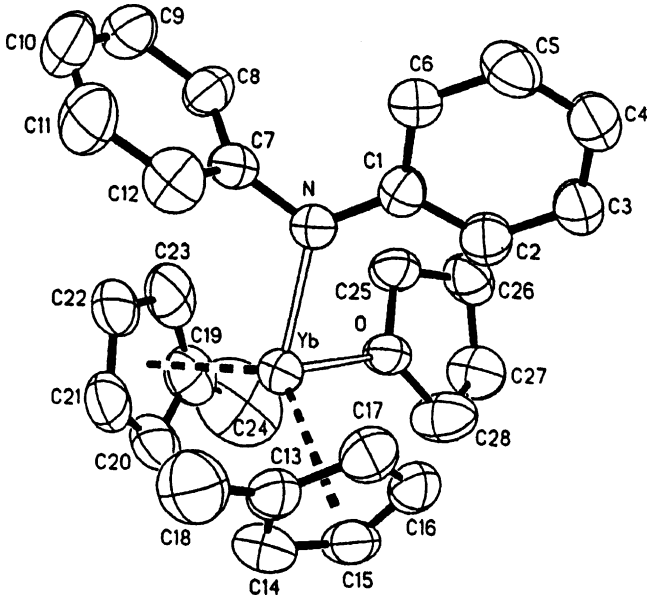

Fig. 12. ORTEP view of the complex $(MeC_5H_4)_2YbNPh_2(THF)$.

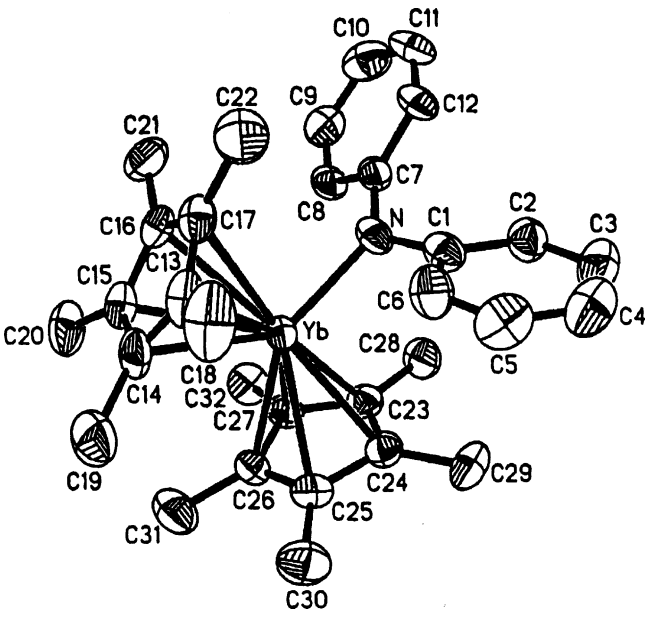

Fig. 13. ORTEP view of the complex $Cp^*_2YbNPh_2$.

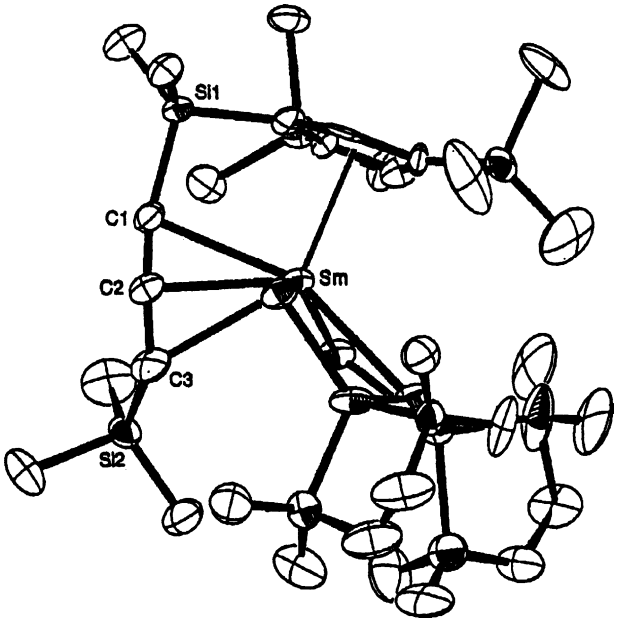

Fig. 14. ORTEP view of the complex $\{[(Me_3Si)_2(C_5H_2)]SiMe_2(\eta^3\text{-}C{=}C{=}C[H]SiPh_3)\}Sm[I_2Li(TMEDA)]$.

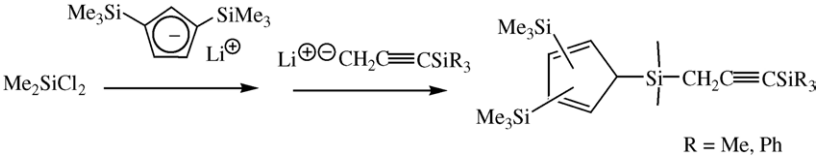

Scheme 9. Synthetic route to the formation of the bridged Cp′-$SiMe_2$allenyl/propargyl ligands.

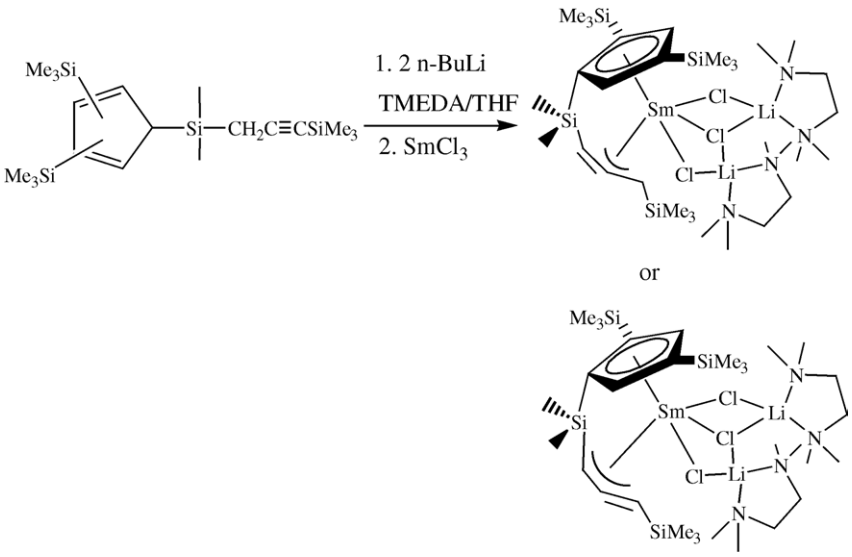

Scheme 10. Formation of the complex $\{[(Me_3Si)_2(C_5H_2)]SiMe_2(\eta^3\text{-}C{=}C{=}C[H]SiMe_3)\}SmCl_3Li_2(TMEDA)_2$.

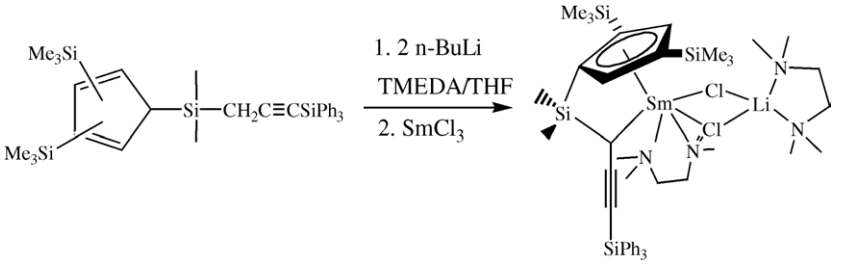

Scheme 11. Formation of the complex $\{[(Me_3Si)_2(C_5H_2)]SiMe_2(\eta^1\text{-}CHC{\equiv}CSiPh_3)\}Sm\text{-}(TMEDA)[Cl_2Li(TMEDA)]$.

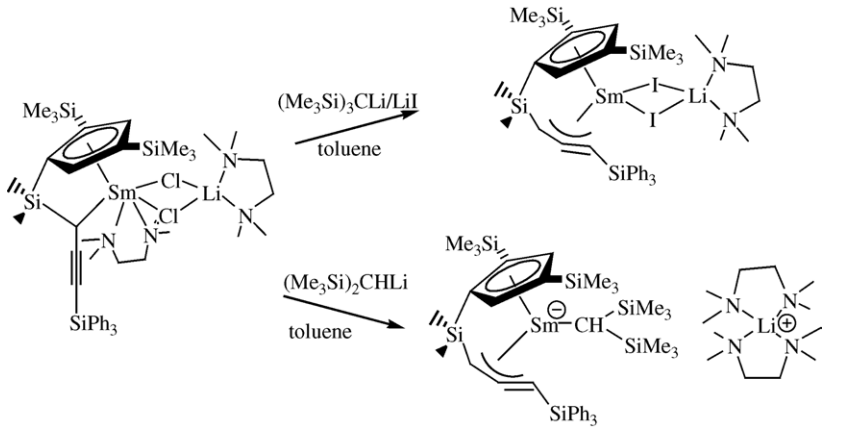

Scheme 12. Conversion of the bonding mode from η^1-propargyl to η^3-allenyl complex in $\{[(Me_3Si)_2(C_5H_2)]SiMe_2(\eta^1\text{-}CHC{\equiv}CSiPh_3)\}Sm(TMEDA)[Cl_2Li(TMEDA)]$.

Addition of $LaI_3(THF)_3$ to the mixture in THF causes the formation of the half-sandwich complexes $[\eta^5{:}\eta^1{:}\eta^1\text{-}C_5H_3(CH_2CH_2NMe_2)_2\text{-}1,2]LaI_2(THF)$ and $[\eta^5{:}\eta^1{:}\eta^1\text{-}C_5H_3(CH_2CH_2NMe_2)_2\text{-}1,3]LaI_2(THF)$ (Figs. 16 and 17), which can be successfully separated because of their different crystal shapes (Scheme 14).

The ligand isomeric mixture reacted with $YbI_2(THF)_2$ to form only $[\eta^5{:}\eta^1{:}\eta^1\text{-}C_5H_3(CH_2CH_2NMe_2)_2\text{-}1,2]YI(THF)_2$ crystals (Fig. 18). The non-crystallizing 1,3-isomer left in solution reacts with Cp^*Na forming the polymeric mixed-metallocene *ate* complex (Scheme 15).

The reaction of $[\eta^5{:}\eta^1{:}\eta^1\text{-}C_5H_3(CH_2CH_2NMe_2)_2\text{-}1,2]YI(THF)_2$ with Cp^*K or $(C_5H_4{}^tBu)Na$ results in the formation of the sandwich complexes $[\eta^5{:}\eta^1{:}\eta^1\text{-}C_5H_3(CH_2CH_2NMe_2)_2\text{-}1,2]YbCp^*$ and $[\eta^5{:}\eta^1{:}\eta^1\text{-}C_5H_3(CH_2CH_2NMe_2)_2\text{-}1,2]Yb(\eta^5\text{-}C_5Me_4{}^tBu)$, respectively (Figs. 19–21).

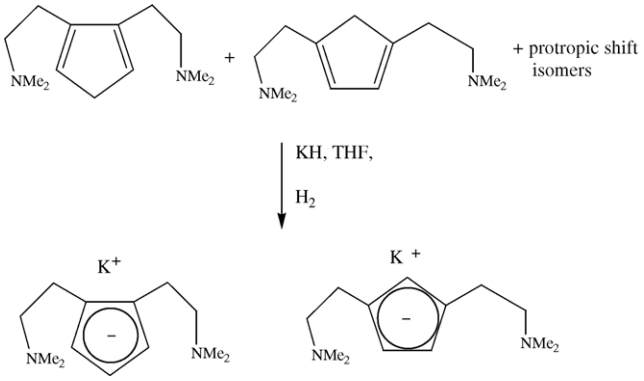

Scheme 13. The mixture of isomeric 1,2- and 1,3-disubstituted cyclopentadienyl ligands.

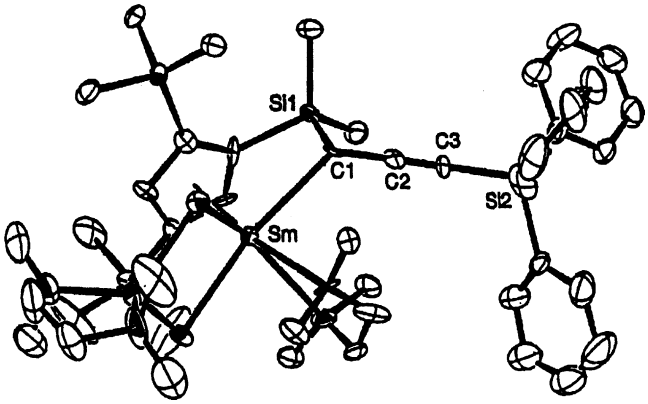

Fig. 15. ORTEP view of the complex $\{[(Me_3Si)_2(C_5H_2)]SiMe_2(\eta^3\text{-}C{=}C{=}C[H]SiPh_3)\}SmClCH(SiMe_3)[Li(TMEDA)_2]$.

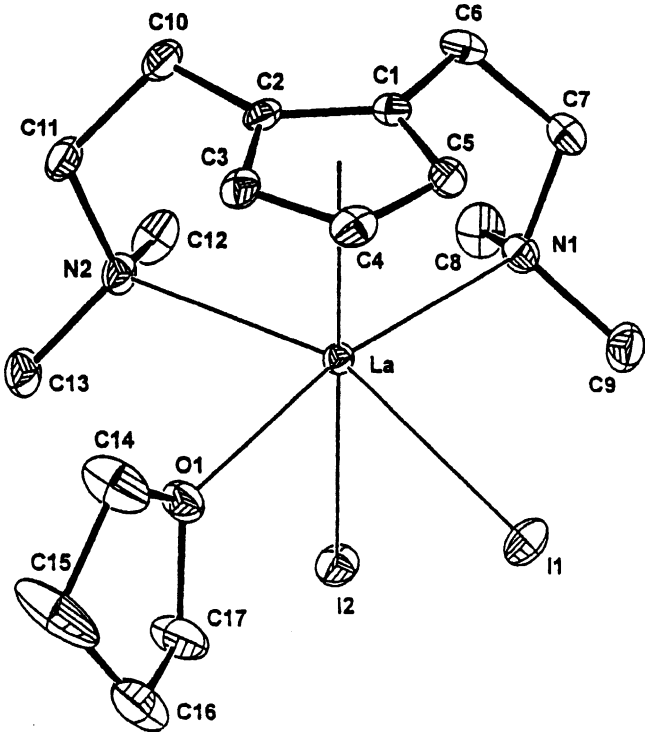

Fig. 16. ORTEP view of the complex $[\eta^5{:}\eta^1{:}\eta^1\text{-}C_5H_3(CH_2CH_2NMe_2)_2\text{-}1,2]LaI_2(THF)$.

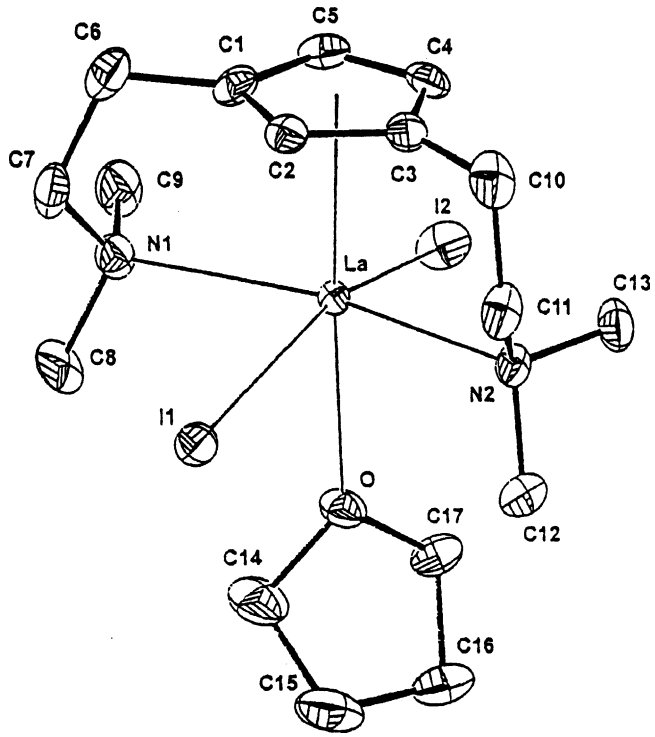

Fig. 17. ORTEP view of the complex $[\eta^5{:}\eta^1{:}\eta^1\text{-}C_5H_3(CH_2CH_2NMe_2)_2\text{-}1,3]LaI_2(THF)$.

The novel compounds have been characterized by elemental analysis, NMR spectroscopy and mass spectrometry.

Cai and co-workers [17] synthesized mono(tetrahydrofurfurylcyclopentadienyl)lanthanide dichloride and bis-(tetrahydrofurfurylcyclopentadienyl)lanthanide chloride complexes. The bis(tetrahydrofurfurylcyclopentadienyl)lanthanide chloride complexes are mentioned in Section 2.2.2. The mono(tetrahydrofurfurylcyclopentadienyl)lanthanide dichlorides were formed by the reaction of lanthanide trichlorides with 1 equiv. of tetrahydrofurfurylcyclopenta-

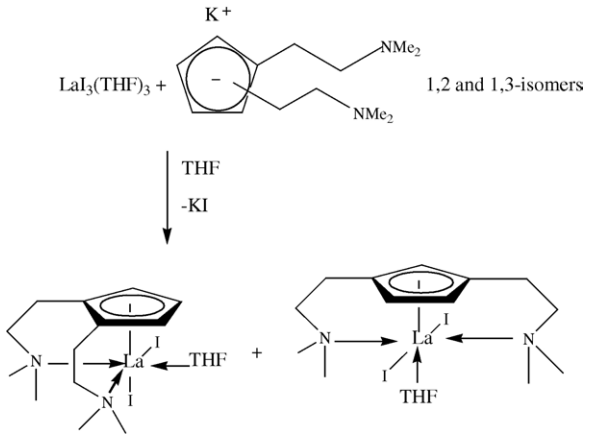

Scheme 14. Formation of the half-sandwich complexes $[\eta^5{:}\eta^1{:}\eta^1\text{-}C_5H_3(CH_2CH_2NMe_2)_2\text{-}1,2]LaI_2(THF)$ and $[\eta^5{:}\eta^1{:}\eta^1\text{-}C_5H_3(CH_2CH_2NMe_2)_2\text{-}1,3]LaI_2(THF)$.

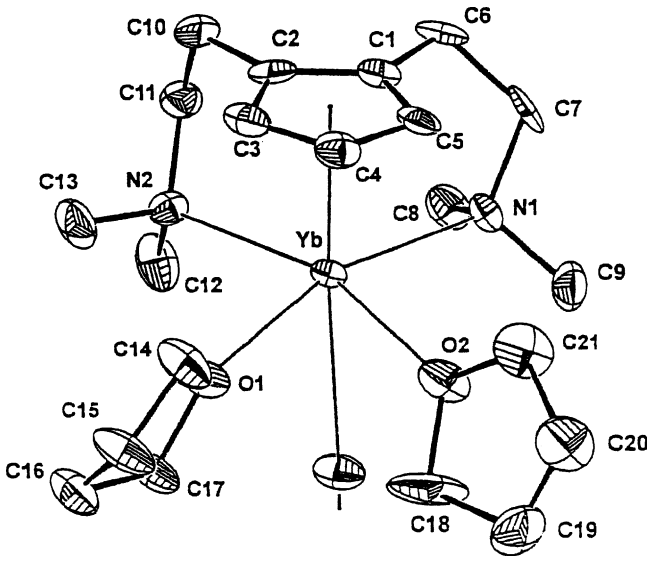

Fig. 18. ORTEP view of the complex $[\eta^5{:}\eta^1{:}\eta^1\text{-}C_5H_3(CH_2CH_2NMe_2)_2\text{-}1,2]YI(THF)_2$.

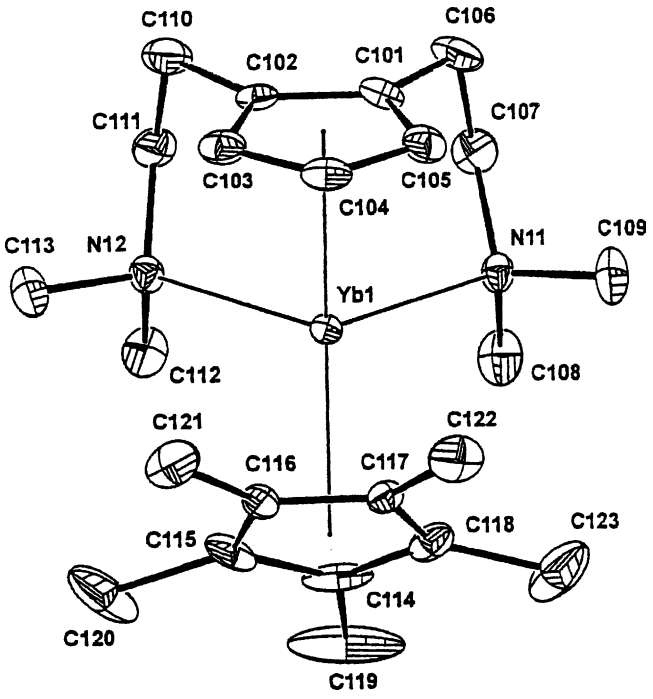

Fig. 19. ORTEP view of the complex $[\eta^5{:}\eta^1{:}\eta^1\text{-}C_5H_3(CH_2CH_2NMe_2)_2\text{-}1,2]YbCp^*$.

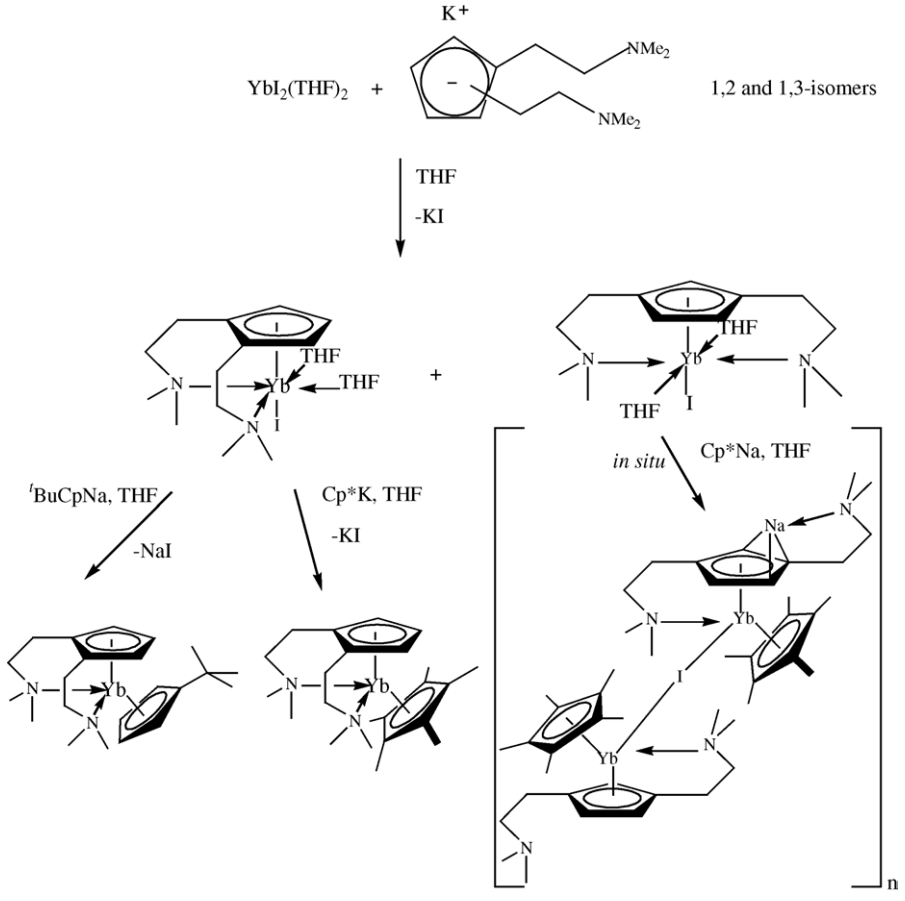

Scheme 15. Formation of the polymeric mixed-metallocene *ate* complex $\{Na[\mu_2\text{-}(\eta^5{:}\eta^1{:}\eta^1\text{-}C_5H_3(CH_2CH_2NMe_2)_2\text{-}1,3)]Cp^*Yb[\mu_2\text{-}(\eta^5{:}\eta^1{:}\eta^1\text{-}C_5H_3(CH_2CH_2NMe_2)_2\text{-}1,3)]Cp^*\}_n$.

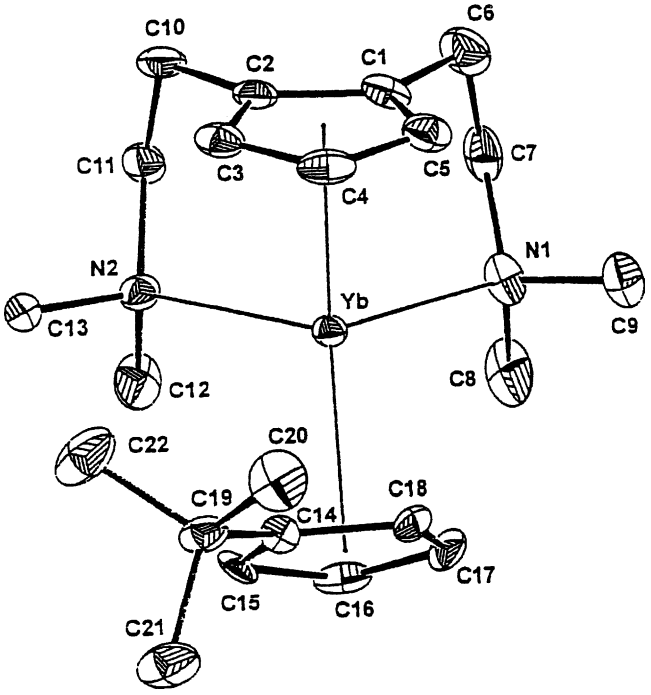

Fig. 20. ORTEP view of the complex $[\eta^5{:}\eta^1{:}\eta^1\text{-}C_5H_3(CH_2CH_2NMe_2)_2\text{-}1,2]Yb(\eta^5\text{-}C_5Me_4{}^tBu)$.

dienyl (Cp^s) sodium salt in THF to give $Cp^sLnCl_2(THF)_2$ (Ln = Dy, Ho, Gd) (Scheme 16).

The complex $Cp^sDyCl_2(THF)_2$ reacts with 1 equiv. of CpNa to yield the mixed-ring complex $[Cp^sCpDyCl]_2$. The complexes were characterized by elemental analysis, IR and mass spectroscopy.

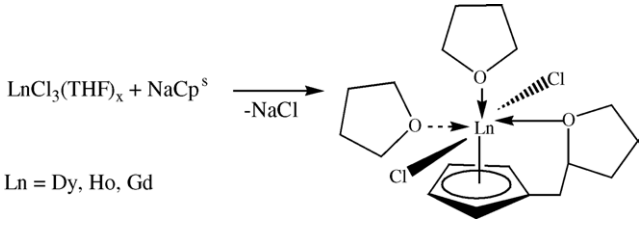

Scheme 16. Formation of the complexes $Cp^sLnCl_2(THF)_2$ (Ln = Dy, Ho, Gd).

Ephritikhine and co-workers [18] synthesized monocyclopentadienyl neodymium complexes. $Nd(BH_4)_3(THF)_3$ reacts with Cp^*K and KC_4Me_4P to give the organometallic derivatives $(Cp^*)Nd(BH_4)_2(THF)$ and $[K(THF)][(C_4Me_4P)_2Nd(BH_4)_2]$. Similarly $Nd(BH_4)_3(THF)_3$ reacts with K_2COT to give a mono(cyclooctatetraenyl)neodymium complex, which is discussed in Section 2.4.

De Oliveira and co-workers [19] presented the synthesis and characterization of chloro(vinylcyclopentadienyl)-lanthanide complexes. Vinylcyclopentadienyl lithium was added in different molar ratios $[LnCl_3]{:}[Li(C_5H_4CH{=}CH_2)]$ of 1:1 or 1:2 to $LnCl_3$ (Ln = La, Sm, Eu, Gd, Dy and Er) to give mono(vinylcyclopentadienyl) complexes of the type $Ln(C_5H_4CH{=}CH_2)Cl_2$ and for neodymium and terbium the bis(vinylcyclopentadienyl) complexes of the type $Ln(C_5H_4CH{=}CH_2)_2Cl$. The reaction of bis(vinylcyclopentadienyl)mercury(II) with powdered dysprosium in THF afforded the tris(vinylcyclopentadienyl)-dysprosium complex $Dy(C_5H_4CH{=}CH_2)_3$. All compounds were characterized by elemental analysis, complexometric titration with EDTA, argentometric and thermal anal-

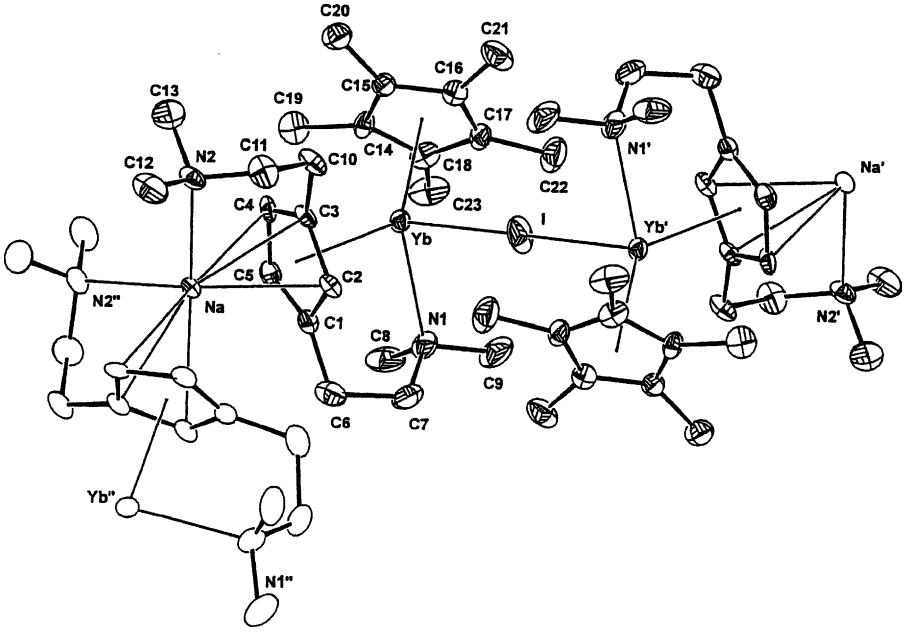

Fig. 21. ORTEP view of the polymeric mixed-metallocene *ate* complex $\{Na[\mu_2\text{-}(\eta^5{:}\eta^1{:}\eta^1\text{-}C_5H_3(CH_2CH_2NMe_2)_2\text{-}1,3)]Cp^*Yb[\mu_2\text{-}(\eta^5{:}\eta^1{:}\eta^1\text{-}C_5H_3(CH_2CH_2NMe_2)_2\text{-}1,3)]Cp^*\}_n$.

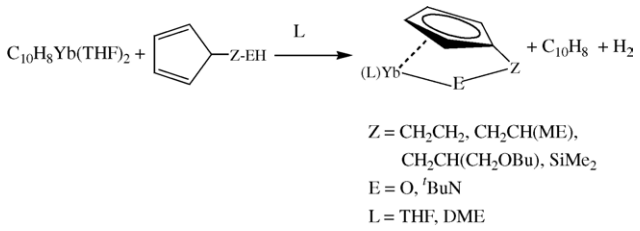

Scheme 17. The reactions of ytterbium naphthalene, $(C_{10}H_8)Yb(THF)_2$, with chelating bifunctional cyclopentadienyl ligands.

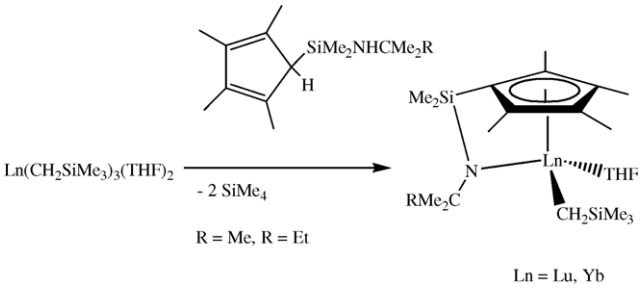

Scheme 18. Formation of the complexes $(\eta^5{:}\eta^1\text{-}C_5Me_4SiMe_2NCMe_2R)Ln(CH_2SiMe_3)(THF)$, Ln = Lu, Yb.

ysis, magnetic susceptibility and vibrational spectra in the IR.

Bochkarev and co-workers [20] published a convenient synthetic route to half-sandwich complexes of divalent ytterbium. Reactions of ytterbium naphthalene, $C_{10}H_8Yb(THF)_2$, with 2-cyclopentadienylethanol, 1-cyclopentadienylpropan-2-ol, 3-cyclopentadienyldimethylsilyl-*tert*-butylamine were studied. The bivalent ytterbium complexes with chelating bifunctional cyclopentadienyl ligands $[(\eta^5\text{-}C_5H_5)CH_2CH_2(\eta^1\text{-}O)]Yb(THF)$, $[(\eta^5\text{-}C_5H_5)CH_2CH_2(\eta^1\text{-}O)]Yb(DME)$, $[(\eta^5\text{-}C_5H_5)CH_2CH(Me)(\eta^1\text{-}O)]Yb(THF)$, $[(\eta^5\text{-}C_5H_5)CH_2CH(CH_2OC_4H_9)(\eta^1\text{-}O)]Yb(THF)$, and $[(\eta^5\text{-}C_5H_5)SiMe_2(\eta^1\text{-}N(^tBu))]Yb(THF)$ were obtained and characterized (Scheme 17).

Okuda and co-workers [21] investigated the synthesis and characterization of dimeric hydrido complexes of lanthanides containing a linked amido-cyclopentadienyl ligand. When the tris[(trimethylsilyl)methyl] complexes of lutetium and ytterbium, $(CH_2SiMe_3)_3Ln(THF)_2$, were treated in pentane solution with 1 equiv. of $(C_5Me_4H)SiMe_2NHCMe_2R$ (R = Me, Et) at 0 °C, the new complexes $(\eta^5{:}\eta^1\text{-}C_5Me_4SiMe_2NCMe_2R)Ln(CH_2SiMe_3)(THF)$ were formed (Scheme 18).

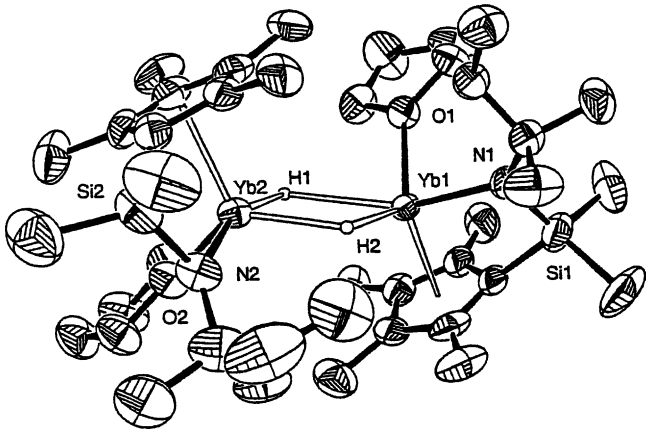

Fig. 22. ORTEP view of the complex of $[(\eta^5{:}\eta^1\text{-}C_5Me_4SiMe_2NCMe_2R)Yb(\mu\text{-}H)(THF)]_2$.

The complexes were characterized by elemental analysis and ^1H, ^{13}C, ^{29}Si, and ^{31}P NMR spectroscopy.

Both the lutetium and ytterbium alkyl complexes were subjected to hydrogenolysis with dihydrogen or with phenylsilane in pentane at room temperature to give the dimeric hydrides $[(\eta^5{:}\eta^1\text{-}C_5Me_4SiMe_2NCMe_2R)Ln(\mu\text{-}H)(THF)]_2$ (Ln = Lu, Yb, Y). Because of the thermal instability of the alkyl complexes of lutetium and ytterbium, it proved advantageous to prepare the hydride complexes in a one-pot procedure without isolating the alkyl complexes (Scheme 19 and Fig. 22).

When the dimeric lutetium and yttrium hydrides are treated with excess PMe_3, exchange against THF occurs (Scheme 20 and Fig. 23) [21].

By mixing equimolar amounts of the lutetium and yttrium hydrido complexes in C_6D_6, the mixed complexes were formed in a statistical 1:2:1 mixture (Scheme 21) [21].

The dimeric chloro complex $[(\eta^5{:}\eta^1\text{-}C_5Me_4SiMe_2NCMe_2R)Y(\mu\text{-}Cl)(THF)]_2$ could be synthesized by allowing in situ formed "$Y(CH_2SiMe_3)_2Cl(THF)_n$" to react with the amino-cyclopentadiene $(C_5Me_4H)SiMe_2NHCMe_2R$ in a σ-bond metathesis [21].

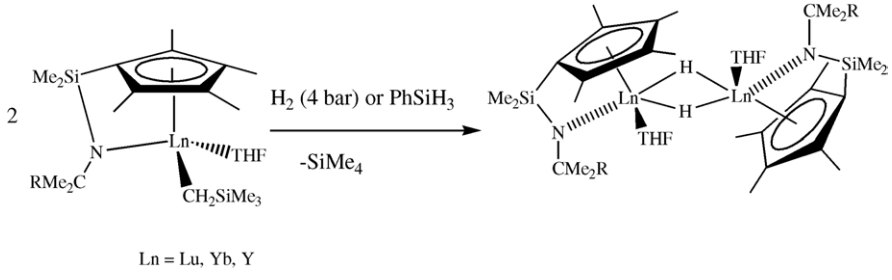

Scheme 19. Formation of the dimeric hydrides complexes $[(\eta^5{:}\eta^1\text{-}C_5Me_4SiMe_2NCMe_2R)Ln(\mu\text{-}H)(THF)]_2$.

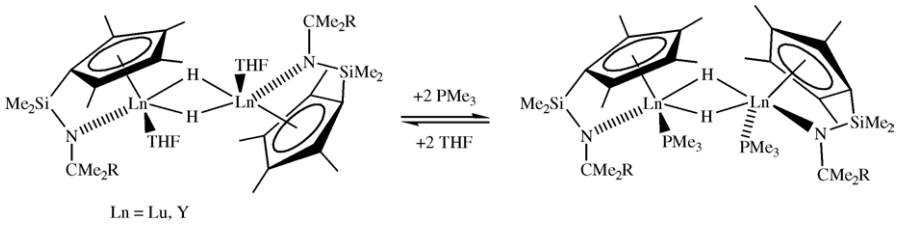

Scheme 20. Exchange reaction of $[(\eta^5{:}\eta^1\text{-}C_5Me_4SiMe_2NCMe_2R)Ln(\mu\text{-}H)(THF)]_2$ with PMe_3.

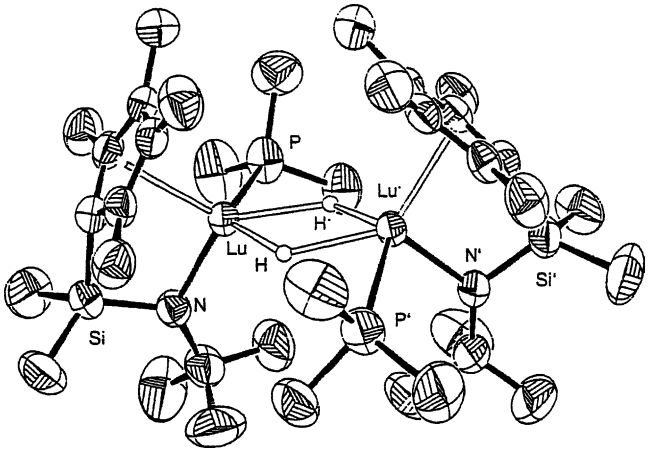

Fig. 23. Molecular structure of the $[(\eta^5{:}\eta^1\text{-}C_5Me_4SiMe_2NCMe_2R)Lu(PMe_3)(\mu\text{-}H)]_2$.

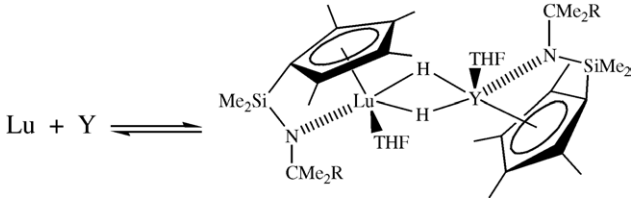

Scheme 21. Equilibration reaction of lutetium and yttrium hydrido complexes.

2.2.2. *Bis(cyclopentadienyl) complexes*

Barbier-Baudry et al. [22] published a conclusion of studies relating the stability of lanthanide hydrides including the bis(cyclopentadienyl)lanthanide hydrides $(^tBuC_5H_4)_2SmH$ and $(^tBuC_5H_4)_2NdH$.

As mentioned in Section 2.2.1, Cai and co-workers [17] synthesized bis(tetrahydrofurfurylcyclopentadienyl)lanthanide chloride complexes with Ln = Sm, Dy (Scheme 22 and Fig. 24).

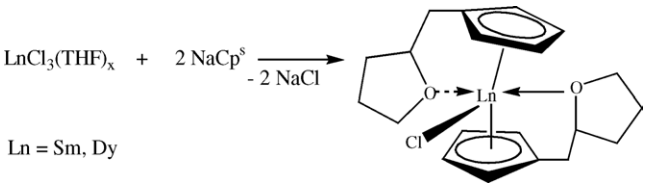

Scheme 22. Formation of the complexes Cp^s_2LnCl (Ln = Sm, Dy).

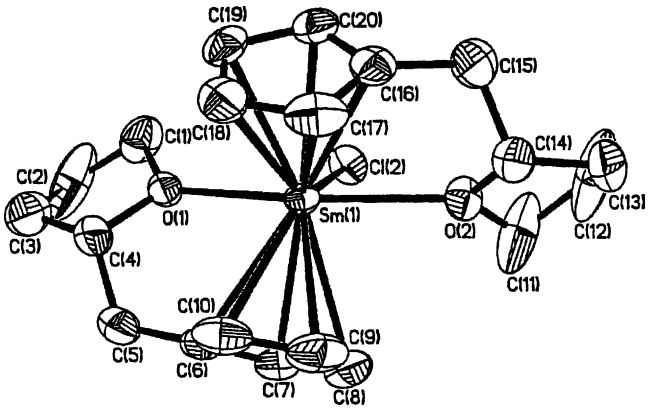

Fig. 24. ORTEP view of the complex Cp^s_2SmCl.

In the complex Cp^s_2SmCl the Sm atom is surrounded by two Cp^s rings, one chlorine atom and two oxygen atoms of the side chain to form a distorted trigonal bipyramid. The coordination number around the central metal is 9 [17].

Treatment of the complex Cp^s_2SmCl with 1 equiv. of $NaPzMe_2$ ($PzMe_2$ = 3,5-dimethylpyrazolate) forms $Cp^s_2SmPzMe_2$ (Fig. 25). X-ray structural analyses show

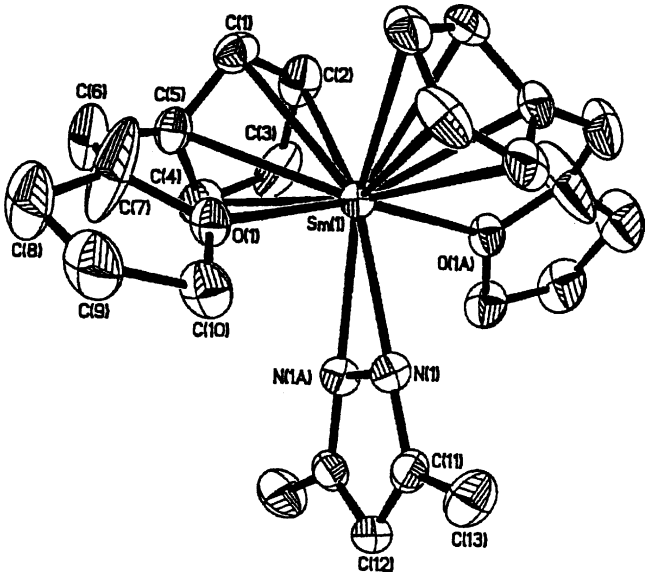

Fig. 25. ORTEP view of the complex $Cp^s_2SmPzMe_2$.

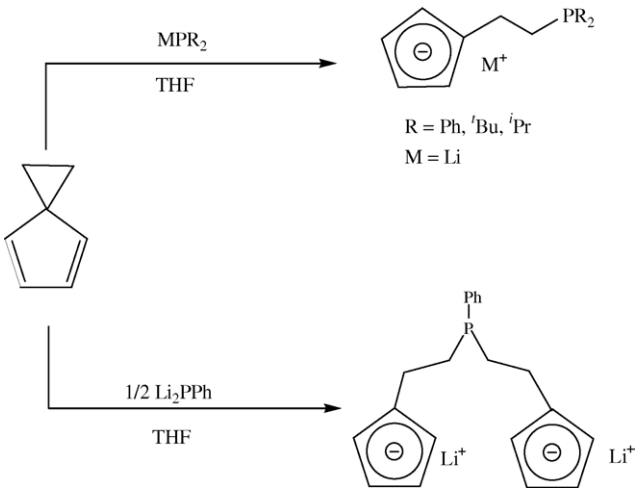

Scheme 23. Synthetic route to lithium phosphanoethylcyclopentadienyl derivatives.

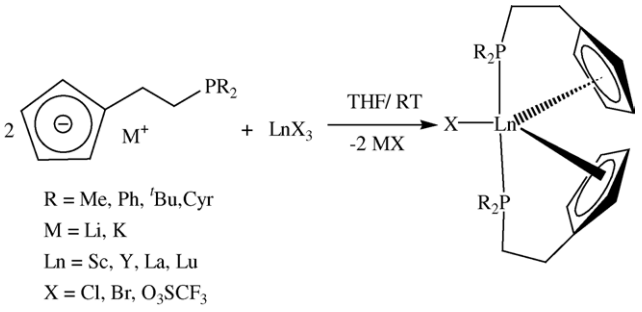

Scheme 24. Synthetic routes to bis(phosphanoethylcyclopentadienyl) lanthanide complexes.

that the complexes Cp^s_2SmCl and $Cp^s_2SmPzMe_2$ are unsolvated monomers. In the latter complex, the Sm atom is coordinated by two Cp^s rings, two nitrogen atoms of 3,5-dimethylpyrazolate and two oxygen atoms of the side chains in a distorted tetragonal–bipyramidal geometry. The coordination number at the Sm atom is 10. The strong intramolecular chelating coordination and the high steric crowding result in a lower activity of $Cp^s_2SmPzMe_2$ towards methylmethacrylate polymerization [17].

De Oliveira and co-workers [23] presented the synthesis of a series of organolanthanide triphenylphosphane

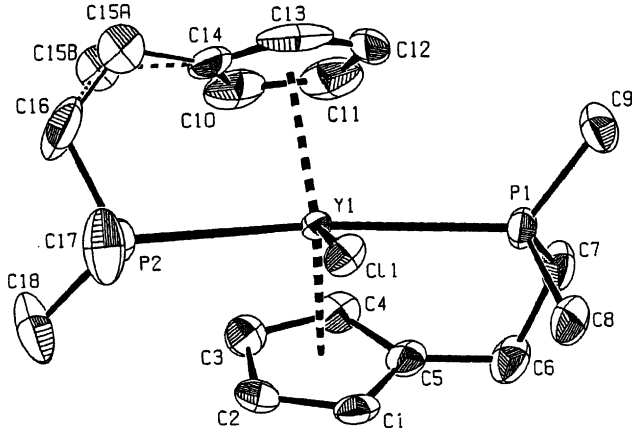

Fig. 26. ORTEP view of the complex $(C_5H_4CH_2CH_2PMe_2)_2YCl$.

adducts. The complexes $Cp_2LnCl(PPh_3)$ (Ln = La, Nd, Eu, Yb, Lu) were characterized by elemental analysis and IR spectroscopy.

Karsch et al. [24] published phosphanoethyl substituted cyclopentadienyl lanthanide complexes of type Cp'_2LnX. The reaction of $M[C_5H_4CH_2PR_2]$ (R = Me, Cy, ^{t}Bu, Ph; M = Li, K) with LnX_3 (Sc, Y, La, Lu, X = Cl^-, $CF_3SO_3^-$) afforded bis(cyclopentadienyl) metal complexes (Scheme 23).

Two equivalents of lithium phosphanoethylcyclopentadienide reacted with Sc, Y, La, Lu to give monomeric, solvent-free complexes (Scheme 24 and Fig. 26).

According to X-ray studies, the central lanthanide atom is surrounded in a trigonal–bipyramidal geometry by two axial phosphano groups and two equatorial cyclopentadienyl groups with the third equatorial site occupied by the halide ligand. Using the dianionic ligand $Li_2[(C_5H_4CH_2CH_2)_2PMe]$ phosphano-bridged *ansa*-metallocene derivatives $[(C_5H_4CH_2CH_2)_2PMe]Ln$ (Ln = Y, Lu; X = Cl^-, $CF_3SO_3^-$) were isolated. The complexes are soluble in toluene, monomeric and free of coordinated solvent ligands [24] (Scheme 25).

Lappert et al. [25] synthesized the ytterbocene(III) iodide $[(\eta^5\text{-}C_5H_3(SiMe_3)_2\text{-}1,3)]_2YbI(THF)$. The complex was obtained by the reaction of 2 equiv. of $Na[C_5H_3(SiMe_3)_2\text{-}1,3]$ with $YbI_3(THF)_2$, which was obtained from Yb metal and an excess of $(ICH_2)_2$ in THF (Fig. 27).

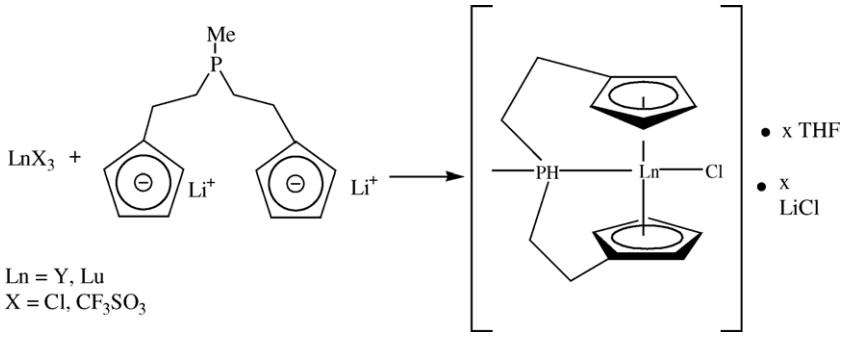

Scheme 25. Formation of the phosphano-bridged *ansa*-metallocene complexes.

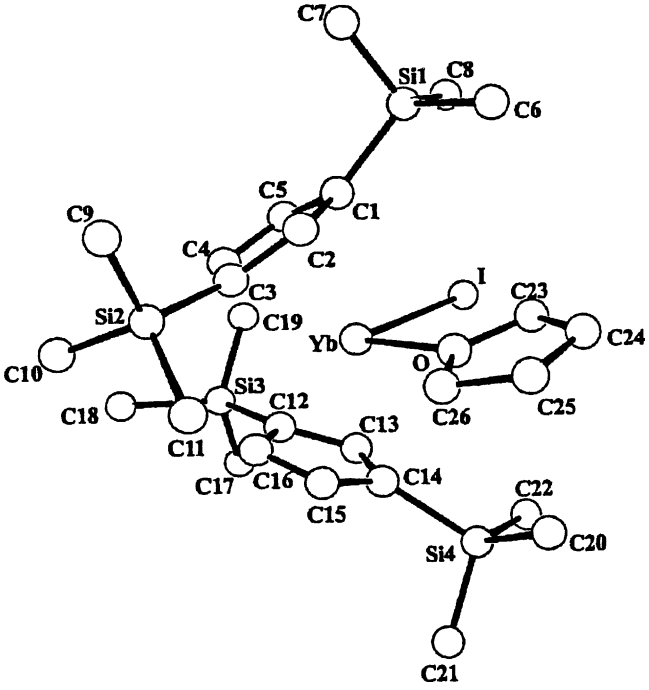

Fig. 27. Molecular structure of $[(\eta^5\text{-}C_5H_3(SiMe_3)_2\text{-}1,3)]_2YbI(THF)$.

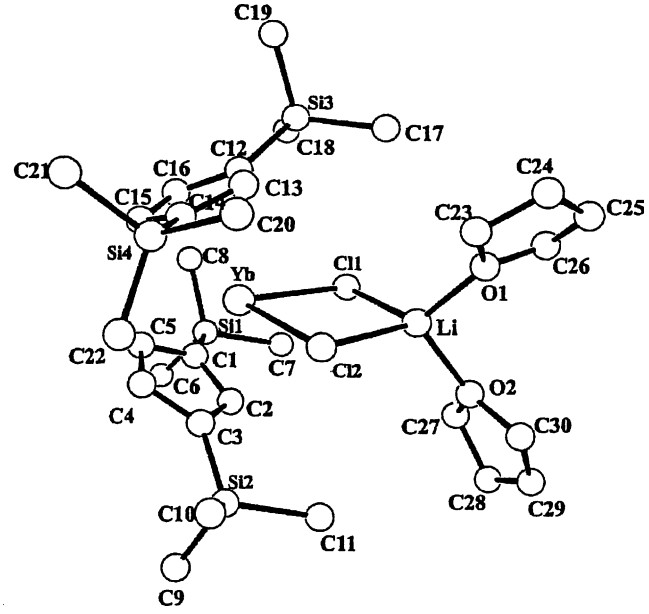

Fig. 28. Molecular structure and atom-labeling scheme of $[(\eta^5\text{-}C_5H_3(SiMe_3)_2\text{-}1,3)_2Yb(\mu\text{-}Cl)_2Li(THF)_2]$.

The heterobimetallic complex $[(\eta^5\text{-}C_5H_3(SiMe_3)_2\text{-}1,3)_2Yb(\mu\text{-}Cl)_2Li(THF)_2]$ was formed with $YbCl_3$ and $Li(\eta^5\text{-}C_5H_3(SiMe_3)_2\text{-}1,3)_2$ (Fig. 28).

Furthermore, the ytterbium(II) complex $[(\eta^5\text{-}C_5H_3(SiMe_3)_2\text{-}1,3)]Yb(OAr)(THF)_x$ ($OAr = OC_6H_2{}^tBu_2\text{-}2,6\text{-}Me\text{-}4$) was obtained during the reaction of either $Na[C_5H_3(SiMe_3)_2\text{-}1,3]$ or $[(\eta^5\text{-}C_5H_3(SiMe_3)_2\text{-}1,3)]_2Yb(THF)$ with $(OAr)_2Yb(THF)_3$. The complex $[(\eta^5\text{-}C_5H_3(SiMe_3)_2\text{-}1,3)]Yb(OAr)(THF)_x$ was characterized by ^1H and ^{171}Yb NMR spectroscopy.

Xie and co-workers [26] synthesized the anionic heterometallic dichlorolanthanocene complexes $[(Me_3Si)_2C_5H_3]_2Ln(\mu\text{-}Cl)_2Li(THF)_4$ (Ln = Er, Yb) and $[(Me_3Si)_2C_5H_3]_2Yb(\mu\text{-}Cl)_2Li(THF)_2$ (Scheme 26).

Treatment of $LnCl_3$ with 2 equiv. of Cp″Li (Cp″ = $(Me_3Si)_2C_5H_3$) in THF gave the ionic compounds $[((Me_3Si)_2C_5H_3)_2Ln(\mu\text{-}Cl)_2][Li(THF)_4]$ (Ln = Er, Yb) in good yields. Recrystallization of the ytterbium complex from toluene afforded the *ate*-compound $[(Me_3Si)_2C_5H_3]_2Yb(\mu\text{-}Cl)_2Li(THF)_2$ (Figs. 29 and 30).

The complex consists of well-separated, alternating layers of discrete tetrahedral anions $[Cp''_2LnCl_2]^-$ and tetrahedral cations $[Li(THF)_4]^+$ in a typical ionic lattice. In the anion, the Ln^{3+} ion is η^5-bonded to two Cp″ ligands and two terminal chloride ions in a distorted tetrahedral geometry. The average distances are 2.667(3) Å in the erbium and 2.641(3) Å in the ytterbium complex. The average Ln–Cl distances of 2.563(1) Å in the erbium and 2.546(1) Å in the ytterbium complex are comparable to each other if Shannon's ionic radii are taken into account [26].

The Yb^{3+} ion is η^5-bonded to two cyclopentadienyl rings and σ-bonded to two doubly bridging chloride ions in a distorted-tetrahedral geometry. The Cl–Yb–Cl angle of 84.89(3) Å is smaller than that in $Cp''_2Nd(\mu\text{-}Cl)_2Li(THF)$, but is significantly smaller than that of 102.77(3)° in $[\{(Me_3Si)_2C_5H_3\}_2YbCl_2][Li(THF)_4]$ probably owing to the bridging unit $Yb(\mu\text{-}Cl)_2Li$ that forces the Cl–Yb–Cl angle to be smaller [26].

Lappert and co-workers [27] synthesized the bis(substituted) cyclopentadienyl lanthanide(III) halides $[Cp^R_2Ln(\mu\text{-}Cl)]_2$ (Ln = Pr, Nd, Sm, Dy, Tb, Y), $[Cp^{tt}_2Ln(\mu\text{-}X)]_2$ (X = Cl, Ln = La, Nd; X = I, Ln = Tm), $[(Cp^{R'}_2SiMe_2)Nd(\mu\text{-}Cl)]_2$ and the bis(substituted cyclopentadienyl)lanthanide(II) complexes $Cp^R_2Ln(THF)_2$ (Ln = Sm, Eu, Yb), $Cp^t_2Yb(THF)_2$, $Cp^{tt}_2Ln(THF)_2$ (Ln = Sm, Yb), Cp^R_2Ln(Ln = Sm, Eu, Yb), Cp^t_2Yb, Cp^{tt}_2Ln (Ln = Sm, Yb) and $(Cp^{R'}_2SiMe_2)Yb(THF)_2$ ($Cp^R = \eta^5\text{-}C_5H_4[CH(SiMe_3)_2]$,

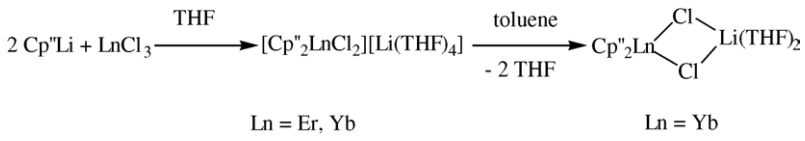

Scheme 26. Formation of the heterometallic dichloroytterbium complex.

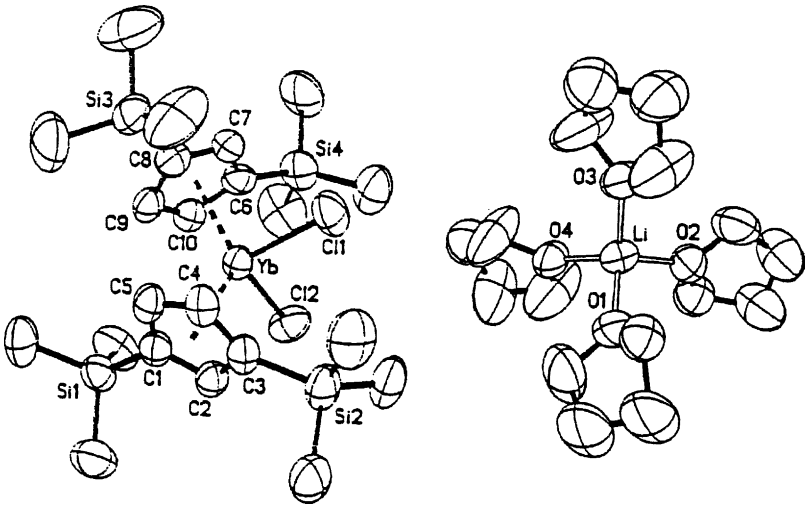

Fig. 29. ORTEP view of the molecular structure of $[Li(THF)_4][((Me_3Si)_2C_5H_3)_2YbCl_2]$.

$Cp^t = \eta^5$-$C_5H_4(SiMe_2{}^tBu)$, $Cp^{tt} = \eta^5$-$C_5H_3(SiMe_2{}^tBu)_2$-1,3, $Cp^{R'} = \eta^5$-$C_5H_3[CH(SiMe_3)_2$-3]) from the appropriate $LnCl_3$, TmI_3, LnI_2 with the selected sodium or potassium cyclopentadienides (Schemes 27 and 28).

The molecular structures of $[Cp_2^RNd(\mu\text{-}Cl)]_2$, $[Cp_2^{tt}Tm(\mu\text{-}I)]_2$, and $(Cp_2^{R'}SiMe_2)Yb(THF)_2$ have been determined by single-crystal X-ray diffraction studies (Figs. 31–33).

The complexes were characterized by ^1H, ^{13}C, ^{29}Si and ^{171}Yb NMR spectroscopy, elemental analysis and mass spectrometry.

Visseaux et al. [28] synthesized base-free metallocenes of samarium and neodymium, using tetra-*iso*-propylcyclopentadienyl as the ligand. The mixed metallocenes $COTSmCp^{4i}$ and $COTNdCp^{4i}$ will be discussed in Section 2.2.5. The bis(tetra-*iso*-propylcyclopentadienyl) samarium complex is obtained from the reaction of 2 equiv. of $NaCp^{4i}$ with SmI_2 (Fig. 34 and Scheme 29).

The Sm–Cp^{4i} distances are 2.51 Å, which is equivalent to that in Cp_2^*Sm (2.53 Å) and the triple-decker complex $(C_5Me_4R)Sm(COT)Sm(C_5Me_4R)$ (2.51 and 2.47 Å for Sm–Cp). The Cp–Sm–Cp angle is 152°, which is larger than in the permethylated analogue.

Deacon et al. [29] published oxidative synthetic routes leading to pyrazolates and pseudo-pyrazolates of lanthanides. Cp_2^*Yb reacted with $Tl(Ph_2pz)$ and Tl(azin)

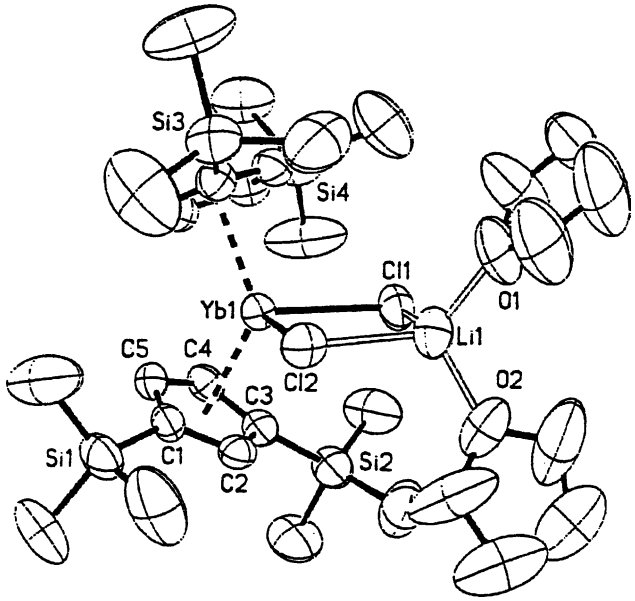

Fig. 30. ORTEP view of the molecular structure of $[(Me_3Si)_2C_5H_3]_2Yb(\mu\text{-}Cl)_2Li(THF)_2$.

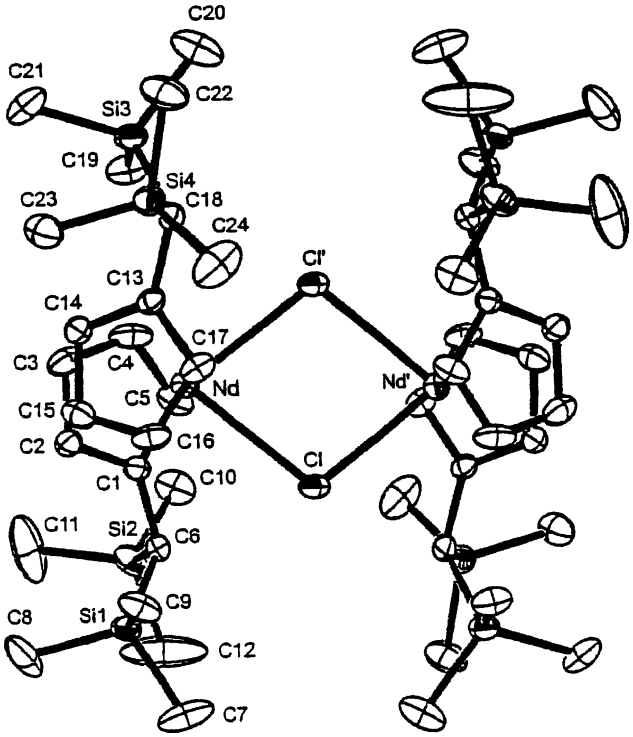

Fig. 31. ORTEP view of the molecular structure of $[Cp_2^RNd(\mu\text{-}Cl)]_2$.

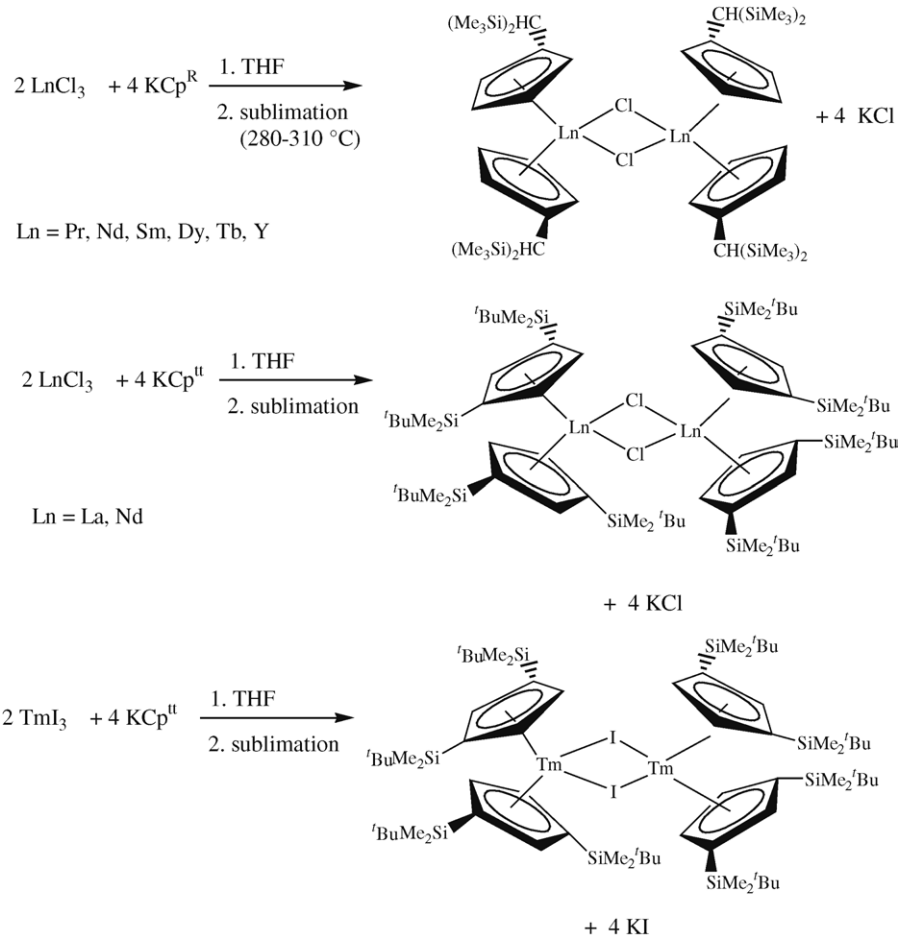

Scheme 27. Synthetic routes to the complexes $[Cp^{R}_{2}Ln(\mu\text{-}Cl)]_2$ (Ln = Pr, Nd, Sm, Dy, Tb, Y), $[Cp^{tt}_{2}Ln(\mu\text{-}X)]_2$ (X = Cl, Ln = La, Nd; X = I, Ln = Tm).

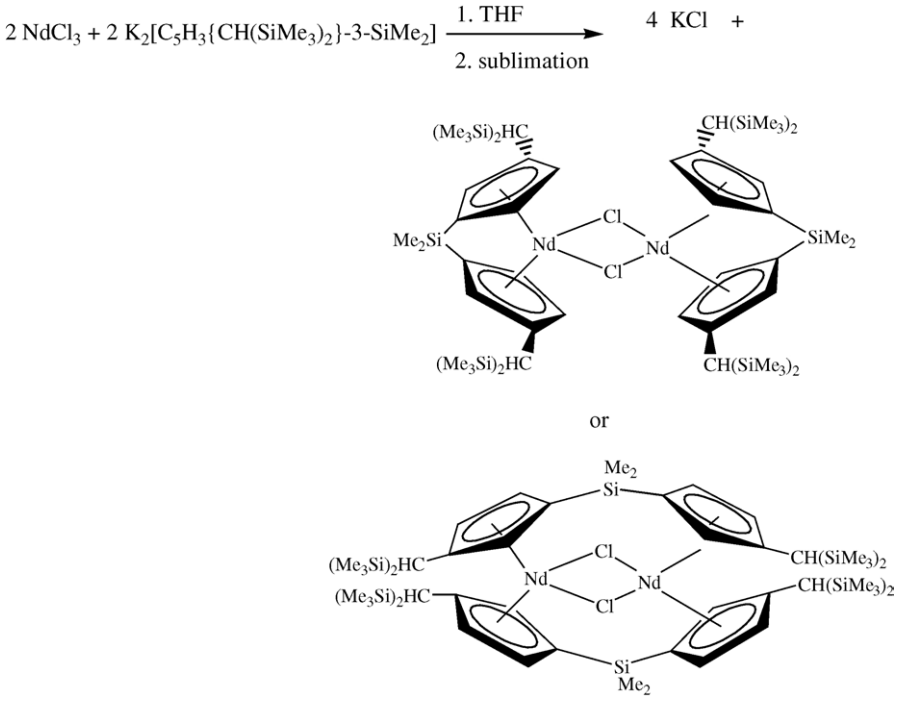

Scheme 28. Synthetic route to the complexes $[(Cp^{R'}_{2}SiMe_2)Nd(\mu\text{-}Cl)]_2$.

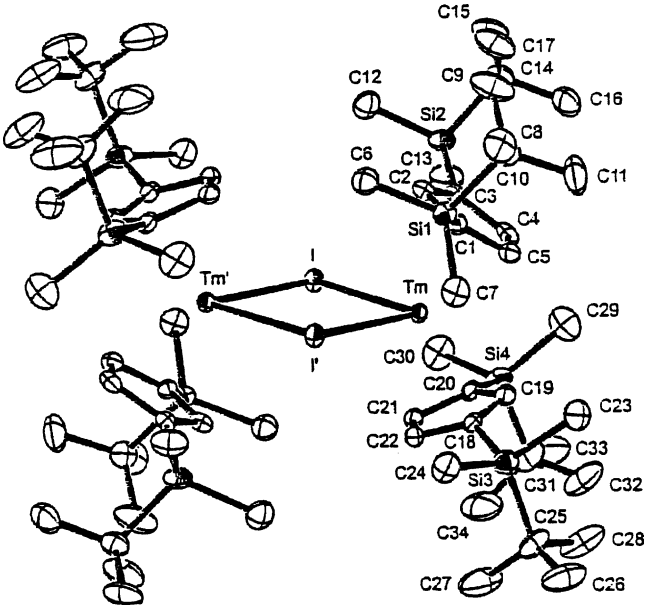

Fig. 32. ORTEP view of the molecular structure of $[Cp''_2Tm(\mu\text{-}I)]_2$.

(Ph_2pz = 3,5-diphenylpyrazolate, azin = 7-azaindolate) yielding $Cp^*_2Yb(Ph_2pz)$ and $Cp^*_2Yb(azin)$ (Scheme 30).

The X-ray crystal structures of $Cp^*_2Yb(Ph_2pz)$ and $Cp^*_2Yb(azin)$ show eight-coordinated monomers with the

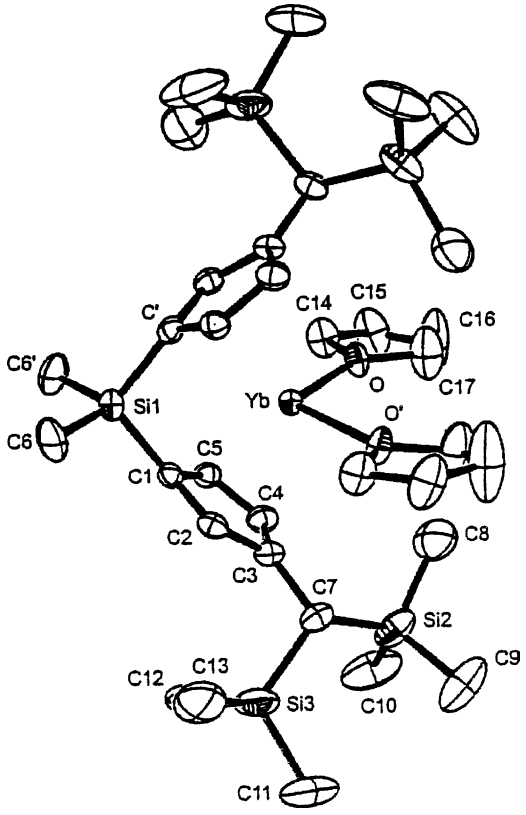

Fig. 33. ORTEP view of the molecular structure of $(Cp^{R'}_2SiMe_2)Yb(THF)_2$.

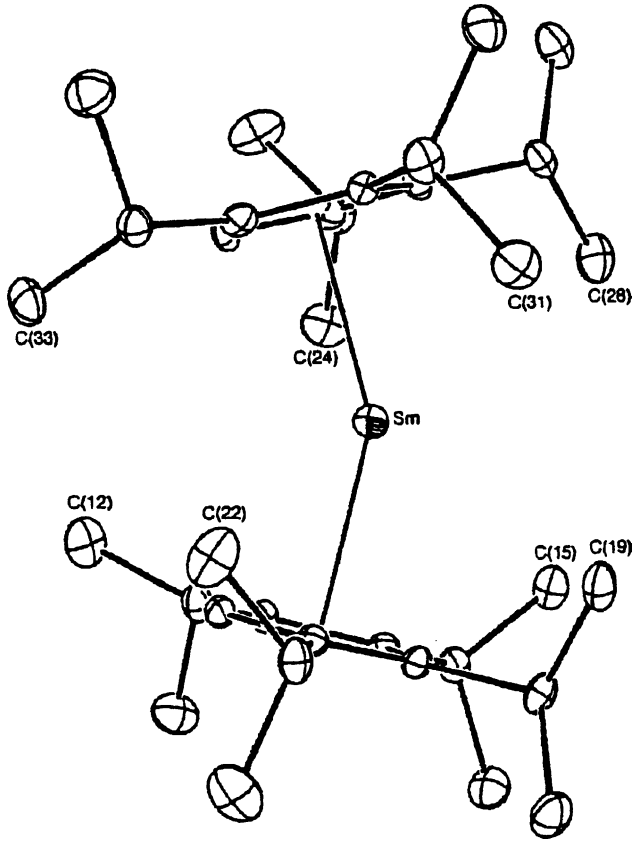

Fig. 34. ORTEP view of $(Cp^{4i})_2Sm$.

Cp^* ligands η^5-bonded to the ytterbium atom and the diaza ligand chelating edge-on through the nitrogen atoms (Figs. 35 and 36).

Treatment of neodymium metal with $Tl(Ph_2pz)$ yields $Nd(Ph_2pz)_3(DME)_2$, which is a nine-coordinate monomer with three η^2-pyrazolate ligands and one chelating as well as a unidentate DME ligand.

Oxidation of Cp^*_2Sm with $[Tl(1,4,2\text{-}P_2SbC_2{}^tBu_2)]/[Tl(1,2,4\text{-}P_3C_2{}^tBu_2)]$ (approximately 4:1) gave a mixture of $Cp^*_2Sm(1,2,4\text{-}P_3C_2{}^tBu_2)$ and $Cp^*_2Sm(1,4,2\text{-}P_2SbC_2{}^tBu_2)$. The former was shown to be a nine-coordinate monomer

$$SmI_2 + 2\ NaCp^{4i} \xrightarrow{THF} (Cp^{4i})_2Sm$$

Scheme 29. Formation of the unsolvated metallocene $(Cp^{4i})_2Sm$.

$$Cp^*_2Yb + TlL \xrightarrow{S} [Cp^*_2Yb(L)] + Tl\downarrow$$

L = Ph_2pz, S = DME; L = azin, S = THF

Scheme 30. Oxidation of Cp^*_2Yb with $Tl(Ph_2pz)$ and Tl(azin) to give $Cp^*_2Yb(Ph_2pz)$ and $Cp^*_2Yb(azin)$.

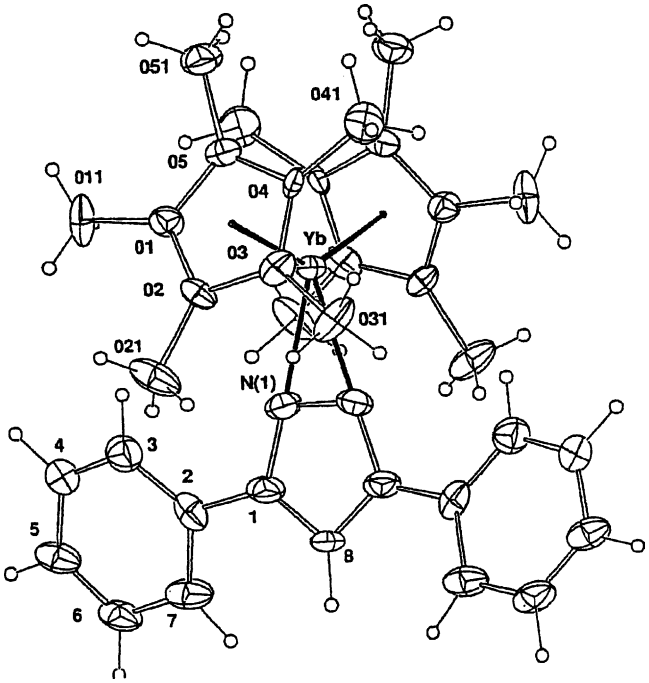

Fig. 35. ORTEP view of the complex $Cp^*_2Yb(Ph_2pz)$.

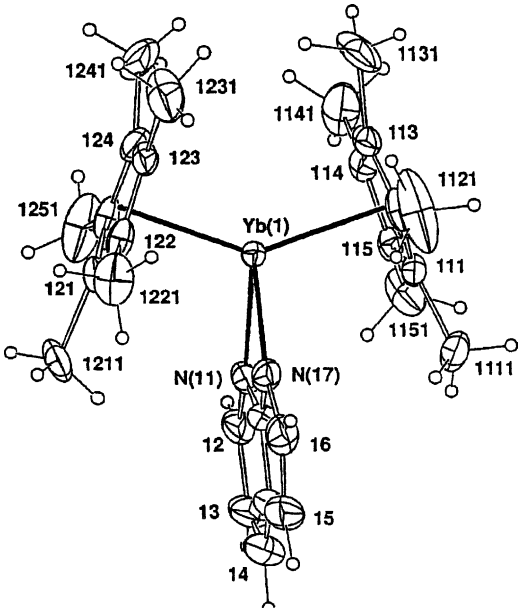

Fig. 36. ORTEP view of the complex $Cp^*_2Yb(Ph_2pz)$.

with novel pseudo-pyrazolate η^2-(P_2)-[1,2,4-$P_3C_2{}^tBu_2$] coordination of the triphosphacyclopentadienide ligand. After metathesis routes to $Ln(1,4,2\text{-}P_2SbC_2{}^tBu_2)_n$ complexes failed, redox transmetalation between ytterbium metal and $Tl(1,4,2\text{-}P_2EC_2{}^tBu_2)$ (E = Sb, P) containing a substantial impurity of $[Li(tmeda)_2][1,4,2\text{-}P_2EC_2{}^tBu_2]$ yielded the first lanthanide diphosphastibacyclopentadienide complex in a mixture with $1,2,4\text{-}P_3C_2{}^tBu_2$ species [29].

Castillo and Tilley [30] synthesized $Cp^*_2SmSiH_3$ complexes via σ-bond metathesis of the Si–C–bond of phenylsilane. Reaction of $PhSiH_3$ with the samarium complexes $[Cp^*_2Sm(\mu\text{-}H)]_2$ leads to redistribution at silicon, yielding benzene, silane, Ph_2SiH_2, Ph_3SiH and dehydrocoupling products.

$[Cp^*_2SmSiH_3]_3$ is a rare example of a lanthanide silyl complex and represents the first example of an f-element-SiH_3 derivative. This complex activates the S–O bond of dimethyl sulfoxide (DMSO) to form the bridged species $Cp^*_2Sm(DMSO)OSiH_2OSm(DMSO)Cp^*_2$ (Scheme 31). The

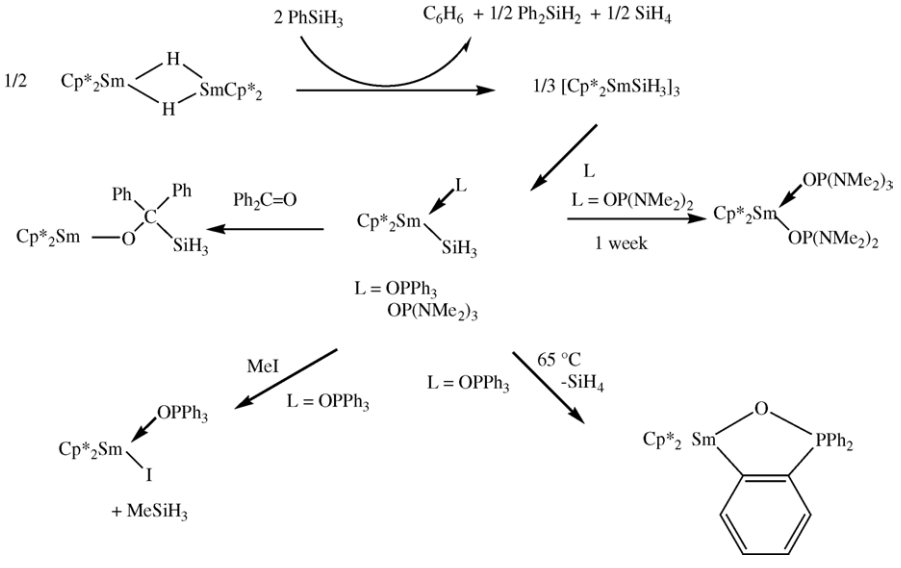

Scheme 31. Reactions of $PhSiH_3$ with the samarium complex $[Cp^*_2Sm(\mu\text{-}H)]_2$.

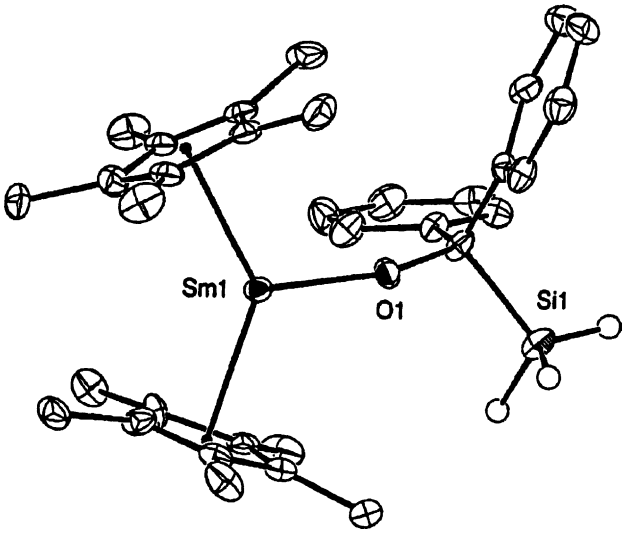

Fig. 37. ORTEP view of the complex $Cp^*_2SmOCPh_2SiH_3$.

hard Lewis bases Ph_3PO and HMPA (HMPA = $(Me_2N)_3PO$) react with the Sm–SiH_3 complex to produce the base adducts $Cp^*_2SmSiH_3(OPPh_3)$ and $Cp^*_2SmSiH_3$(HMPA), respectively [30]. Fig. 37 depicts the molecular structure of $Cp^*_2SmOCPh_2SiH_3$.

Schumann and co-workers [31] synthesized two catalytically active samarocene complexes, $Cp^*_2Sm(^i$Pr-carben) and $[(C_5Me_4Et)_2Sm(CH_3)Al(CH_3)_3]_2$, and investigated their catalytic activity in the living polymerization of mesogenic methacrylates (Fig. 38). $Cp^*_2Sm(THF)_2$ reacts with 1,3-diisopropyl-4,5-dimethylimidazoline-2-ylidene, $C_3N_2Me_2{}^iPr_2$ (=^{i}Pr-carben), under formation of $Cp^*_2Sm(^i$Pr-carben). The Sm–C, C–C and the exocyclic N–C bond lengths are in the normal range.

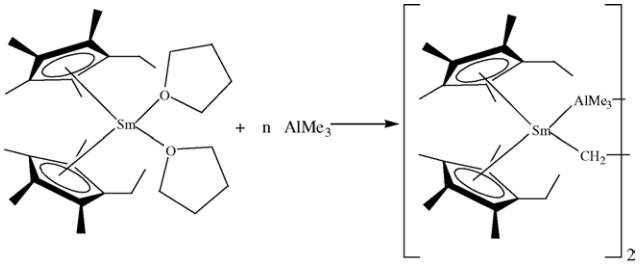

Scheme 32. Formation of the heterobimetallic samarocene complex $[(C_5Me_4Et)_2Sm(\mu\text{-}Me)Al(Me)_3]_2$.

The heterobimetallic complex $[(C_5Me_4Et)_2Sm(\mu\text{-}Me)Al(Me)_3]_2$ is easily formed by the reaction of the THF adduct of bis[(ethyltetramethylcyclopentadienyl)]samarium(II) with $AlMe_3$ [31] (Scheme 32 and Fig. 39).

Andersen and co-workers [32] investigated the syntheses of the base-free ytterbocenes Cp^*_2Yb, $(Me_4C_5H_4)_2Yb$ and $[1,3\text{-}(Me_3C)_2C_5H_3]_2Yb$. All these complexes have been prepared from their diethyl ether adducts by the toluene reflux method: a toluene solution must be refluxing vigorously before the system is exposed to dynamic vacuum (Scheme 33 and Figs. 40 and 41).

In order to get the ether-free ytterbocene derived from $(Me_4C_5H)_2Yb(OEt_2)$, the complex was dissolved in toluene and crystallized slowly at −40 °C [32] (Fig. 42).

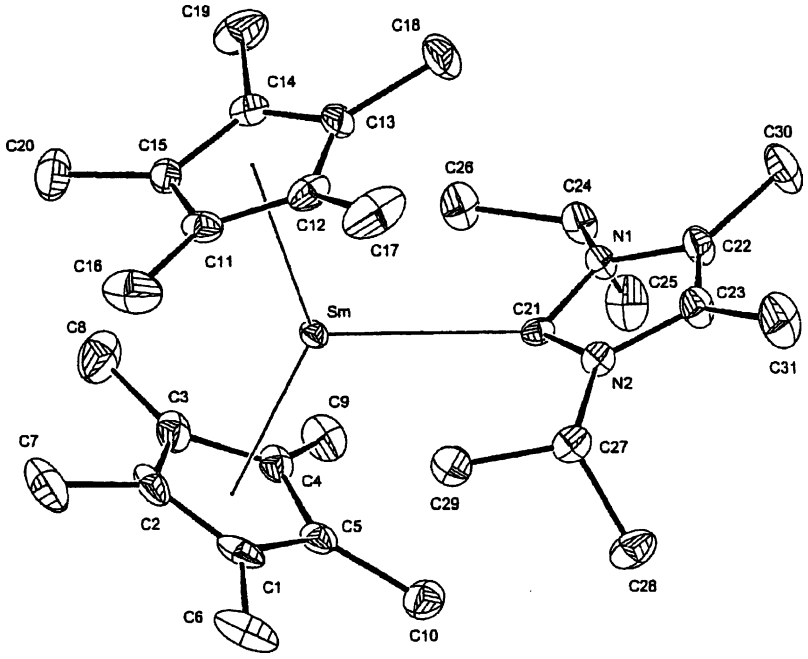

Fig. 38. ORTEP view of the complex $Cp^*_2Sm(^i$Pr-carben).

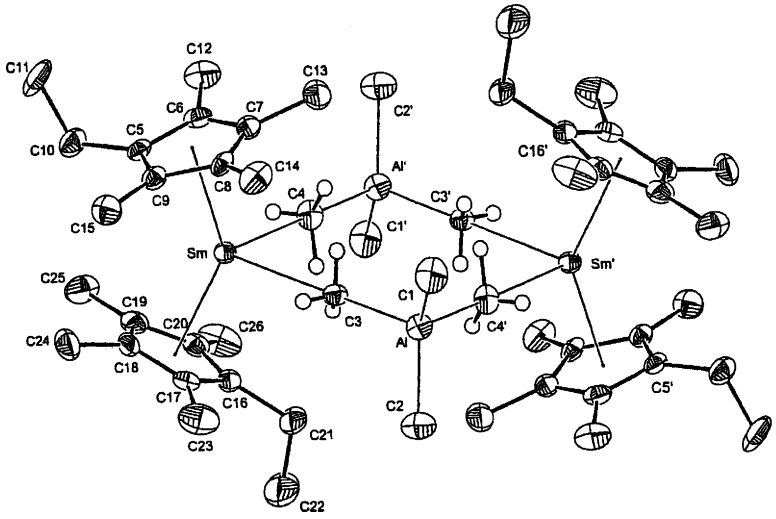

Fig. 39. ORTEP view of the heterometallic samarocene complex $[(C_5Me_4Et)_2Sm(\mu\text{-}Me)Al(Me)_3]_2$.

$$Cp'_2Yb(OEt_2) \xrightarrow[\text{reflux, vac}]{\text{toluene}} Cp'_2Yb \quad (Cp' = Me_5C_5,\ 1,3\text{-}(Me_3C)_2C_5H_3)$$

Scheme 33. Formation of the complexes Cp'_2Yb.

The structures of these base-free molecules have been determined by X-ray crystallography. The complexes exhibit bent structures in the solid state with centroid–metal–centroid angles ranging from 132° to 147°. Cp^*_2Yb forms complexes with *ortho*-, *meta*- and 1,2-dimethyl-*ortho*-carborane. The sterically and electronically unsaturated ytterbium center in this complex is expected to coordinate any molecule with a permanent dipole moment. The dipole moment of *ortho*-carborane is 4.31 Da. When *ortho*-carborane and Cp^*_2Yb are mixed in hexane, an immediate precipitation of a green solid is observed. The solid can be recrystallized from hot toluene to give dark green needles in good yield. This complex shows thermochroism: at lower temperatures the complex is green and turns reversibly orange at 130 °C (Fig. 43).

Carboranes with smaller dipole moments like *meta*-carborane and 2-dimethyl-*ortho*-carborane also form complexes with Cp^*_2Yb, which are more soluble and can be crystallized from hexane at −25 °C [32] (Fig. 44).

Shen and co-workers [33] published novel anionic lanthanocene amide complexes. Treatment of $(MeC_5H_4)_2LnCl$ with $NaNPh_2$ in THF afforded the supramolecular amide complexes $[Na(THF)_2(\mu\text{-}\eta^5\text{:}\eta^5\text{-}MeC_5H_4)_2Ln(NPh_2)_2]_n$ (Ln = Sm, Er). Both complexes have an alternating Cp–Ln–Cp–Na chain structure, and each lanthanide atom is coordinated by two η^5-MeC_5H_4 rings and two NPh_2

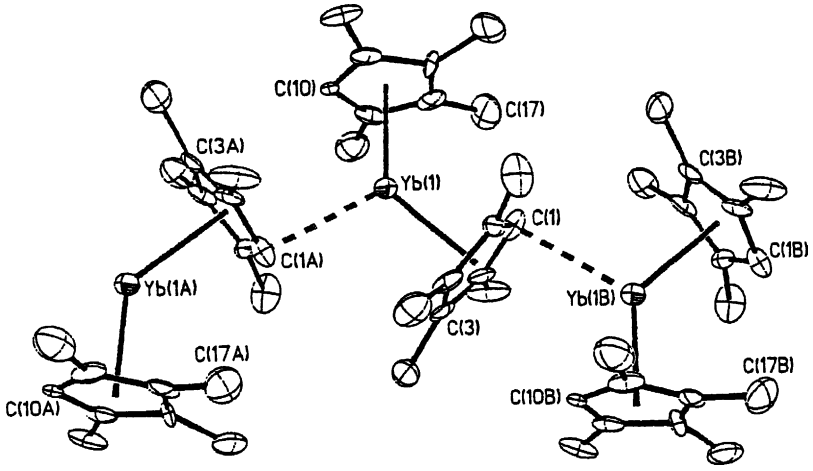

Fig. 40. ORTEP view of the base-free ytterbocene complex Cp^*_2Yb.

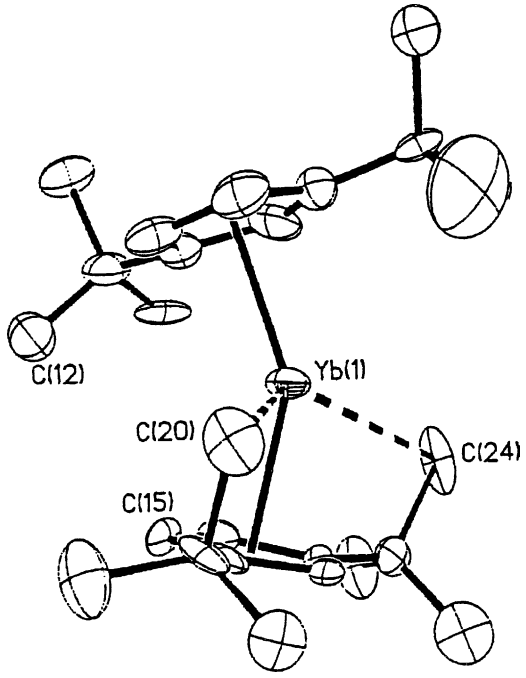

Fig. 41. ORTEP view of the base-free ytterbocene complex [1,3-$(Me_3C)_2C_5H_3]_2Yb$.

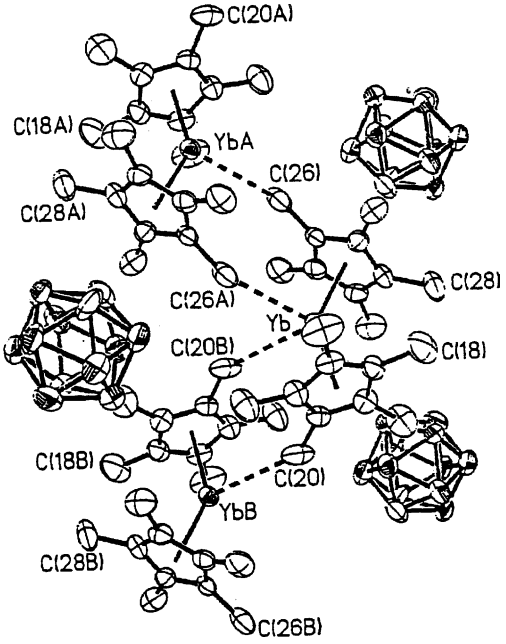

Fig. 43. ORTEP view of the complex $Cp^*_2Yb(o\text{-}H_2C_2B_{10}H_{10})$.

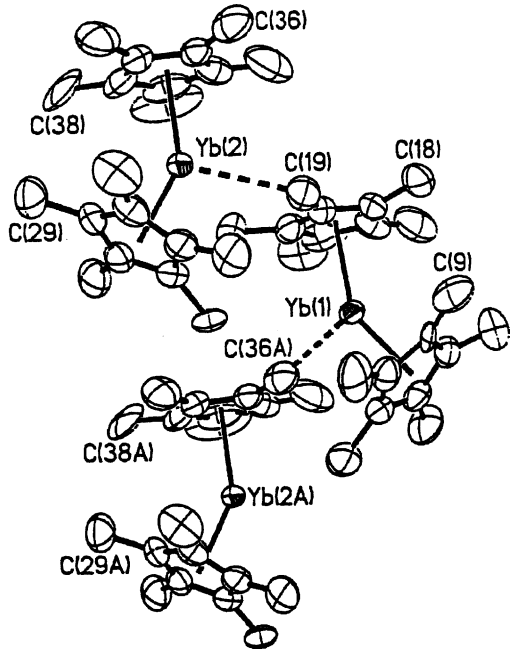

Fig. 42. ORTEP view of the base-free ytterbocene complex $(Me_4C_5H)_2Yb$.

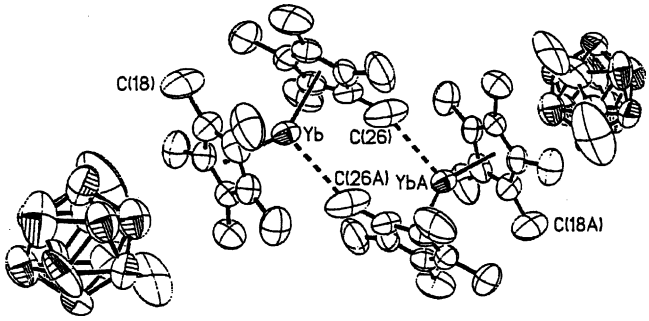

Fig. 44. ORTEP view of the complex $Cp^*_2Yb(o\text{-}Me_2C_2B_{10}H_{10})$.

ligands, while Na is coordinated by two η^5-MeC_5H_4 rings and two THF ligands without interacting with the amido ligands (Scheme 34 and Figs. 45–47).

Deacon et al. [34] investigated the solubility of bis-(cyclopentadienyl)samarium(II) in THF/ether mixtures. The result of their investigation is that bis(cyclopentadienyl)-samarium(II), also obtained from the reaction of samarium with Cp_2Hg, is not soluble in a THF:ether mixture. Deacon et al. [35] also synthesized the bis(cyclopentadienyl)-fluoroytterbium(III) complexes $[Cp_2YbF]_3$, $[(MeCp)_2YbF]_4$, $[Cp_2YbF(OPh_3)]_2$ and $[(MeCp)_2YbF(THF)]_4$. Oxidation of bis(cyclopentadienyl)ytterbium(II) with perfluoro(methylcyclohexane) or perfluorodecalin in DME gave unsolvated $[Cp_2YbF]_3$. The analogous reaction of bis(methylcyclopentdienyl)ytterbium(II) yielded unsolvated $[(MeCp)_2YbF]_4$, whereas in THF the fluorination reaction provides $[(MeCp)_2YbF(THF)]_4$ (Scheme 35).

Treatment of $(Cp)_2YbF(THF)$ with triphenylphosphane oxide gave $[Cp_2YbF(OPh_3)]_2$ (Scheme 36).

X-ray structure determinations of these cyclopentadienyl fluoro complexes showed that $[Cp_2YbF]_3$ is trimeric with formal eight coordination around ytterbium and a

planar $(YbF)_3$ ring, whereas $[(MeCp)_2YbF]_4$ is an eight-coordinated tetramer having a puckered $(YbF)_4$ ring with F–Yb–F angles of 90° and Yb–F–Yb angles close to 180°. Both $[(MeCp)_2Yb(THF)]_4$ and $[Cp_2YbF(OPPh_3)]_2$ are nine-coordinate fluoride-bridged dimers [35] (Figs. 48–50).

Sitzmann et al. [36] published the synthesis of metallocenes of samarium, europium and ytterbium with the especially bulky cyclopentadienyl ligands tetra(*iso*-propyl)cyclopentadienide, $C_5H(CHMe_2)_4^-$, tri(*tert*-butyl)-cyclopentadienide, $C_5H_2(CMe_3)_3^-$ and penta(*iso*-propyl)-cyclopentadienide, $C_5(CHMe_2)_5^-$. Octa(*iso*-propyl)metallocenes of the lanthanides Sm, Eu, Yb can easily be obtained

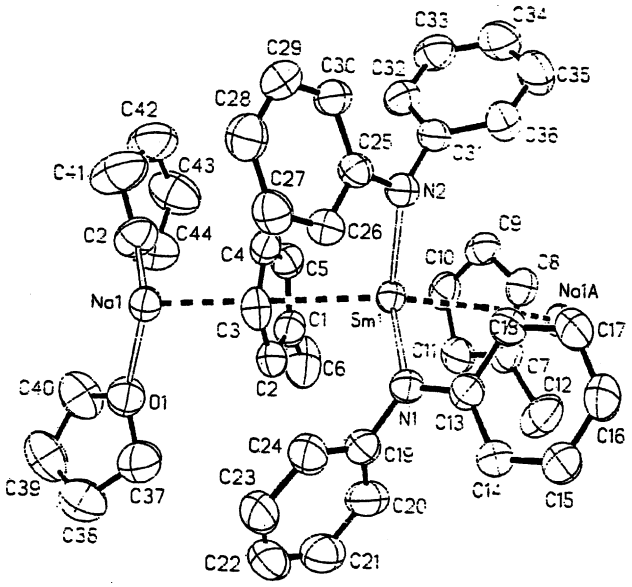

Fig. 45. ORTEP view of the molecular structure of $[Na(THF)_2(\mu\text{-}\eta^5{:}\eta^5\text{-}MeC_5H_4)_2Sm(NPh_2)_2]_n$.

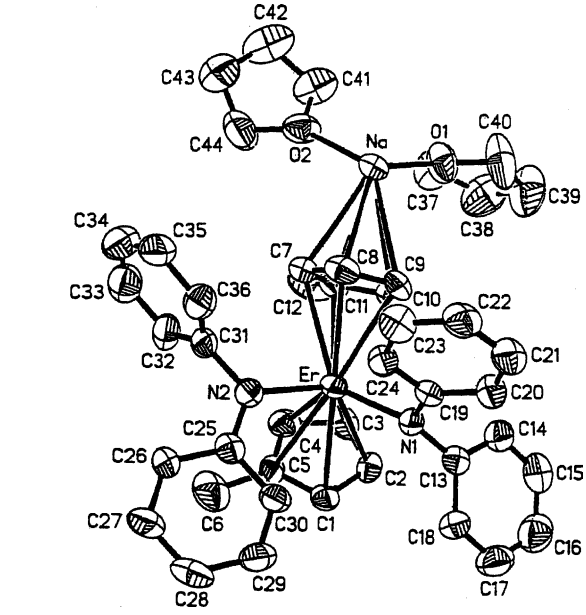

Fig. 46. ORTEP view of the molecular structure of $[Na(THF)_2(\mu\text{-}\eta^5{:}\eta^5\text{-}MeC_5H_4)_2Er(NPh_2)_2]_n$.

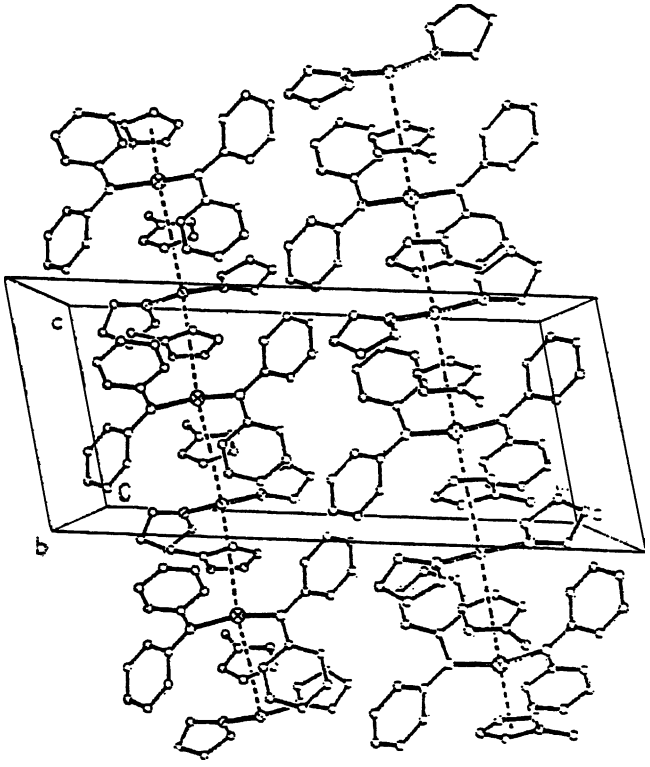

Fig. 47. Unit cell of $[Na(THF)_2(\mu\text{-}\eta^5{:}\eta^5\text{-}MeC_5H_4)_2Ln(NPh_2)_2]_n$ (Ln = Sm, Er).

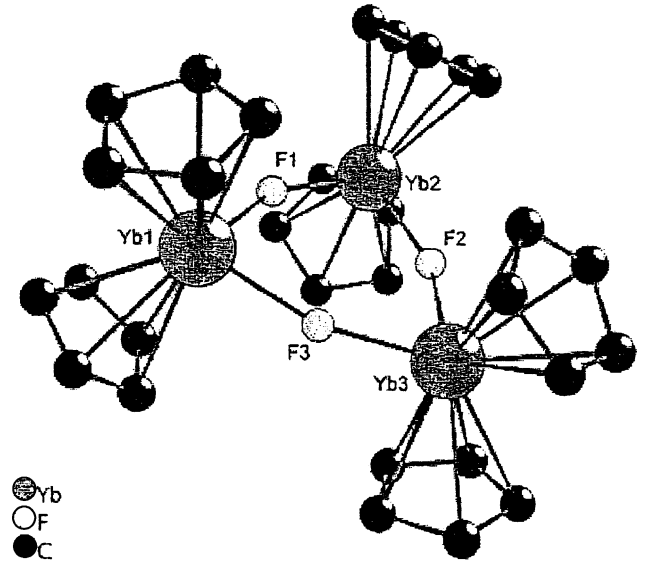

Fig. 48. The molecular structure of $[Cp_2YbF]_3$.

$$(MeC_5H_4)_2LnCl + 2\ NaNPh_2 \xrightarrow[-NaCl]{THF} (1/n)[Na(THF)_2(MeC_5H_4)_2Ln(NPh_2)_2]_n$$

Ln = Sm, Er

Scheme 34. Formation of supramolecular amide complexes of samarium and erbium.

$$3\ Cp_2Yb(DME) + C_{10}F_{18} \xrightarrow[DME]{} 3\ [Cp_2YbF]_3 + \text{unsaturated fluorocarbons}$$

$$4\ (MeCp)_2Yb((THF) + C_{10}F_{18} \longrightarrow 3\ [(MeCp)_2YbF]_3 + \text{unsaturated fluorocarbons}$$

Scheme 35. Formation of new bis(cyclopentadienyl)fluoroytterbium(III) complexes.

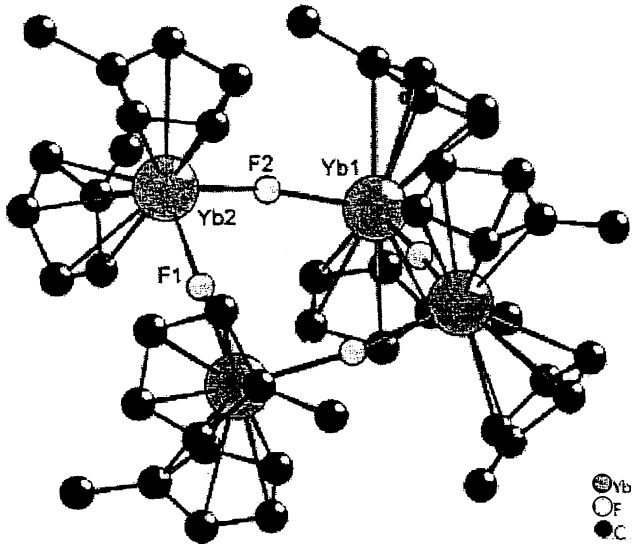

Fig. 49. The molecular structure of $[(MeCp)_2YbF]_4$.

$$3\ [Cp_2YbF(THF)]_2 + 2\ Ph_3PO \longrightarrow 3\ [Cp_2YbF(OPPh_3)]_2 + 2\ THF$$

Scheme 36. Formation of the complex $[Cp_2YbF(OPPh_3)]_2$.

from the diiodides of the corresponding rare-earth elements (Scheme 37 and Fig. 51).

The hexa(*tert*-butyl)metallocenes (Sm, Eu, Yb) show no tendency towards coordination of donor solvent molecules or alkali metal salts [36] (Scheme 38 and Fig. 52).

The deca(*iso*-propyl)metallocenes have been synthesized from the metal and the free penta(*iso*-propyl)cyclopentadienyl radical [36] (Scheme 39 and Fig. 53).

The three europocenes octa(*iso*-propyl)europocene, hexa(*tert*-butyl)europocene and deca(*iso*-propyl)europocene show fluorescence in daylight or under UV irradiation (336 nm).

The europocenes octa(*iso*-propyl)europocene and hexa(*tert*-butyl)europocene are bent sandwich complexes, whereas for the deca(*iso*-propyl)europocene axial symmetry with parallel five-membered rings has been found [36].

Qian and co-workers [37] synthesized monomeric lanthanocene aryloxide complexes of the type $Cp_2Ln(OC_{14}H_{13}NO)$ (Ln = Sm, Er, Dy, Y). The reaction of tris(cyclopentadienyl)lanthanides with the tridentate Schiff-base *N*-1-(*ortho*-methoxyphenyl)salicylideneamine in THF at room temperature afforded the monomeric lanthanocene Schiff-base complexes $Cp_2Ln(OC_{14}H_{13}NO)$ (Ln = Sm, Er, Dy, Y), which have been characterized by elemental analysis and mass spectra. The X-ray determination of the complex $Cp_2Sm(OC_{14}H_{13}NO)$ showed that the complex is monomeric and the metal center is coordinatively saturated by two cyclopentadienyl rings and two oxygens and one nitrogen from the Schiff-base ligand (Scheme 40 and Fig. 54).

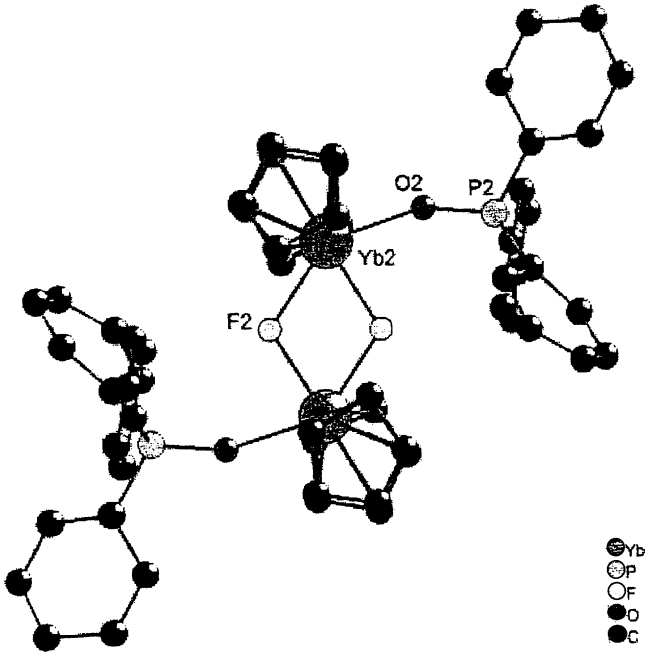

Fig. 50. The molecular structure of $[Cp_2YbF(OPPh_3)]_2$.

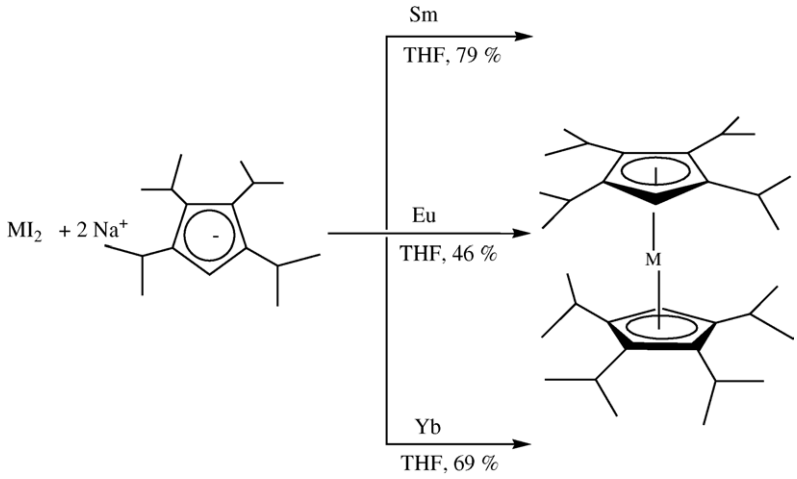

Scheme 37. Synthetic routes to octa(*iso*-propyl)metallocenes (Ln = Sm, Eu, Yb).

The average Sm–C bond distance is 2.723(7) Å, while those of the metal center to the Schiff-base oxygens and nitrogen atoms are 2.232(4), 2.572(4) and 2.534(4) Å, respectively [37].

Schumann et al. [38] investigated the synthesis of lanthanidocene complexes involving tridentate ligation of a tetrahydroborato ligand. Such lanthanidocene complexes play an important role in homogeneous catalysis. Treatment of samarium trichloride with *iso*-propyltetramethylcyclopentadienyl sodium in refluxing THF for 3 h followed by the addition of 1 equiv. of $NaBH_4$ and further refluxing for 3 h yielded the complex bis(η^5-*iso*-propyltetramethylcyclopentadienyl)samarium(III)(tetrahydroborato)(THF) (Scheme 41 and Fig. 55).

The complex shows a distorted tetrahedral arrangement around the central Sm(III) atom. It consists of two η^5-*iso*-propyltetramethylcyclopentadienyl ligands, one tetrahydroborato (BH_4^-) ligand and one coordinating THF molecule. The BH_4^- unit of the complex coordinates as a tridentate

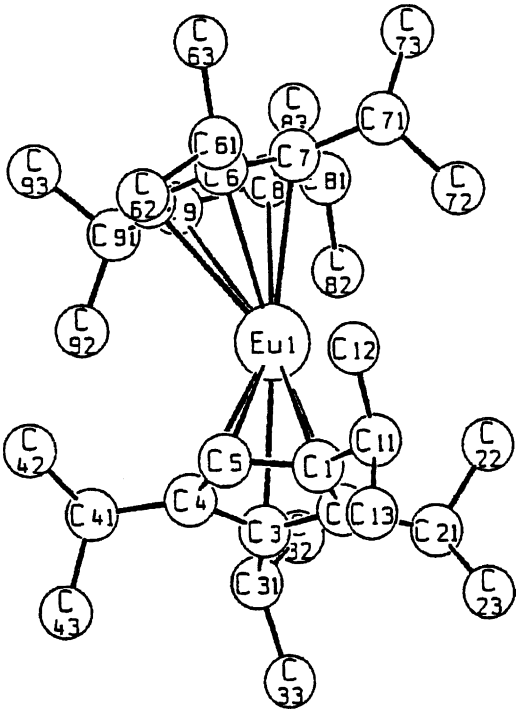

Fig. 51. Molecular structure of octa(*iso*-propyl)europocene.

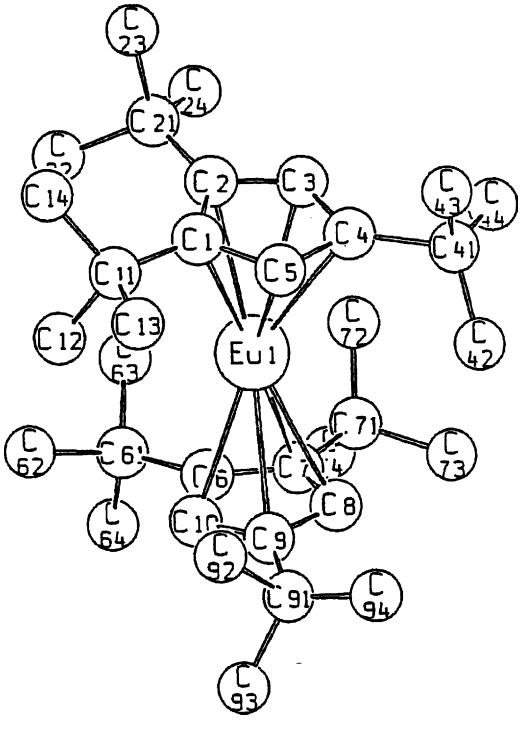

Fig. 52. Molecular structure of hexa(*tert*-butyl)europocene.

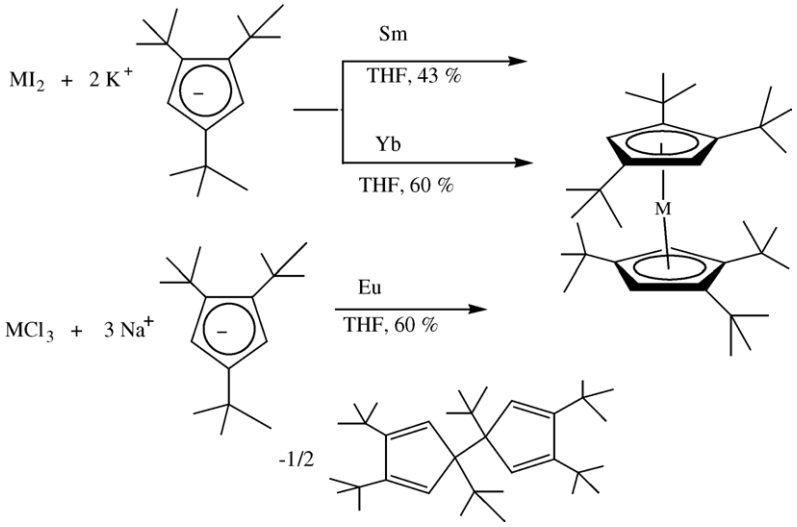

Scheme 38. Synthetic routes to hexa(*tert*-butyl)metallocenes (Ln = Sm, Eu, Yb).

ligand with three bridging H atoms and one terminal H atom. The η^5-*iso*-propyltetramethylcyclopentadienyl ligands in this bent-sandwich complex adopt a staggered conformation [38].

Pernin and Ibers [39] published the synthesis and properties of bis(cyclopentadienyl)imidodiphosphinochalcogenido lanthanides. The complexes $Cp_2Ln[N(QPPh_2)_2]$ (Ln = La, Gd, Er, Yb for Q = Se; Ln = Yb for Q = S) have been synthesized from the corresponding lanthanide tris(cyclopentadienyl) compounds and $H[N(QPPh_2)_2]$ (Scheme 42).

The structures of the complexes consist of a Cp_2Ln fragment, coordinated in an η^3-fashion by two chalcogen atoms and an N atom of the imidodiphosphinochalcogenido ligand $[N(QPPh_2)_2]^-$. In the complex $Cp_2Yb[N(SePPh_2)_2]$ the Cp_2Yb moiety is coordinated in η^2-fashion by two Se atoms of the $[N(SePPh_2)_2]^-$ ligand (Figs. 56 and 57).

Bochkarev and co-workers [40] investigated the reactions of some halides, cyclopentadienyl dichlorides and bis(cyclopentadienyl) chlorides of lanthanides with alkali metal adducts of *trans*-stilbene, $M^+[PhCHCHPh]^-$ (M = Li, Na). The reaction of $SmI_2(THF)_2$ with metallic lithium and *trans*-stilbene in a 1:2.2 molar ratio in DME gave a stilbene complex of divalent samarium, $(PhCHCHPh)Sm(DME)_2$. This complex subsequently reacts with hydrogen in THF to give $SmH_2(THF)_2$ and 1,2-diphenylethane (Scheme 43).

The complex $(PhCHCHPh)Sm(DME)_2$ was found to be an efficient catalyst in the block polymerization of styrene; however, it is inert towards propylene. This stilbene complex of divalent samarium, $(PhCHCHPh)Sm(DME)_2$, reacts with hexamethyldisilazane in DME to give the divalent samarium amide $[(Me_3Si)_2N]_2Sm(DME)_2$ and 1,2-diphenylethane [40] (Scheme 44).

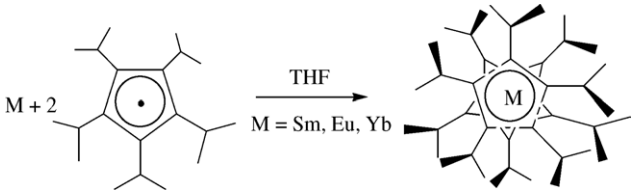

Scheme 39. Synthetic routes to deca(*iso*-propyl)metallocenes (Ln = Sm, Eu, Yb).

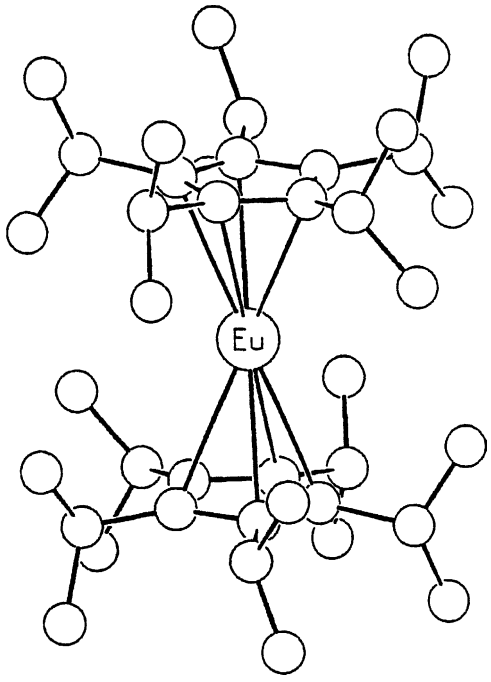

Fig. 53. Molecular structure of deca(*iso*-propyl)europocene.

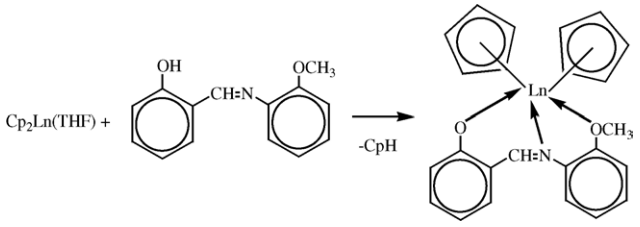

Scheme 40. Preparation of monomeric lanthanocene Schiff-base complexes $Cp_2Ln(OC_{14}H_{13}NO)$ (Ln = Sm, Er, Dy, Y).

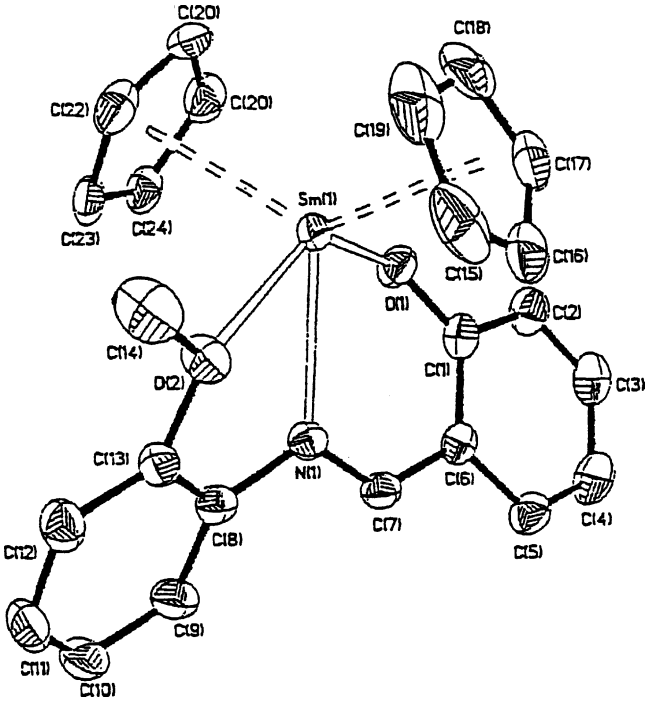

Fig. 54. ORTEP view of the molecular complex of $Cp_2Sm(OC_{14}H_{13}NO)$.

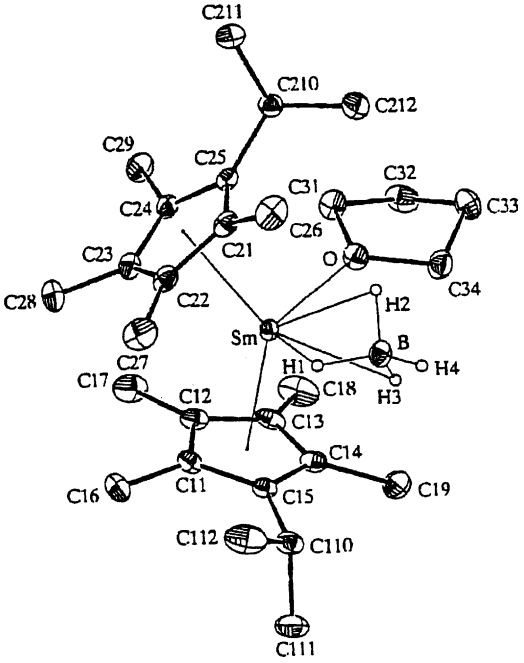

Fig. 55. ORTEP view of the complex bis(η^5-*iso*-propyltetramethylcyclopentadienyl)samarium(III)(tetrahydroborato)(THF).

$$Cp_3Ln + HN(QPPh_2)_2 \longrightarrow Cp_2Ln[N(QPPh_2)_2] + CpH$$

Ln = La, Gd, Er, Yb; Q = Se
Ln = Yb Q = S

Scheme 42. Synthesis of the complexes $Cp_2Ln[N(QPPh_2)_2]$ (Ln = La, Gd, Er, Yb; Q = S, Se).

The binuclear complexes $(Cp^*_2Sm)_2(\mu\text{-}\eta^2\text{:}\eta^4\text{-PhCHCHPh})$ and $(Cp^*_2Sm)_2(\mu\text{-}\eta^2\text{:}\eta^4\text{-PhCHCH}_2)$ were prepared by the reaction of Cp^*_2Sm with *cis*-stilbene and styrene, respectively. The reactions of $LaCl_3$, LaI_3, $NdCl_3$, NdI_3 and $LuCl_3$ with 3 equiv. of $M^+[PhCHCHPh]^-$ (M = Li, Na) in THF or DME resulted in the formation of dark-colored solutions and in the precipitation of NaCl, but the isolation of pure Ln(III) stilbene derivatives was not possible. In contrast, the reaction of $CpLuCl_2(THF)_3$ with $Na^+[PhCHCHPh]^-$ in a molar ratio of 1:2 in DME gave an *ate* complex in 47% yield [40] (Scheme 45).

Evans et al. [41] studied the reactions of $Cp^*_2Sm(THF)_2$ and Cp^*_2Sm with $Al(CH_2CHMe_2)_3$. The reactions afforded several products including the *iso*-butyl-bridged Sm–Al heterobimetallic species $Cp^*_2Sm[(\mu\text{-}CH_2CHMe_2)_2\text{-}Al(CH_2CHMe_2)_2]$. In contrast, no reaction was observed between $Al(CMe_3)_3$ and Cp^*_2Sm, but $Cp^*_2Sm(THF)_2$ reacted to lose THF under formation of $Al(CMe_3)_3(THF)$ and Cp^*_2Sm.

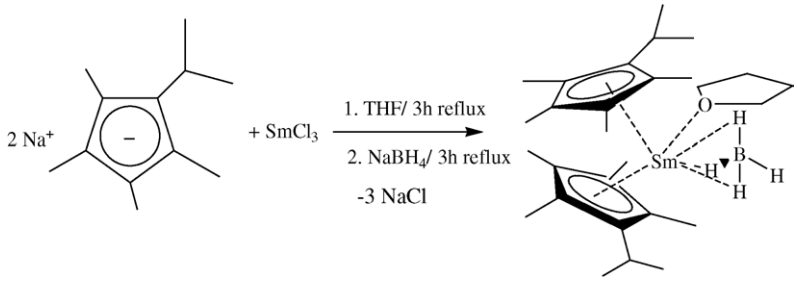

Scheme 41. Synthesis of the complex bis(η^5-*iso*-propyltetramethylcyclopentadienyl)samarium(III)(tetrahydroborato)(THF).

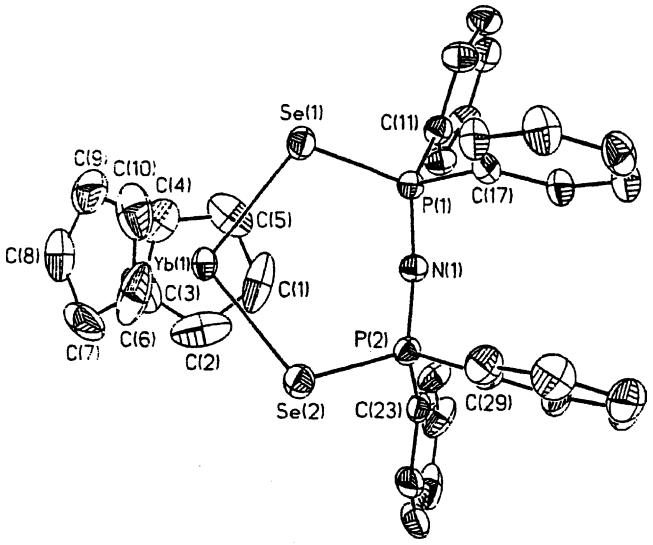

Fig. 56. ORTEP view of the complex $Cp_2Yb[\eta^2\text{-}N(SePPh_2)]_2$.

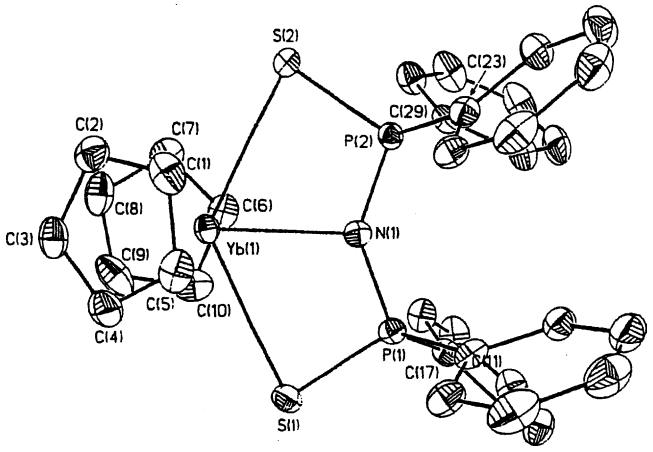

Fig. 57. ORTEP view of the complex $Cp_2Yb[\eta^2\text{-}N(SPPh_2)]_2$.

$$SmI_2(THF)_2 + 2\,Li + 2\,trans\text{-}PhCH{=}CHPh \xrightarrow[-2\,LiI]{DME} (PhCHCHPh)Sm(DME)_2$$

$$(PhCHCHPh)Sm(DME)_2 + H_2 \xrightarrow{THF} SmH_2(THF)_2 + PhCH_2CH_2Ph$$

Scheme 43. Reaction of samarium diiodide with metallic lithium and *trans*-stilbene, followed by the reaction with hydrogen.

$$(PhCHCHPh)Sm(DME)_2 + 2\,(Me_3Si)_2NH \xrightarrow[-H_2]{DME} [(Me_3Si)_2N]_2Sm(DME)_2 + PhCH_2CH_2Ph$$

Scheme 44. Formation of the samarium(II) amide $[(Me_3Si)_2N]_2$-$Sm(DME)_2$.

$$CpLuCl_2(THF)_3 + 2\,Na[PhCHCHPh] \xrightarrow[-2\,NaCl]{DME}$$

$$\{CpLu[\mu\text{-}CH(Ph)CH(Ph)CH(Ph)CH(Ph)]\}Na(DME)_3$$

Scheme 45. Reaction of $CpLuCl_2(THF)_3$ with $Na^+[PhCHCHPh]^-$.

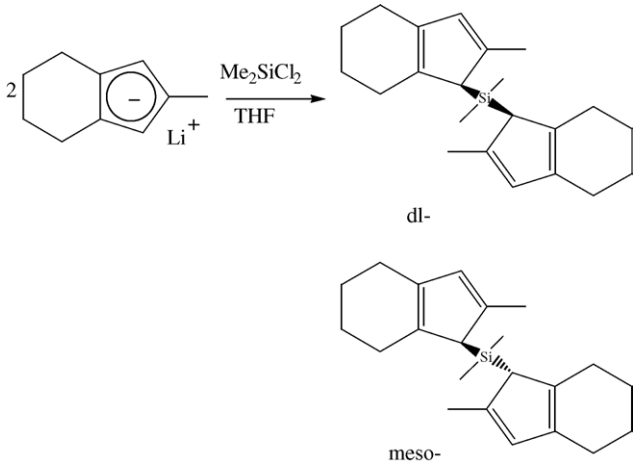

Scheme 46. Synthesis of the annelated trisubstituted cyclopentadiene ligands.

2.2.3. *ansa*-Cyclopentadienyl complexes

Haltermann et al. [42] published the three-step synthesis of 2-methyl-4,5,6,7-tetrahydro-1*H*-indene. This annelated trisubstituted cyclopentadiene was bridged selectively to form ethylene- or dimethylsilyl-bridged bis(2-methyl-4,5,6,7-tetrahydro-1*H*-inden-1-yl) ligands (Scheme 46).

YCl_3 and $LuCl_3$ reacted with the ligand bis(2-methyl-4,5,6,7-tetrahydroinden-1-yl)dimethylsilane after lithiation to form *meso*/*dl* stereoisomeric mixtures [42] (Scheme 47).

Qian et al. [43] synthesized a series of new silylene-bridged fluorenyl cyclopentadienyl *ansa*-lanthanocene chlorides with C_s-symmetry, $[R_2Si(Flu)(R'(Cp))Ln(\mu\text{-}Cl)]_2$ ($Flu = C_{13}H_8$, $Cp = C_5H_3$) (R = Me, R′ = H, Ln = Y, Lu, Dy, Er) and R = Ph, R′ = ^{t}Bu, Ln = Dy. The complexes were synthesized by the reaction of anhydrous lanthanide chlorides with the dilithium salt of the ligand $Me_2Si(FluH)(CpH)$. The complexes were characterized by X-ray diffraction studies (Scheme 48 and Figs. 58 and 59).

Treatment of the resulting chlorides with $ME(SiMe_3)_2$ (M = Li or K, E = N, CH) gave the amide and hydrocarbyl derivatives $Me_2Si(Flu)(Cp)LnE(SiMe_3)_2$ (E = N, Ln = Dy, Er; E = CH, Ln = Dy) (Scheme 48). All these amide and hydrocarbyl complexes show chelating structures and exhibit an intramolecular γ-agostic Ln–Me–Si interaction. These complexes are active in the polymerization of methyl methacrylate (Section 2.6) [43] (Figs. 60 and 61).

Anwander and co-workers [44] published the synthesis of C_2-symmetric *ansa*-lanthanidocene amides via silylamine elimination. According to Scheme 49, reaction with the bis(dimethylsilyl)amide precursors gave the corresponding *ansa*-lanthanidocene amides complexes (Figs. 62–64).

Hou et al. [45] published the synthesis and polymerization reaction of a series of Cp^*/ER-ligated lanthanide(II) complexes (ER = OAr, SAr, NR^1R^2). Reactions of $Cp^*_2Sm(THF)_2$ with 1 equiv. of KER in THF gave the Sm(II) complexes $[Cp^*Sm(THF)_m(ER)(Cp^*)K(THF)_n]_\infty$ ($m = 0$ or 1; $n = 1$ or 2; ER = $OC_6H_2{}^tBu_2$-2,6-Me-4, $OC_6H_3{}^tPr_2$-2,6, $SC_6H_2{}^tPr_3$-

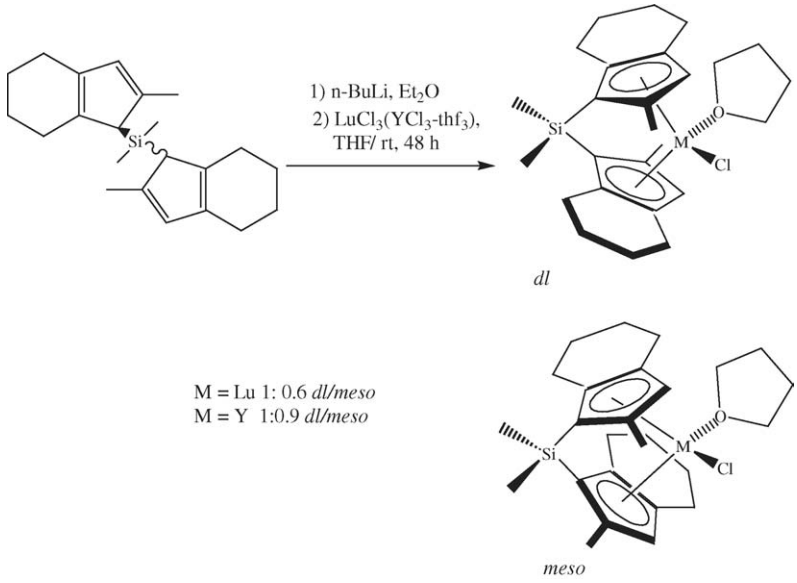

Scheme 47. Formation of the *dl*/*meso* stereoisomeric complexes in dependence of the central metals M = Y, Lu.

2,4,6, $NHC_6H_2{}^tBu_2$-2,4,6, or $N(SiMe_3)_2$) in high yields. This type of heteroleptic samarium(II) complexes acts as a unique catalytic system, which cannot only polymerize styrene and ethylene, but also copolymerize these monomers to block styrene–ethylene copolymers. The results of the polymerization reactions are presented in Section 2.7 (Schemes 50 and 51 and Fig. 65).

The similar reaction of $Cp^*_2Yb(THF)_2$ with 1 equiv. of $KN(SiMe_3)_2$ yielded the corresponding Yb(II) complex $[Cp^*Yb(N(SiMe_3)_2)(Cp^*)K(THF)_2]_\infty$. The reaction of the dimethylsilyl-bridged bis(tetramethylcyclopentadienyl) samarium(II) complex $Me_2Si(C_5Me_4)_2Sm(THF)_2$ with 1 equiv. of KOAr in THF gave $[Me_2Si(C_5Me_4)(\mu\text{-}C_5Me_4)K(THF)_nSm(OAr)]_\infty$, which can be viewed as

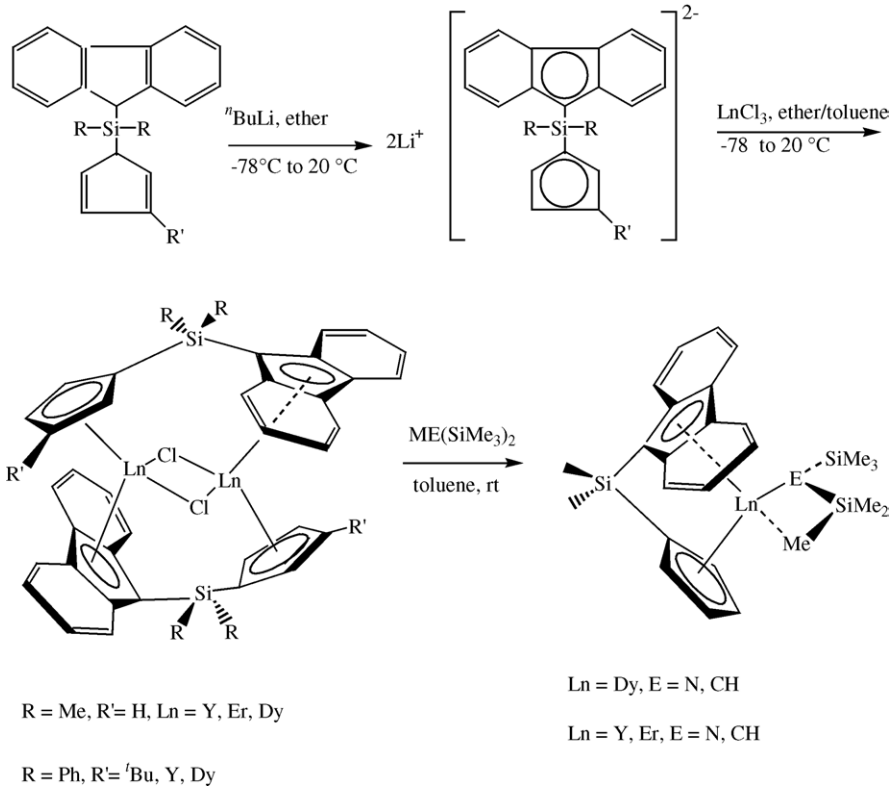

Scheme 48. Synthetic routes to C_s-symmetric *ansa*-organolanthanocene chlorides.

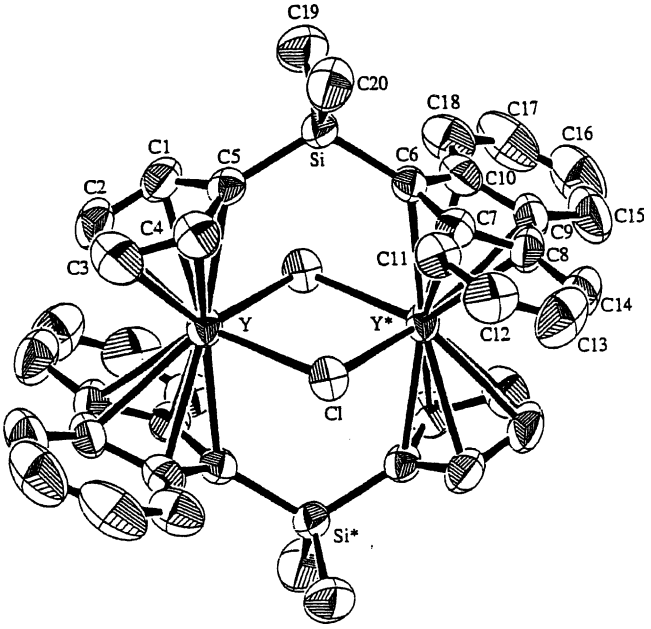

Fig. 58. ORTEP view of the complex $[Me_2Si(C_{13}H_8)(C_5H_4)Y(\mu\text{-}Cl)]_2 \cdot (1/2)$toluene.

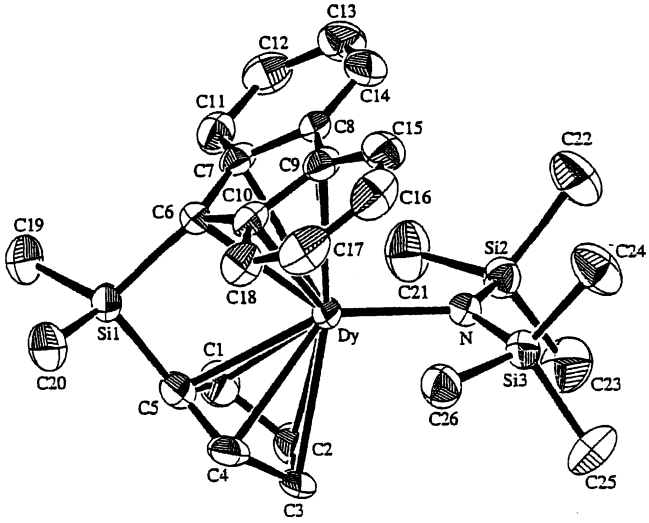

Fig. 60. ORTEP view of the complex $[Me_2Si(C_{13}H_8)(C_5H_4)]DyN(TMS)_2$.

a C_5Me_4/OAr-ligated Sm(II) species coordinated by the dimethylsilyl-bridged, neutral "C_5Me_4K" ligand [45] (Scheme 52 and Fig. 66).

The use of $NaN(SiMe_3)_2$ instead of $KN(SiMe_3)_2$ in the reaction with $Cp^*_2Ln(THF)_2$ afforded the "$Cp^*Na(THF)_3$"-coordinated Sm(II) and Yb(II) complexes. In contrast to the "Cp^*K"-coordinated complexes, which adopt a polymeric structure through intermolecular $K\cdots Cp^*$ interactions, the "Cp^*Na"-coordinated complexes are monomers owing to the

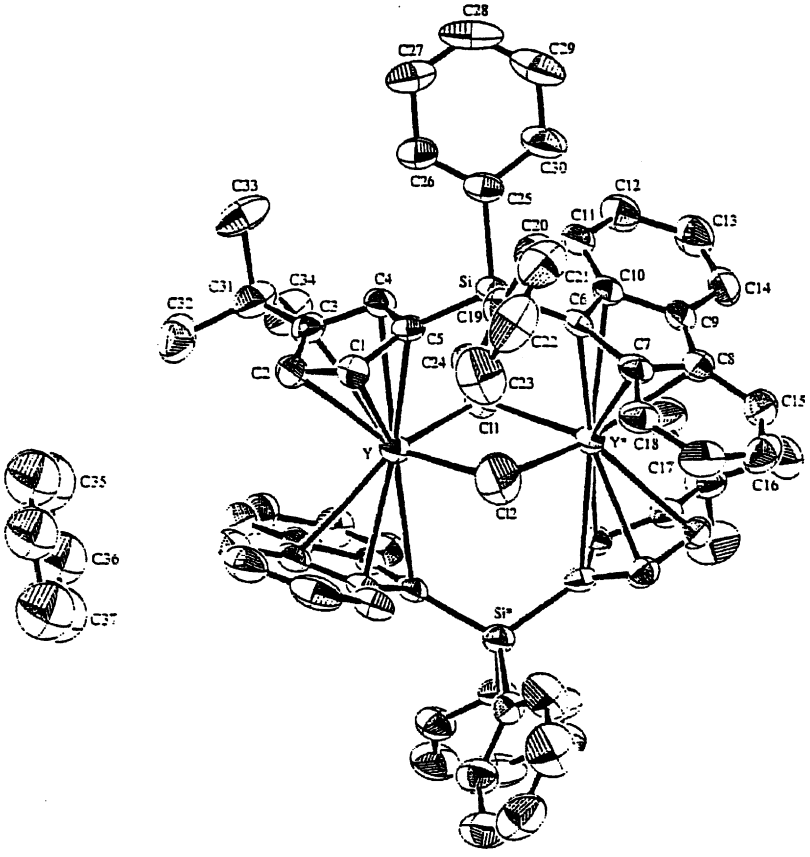

Fig. 59. ORTEP view of the complex $[Ph_2Si(C_{13}H_8)(^tBuC_5H_4)Y(\mu\text{-}Cl)]_2 \cdot (1/2)$toluene.

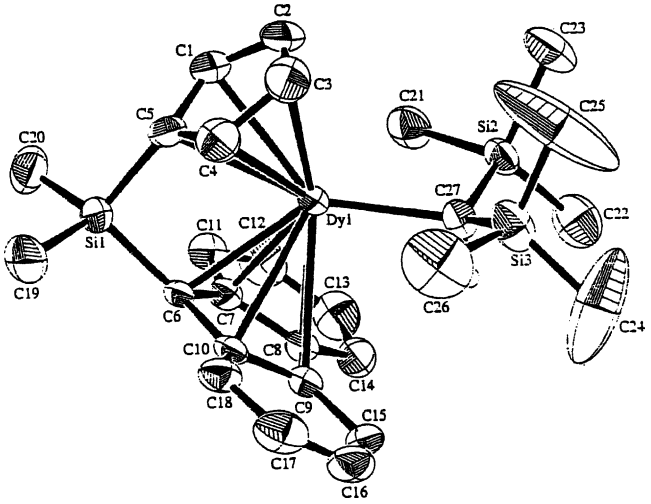

Fig. 61. ORTEP view of the complex $[Me_2Si(C_{13}H_8)(C_5H_4)]DyCH(TMS)_2$.

coordination of THF to the sodium ion [45] (Scheme 53 and Fig. 67).

2.2.4. Tris(cyclopentadienyl) complexes

Lappert and co-workers [46] investigated non-classical organolanthanide chemistry. They treated Cp^t_3Ln or Cp''_3Ln ($Cp^t = \eta^5$-$C_5H_4SiMe_2{}^tBu$, $Cp'' = \eta^5$-$C_5H_3(SiMe_3)_2$-1,3, Ln = La, Ce) with potassium and [18]-crown-6 in toluene and obtained the potassium salts $[K([18]\text{-crown-6})(\eta^2\text{-PhMe})_2][(Cp^t_3Ln)_2(\mu\text{-H})]$ and $[K([18]\text{-crown-6})(\eta^2\text{-PhMe})_2][(Cp''_2Ln)_2(\mu\text{-}\eta^6\text{:}\eta^6\text{-PhMe})]$ (Scheme 54 and Fig. 68).

Herrmann and co-workers [47] investigated the theoretical evidence for a symmetric Ln···(Si–H)β-diagostic interaction in *ansa*-lanthanidocene complexes. Density functional calculations on *ansa*-bridged rare-earth disilylamide

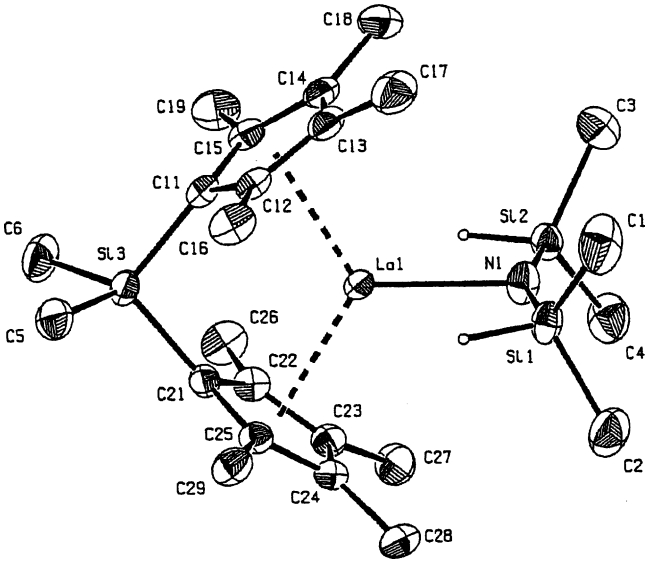

Fig. 62. PLATON plot of $[Me_2Si(Cp'')_2]La[N(SiHMe_2)_2]$.

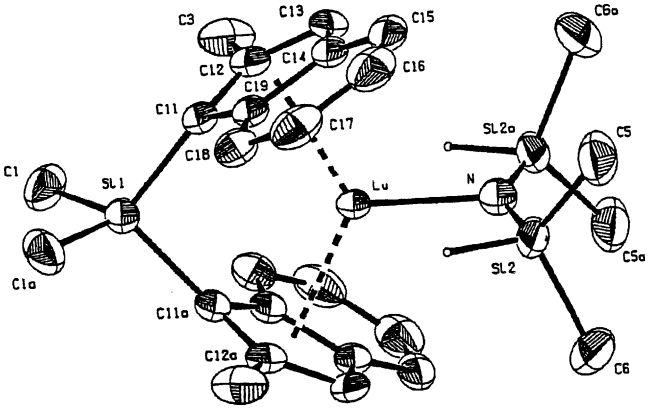

Fig. 63. PLATON plot of $[Me_2Si(2\text{-Me-}C_9H_5)_2]Lu[N(SiHMe_2)_2]$.

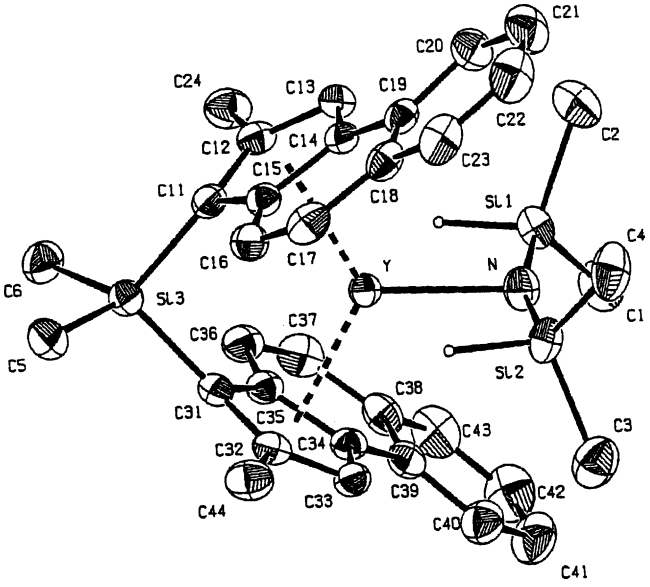

Fig. 64. PLATON plot of $[Me_2Si(2\text{-Me-}4,5\text{-Benz-Ind})_2]Y[N(SiHMe_2)_2]$.

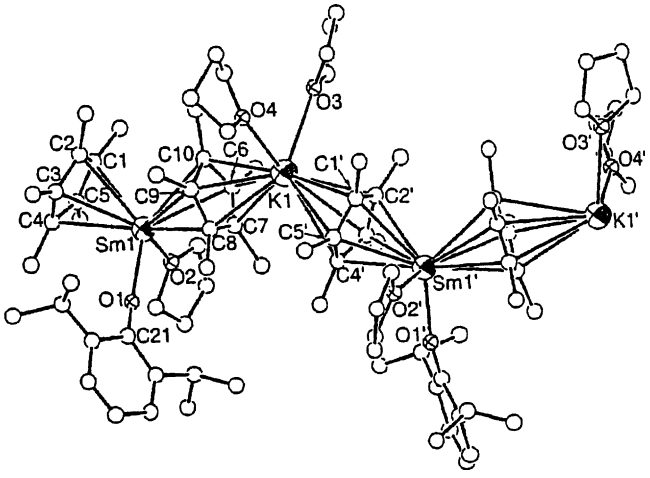

Fig. 65. ORTEP view of the complex $[Cp^*Sm(THF)(SC_6H_2{}^iPr_3\text{-}2,4,6)(Cp^*)K(THF)]_\infty$.

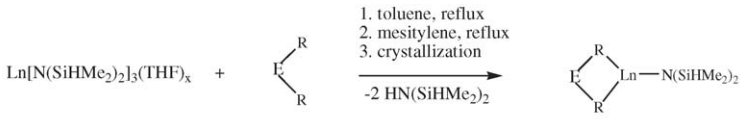

R	E	Ligand precursor	Ln(yield)
	Me_2Si	$Me_2Si(Cp''H)_2$	Y (82 %) La (96 %)
	Me_2C	$Me_2C(IndH)_2$	*rac*-Y (14 %)
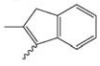	Me_2Si	$Me_2Si(2\text{-Me-IndH})_2$	*rac*-Sc (20 %) *rac*-Y (52 %) *rac*-La (49 %) *rac*-Nd (44 %) *rac*-Lu (32 %)
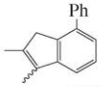	Me_2Si	$Me_2Si(2\text{-Me-4-Ph-IndH})_2$	Y (11 %)[a] *rac*-La (13 %)
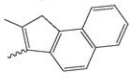	Me_2Si	$Me_2Si(2\text{-Me-4,5-Benz-IndH})_2$	*rac*-Y (72 %) *rac*-La (47 %) *rac*-Lu (54 %)
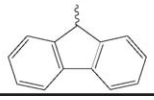	Me_2Si	$Me_2Si(FluH)_2$	Y (7 %)

Scheme 49. Synthesis of C_2-symmetric *ansa*-lanthanidocene amide complexes according to the extended silylamide route.

complexes confirm the presence of a new type of symmetric Ln···(Si–H)β-diagostic interaction. The interaction turns out to be dominated by electrostatic effects, and the presence of vacant f-orbitals appears to be of minor importance for the bonding in this case. It was shown that only central metals of sufficient size allow a diagostic coordination mode owing to steric hindrance.

Amberger and co-workers [48] further investigated the electronic structure of organo f-element complexes. The absorption spectrum of $Cp_3Er{\cdot}CNC_6H_{11}$ has been measured at room temperature. From the spectra, a truncated crystal field (CF) splitting pattern was derived and simulated by fitting the parameters of an empirical Hamiltonian. For 46 assignments, a reduced r.m.s. deviation of 31 cm^{-1} was achieved. On the basis of the wavefunction of the CF ground state from these calculations, the 2.5 K EPR spectrum of magnetically diluted $Cp_3Er{\cdot}CNC_6H_{11}$ could be explained. Using the calculated wavefunctions and eigenvalues, the experimentally determined dependence of μ^2_{eff} of powdered $Cp_3Er{\cdot}CNC_6H_{11}$ could be reproduced by adopting an orbital reduction factor $k = 0.985$.

2.2.5. Complexes with cyclopentadienyl and cyclooctatetraenyl ligands

Qian and co-workers [49] synthesized mixed lanthanide sandwich complexes with cyclooctatetraenyl and cyclopentadienyl ligands containing a chelating ether side chain. $LnCl_3$ reacted with $K_2C_8H_8$ in THF in the ratio 1:1 at room temperature and formed (COT)LnCl·*n*THF, which was then treated with RCpK in THF (RCp = $MeOCH_2CH_2C_5H_4$ or $C_4H_7OCH_2CH_2C_5H_4$) to yield the complexes (RCp)Ln(COT)(THF) (Ln = Nd,

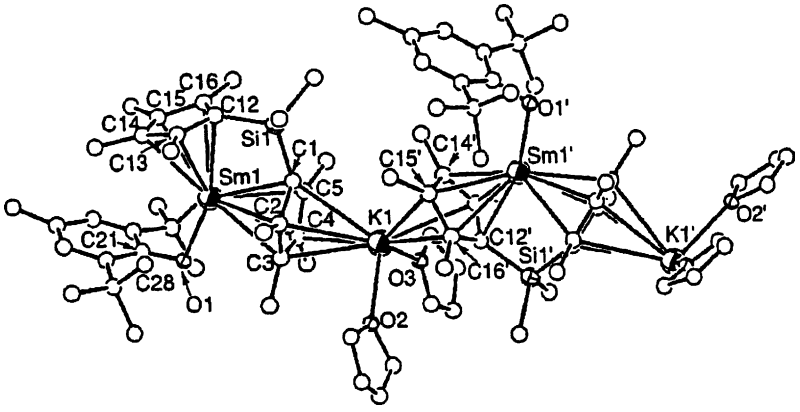

Fig. 66. ORTEP plot of $[Me_2Si(C_5Me_4)(\mu\text{-}C_5Me_4)K(THF)_nSm(OAr)]_\infty$.

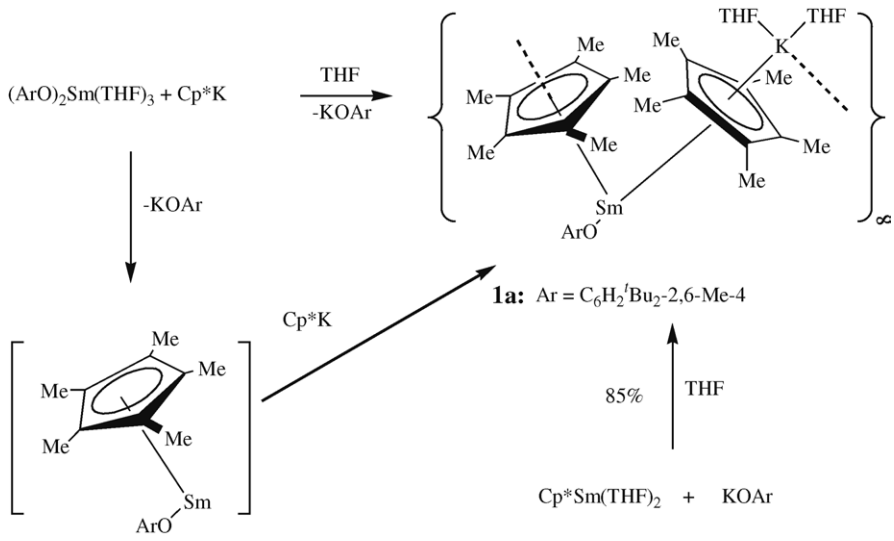

Scheme 50. Synthesis of samarium(II) complex with mixed Cp^*/ER ligands.

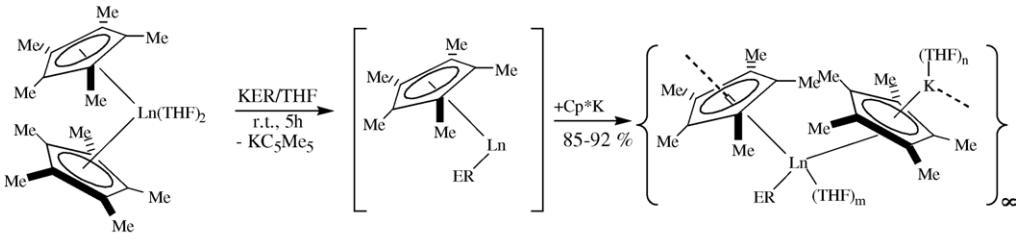

Ln = Sm, ER = $OC_6H_2{}^tBu_2$-2,6-Me-4; m = 0; n = 2
Ln = Sm, ER = $OC_6H_3{}^iPr_2$-2,6; m = 1; n = 2
Ln = Sm, ER = $OC_6H_3{}^iPr_2$-2,6; m = 0; n = 1
Ln = Sm, ER = $SC_6H_2{}^iPr_3$-2,4,6; m = 1; n = 1
Ln = Sm, ER = $SC_6H_2{}^iPr_3$-2,4,6; m = 0; n = 1
Ln = Sm, ER = $NHC_6H_2{}^tBu_3$-2,4,6; m = 0; n= 2
Ln = Sm, ER = $N(SiMe_3)_2$; m = 0; n = 2
Ln = Yb; ER = $N(SiMe_3)_2$; m = 0; n= 2

Scheme 51. Synthesis of the Cp^*/ER-ligated lanthanide(II) complexes with the neutral "Cp^*K" ligand.

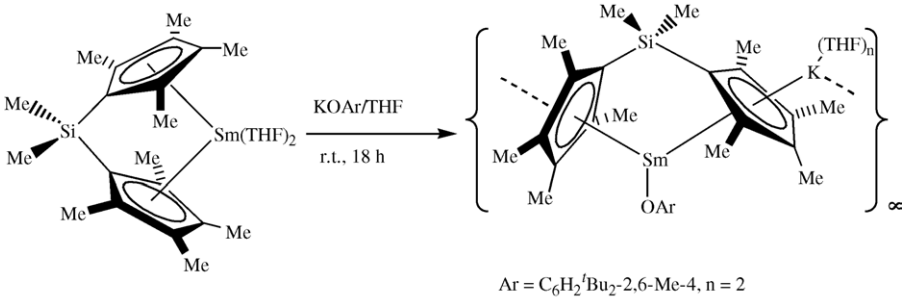

Ar = $C_6H_2{}^tBu_2$-2,6-Me-4, n = 2
or
Ar = $C_6H_3{}^tBu_2$-2,6, n = 1

Scheme 52. Synthesis of $[Me_2Si(C_5Me_4)(\mu\text{-}C_5Me_4)K(THF)_nSm(OAr)]_\infty$.

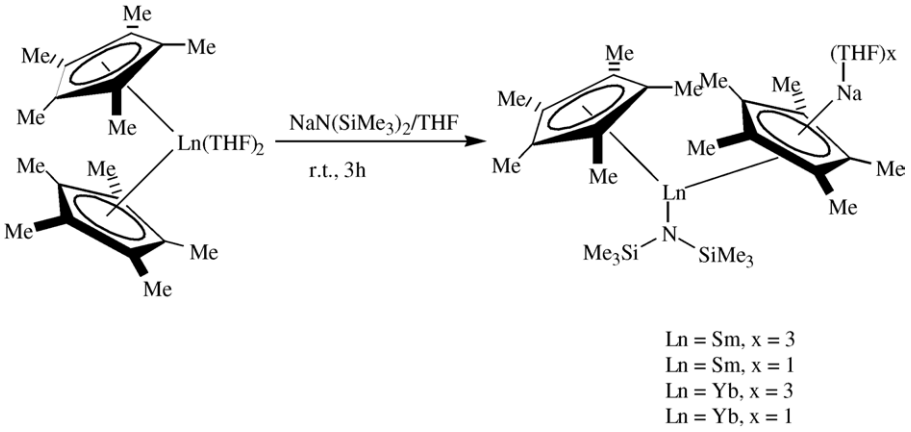

Scheme 53. Formation of the monomeric lanthanide complexes $Cp^*Na(THF)_xCp^*LnN(SiMe_3)_2$ (Ln = Sm, Yb).

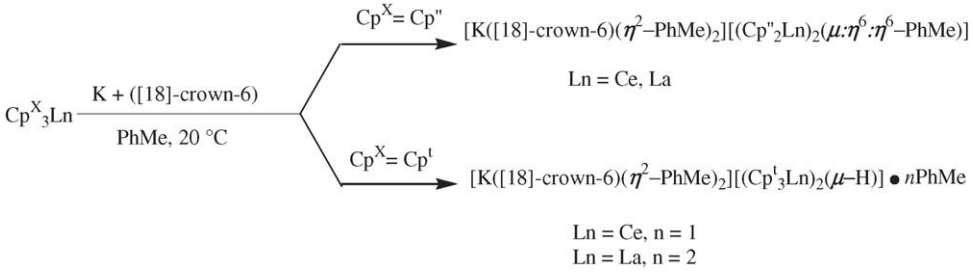

Scheme 54. Synthetic routes to the complexes $[K([18]\text{-crown-6})(\eta^2\text{-PhMe})_2][(Cp^t_3Ln)_2(\mu\text{-H})]$ and $[K([18]\text{-crown-6})(\eta^2\text{-PhMe})_2][(Cp''_2Ln)_2(\mu\text{-}\eta^6\text{:}\eta^6\text{-PhMe})]$.

Sm, RCp = $MeOCH_2CH_2C_5H_4$; Ln = La, Nd, Sm, RCp = $C_4H_7OCH_2CH_2C_5H_4$) (Schemes 55 and 56).

The crystal structures of the complexes (η^5-$MeOCH_2CH_2C_5H_4$)Nd(COT)(THF) and (η^5-$C_4H_7OCH_2$-C_5H_4)La(COT)(THF) were determinated by X-ray diffraction and revealed that the oxygen atom of the ether group on the cyclopentadienyl ring is coordinated to the central metal atom [49] (Fig. 69).

The average bond lengths Nd–C(η^8) and Nd–C(η^5) are 2.697(2) and 2.749(2) Å, respectively, while the Nd–O(THF) and Nd–O(η^1) distances are 2.580(1) and 2.619(1) Å, respectively [49] (Fig. 70).

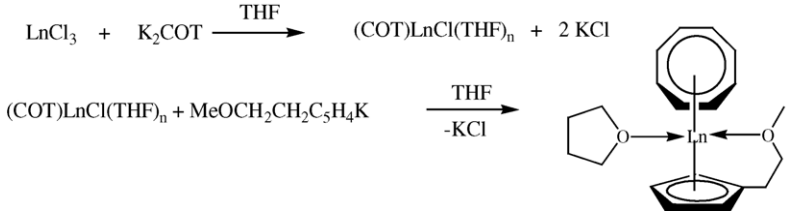

Scheme 55. Formation of the complexes (RCp)Ln(COT)(THF) (Ln = Nd, Sm, RCp = $MeOCH_2CH_2C_5H_4$).

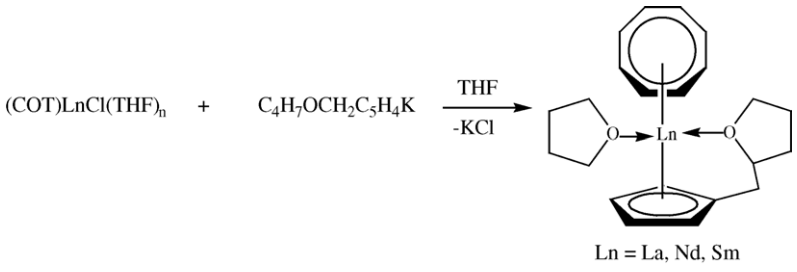

Scheme 56. Formation of the complexes (RCp)Ln(COT)(THF) (Ln = La, Nd, Sm, RCp = $C_4H_7OCH_2CH_2C_5H_4$).

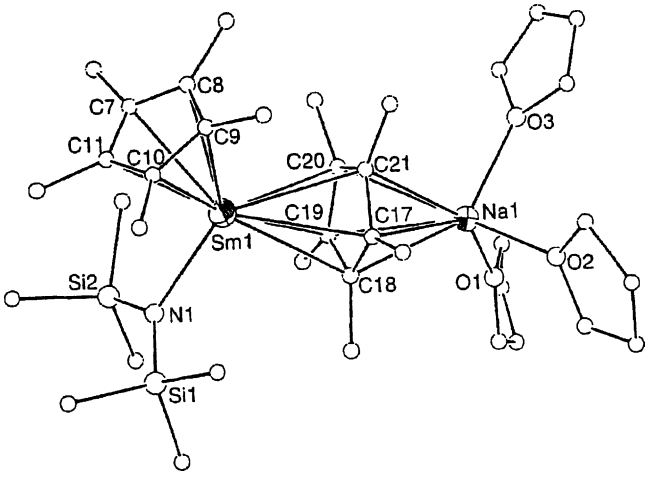

Fig. 67. ORTEP plot of the monomeric samarium complex $Cp^*Na(THF)_x$ $Cp^*SmN(SiMe_3)_2$.

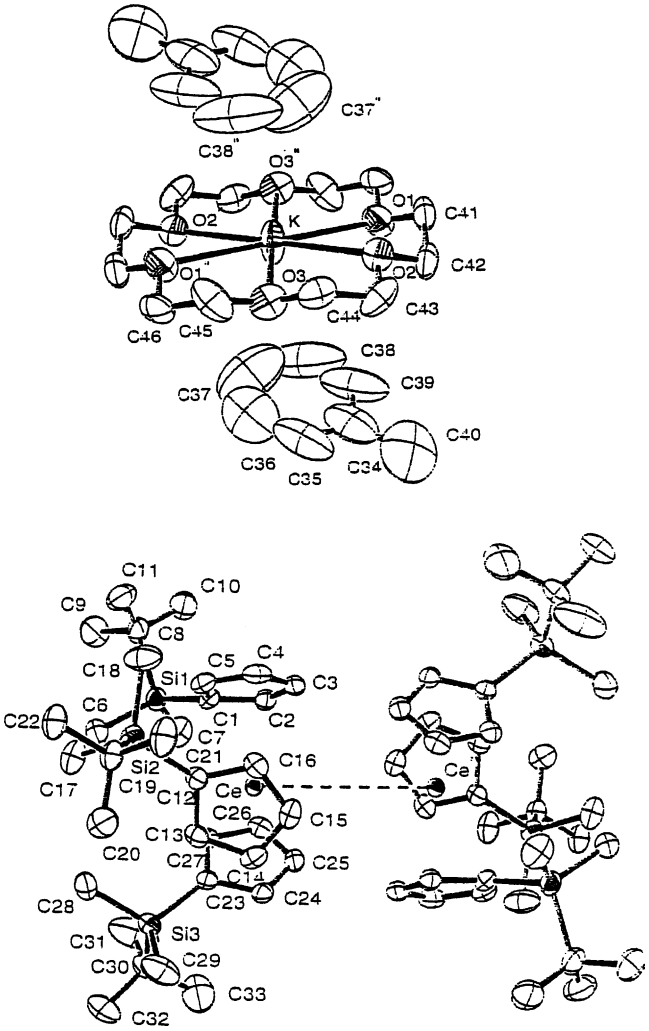

Fig. 68. ORTEP view of the complex [K([18]-crown-6)(η^2-PhMe)$_2$] [($Cp^t_3Ce)_2$(μ-H)]·PhMe.

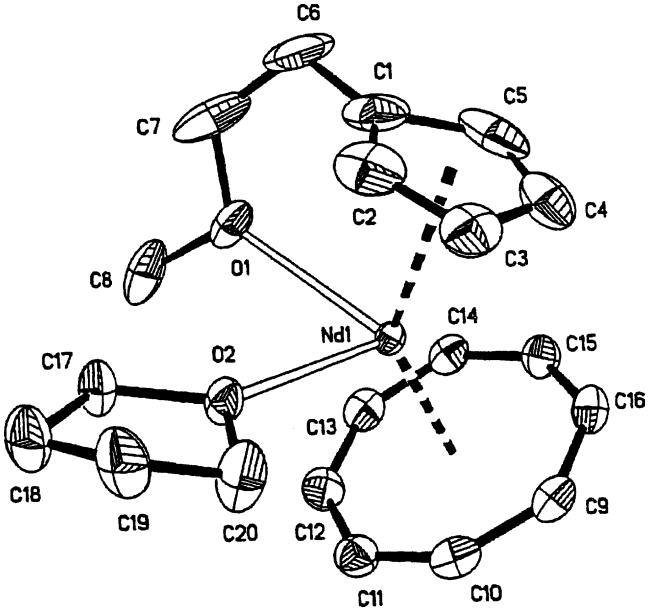

Fig. 69. ORTEP view of the molecular structure of (η^5-$MeOCH_2CH_2$ C_5H_4)Nd(COT)(THF).

The average bond lengths La–C(η^8) and La–C(η^5) are 2.740(8) and 2.842(7) Å, respectively. The La–O(THF) and La–O–(η^1) distances are 2.607(4) and 2.633(4) Å [48].

Visseaux et al. [28] investigated the synthesis of THF-free metallocene of early lanthanides with highly substituted cyclopentadienyl and cyclooctatetraenyl ligands. The complexes were obtained by the reaction of (COT)LnCl(THF)$_2$ (Ln = Sm, Nd) with 1 equiv. of $NaCp^{4i}$ to give the corresponding lanthanide(III) metallocenes (COT)$LnCp^{4i}$ in high yields (Scheme 57 and Fig. 71).

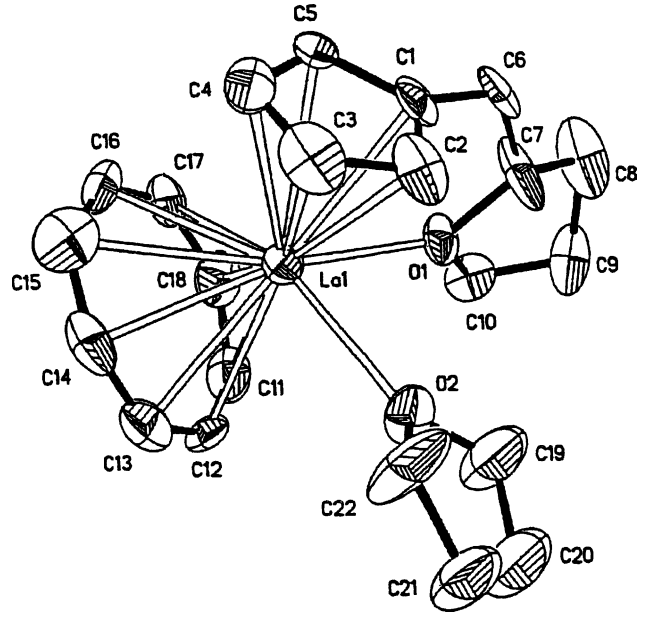

Fig. 70. ORTEP view of the molecular structure of (η^5-$C_4H_7OCH_2$ C_5H_4)La(COT)(THF).

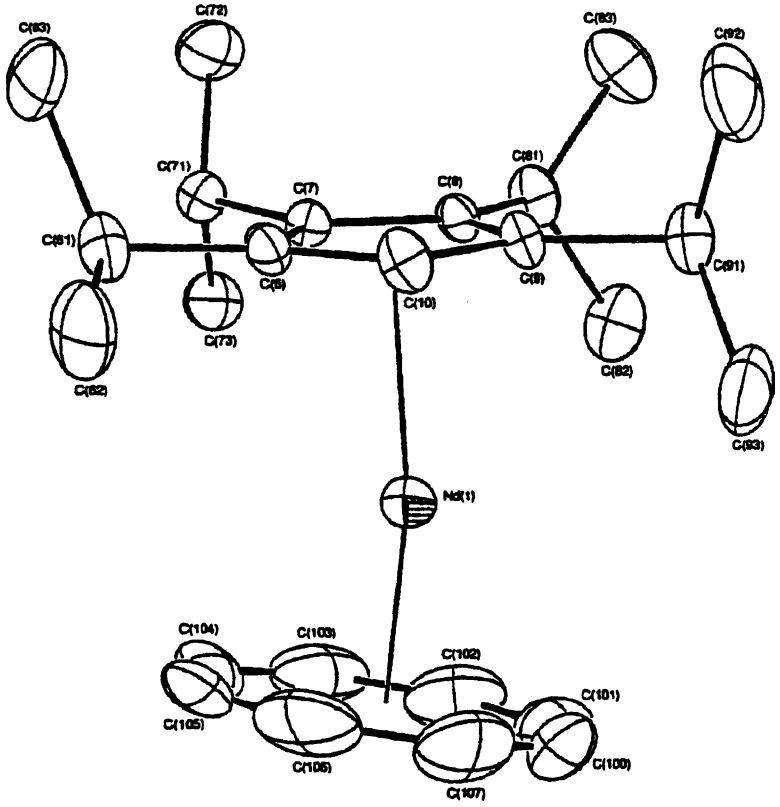

Fig. 71. ORTEP view of the complex (COT)NdCp[4i].

The molecular structure of (COT)LnCp[4i] shows a slight bending; 170.4° for the Cp–Sm–COT angle in (COT)SmCp[4i], 165° in one independent conformer of (COT)NdCp[4i] and 173° in the other.

Schumann et al. [50] synthesized enantiomerically pure sandwich complexes of samarium and lutetium with donor-functionalized cyclopentadienyl ligands. The reaction of K[(*S*)-$C_5H_4CH_2CH(Me)OMe$], K[(*S*)-$C_5H_4CH_2CH(Me)NMe_2$] and K[(*S*)-$C_5H_4CH(Ph)CH_2NMe_2$] with the cyclooctatetraenyl lanthanide chlorides [(COT)Ln(μ-Cl)(THF)]$_2$ (Ln = Sm, Lu) yielded the mixed cyclooctatetraenyl–cyclopentadienyl lanthanide complexes (COT)Sm[(*S*)-η^5:η^1-$C_5H_4CH_2CH(Me)OMe$], (COT)Ln[(*S*)-η^5:η^1-$C_5H_4CH_2CH(Me)NMe_2$] (Ln = Sm, Lu) and (COT)Ln[(*S*)-η^5:η^1-$C_5H_4CH(Ph)CH_2NMe_2$] (Ln = Sm, Lu). The complexes were characterized by ^{1}H, ^{13}C NMR and mass spectra. Single-crystal X-ray determinations of (COT)Lu[(*S*)-η^5:η^1-$C_5H_4CH(Ph)CH_2NMe_2$] and the achiral compound (COT)Ln[η^5:η^1-$C_5H_4CH_2CH_2NMe_2$] were performed (Scheme 58 and Figs. 72 and 73).

In both complexes, the cyclooctatetraenyl ligand is disordered. Through the additional intramolecular coordination of nitrogen of the side chain the coordination number around Lu^{3+} is 9 [50].

$$(COT)LnCl(THF)_2 + NaCp^{4i} \xrightarrow{THF} (COT)Ln(Cp^{4i})$$

Ln = Sm, Nd

Scheme 57. Formation of THF-free metallocenes of samarium and neodymium.

2.3. Complexes with indenyl and fluorenyl ligands

Xie and co-workers [51] published a new versatile carbon-bridged ligand for organolanthanide chemistry, $Me_2C(C_9H_7)(C_2B_{10}H_{11})$. The ligand was prepared by treatment of $Li_2C_2B_{10}H_{10}$ with 1 equiv. of 6,6-dimethylbenzofulvene followed by hydrolysis with saturated aqueous NH_4Cl solution (Scheme 59).

This ligand can be conveniently converted into the monoanion Li[$Me_2C(C_9H_6)(C_2B_{10}H_{11})$] and the dianion Li_2[$Me_2C(C_9H_7)(C_2B_{10}H_{10})$] by treatment with 1 or 2 equiv. of ^{n}BuLi, respectively [51] (Scheme 60).

The dianion reacted with 1 equiv. of SmI_2, followed by reaction (without isolation) with 1 equiv. of the monoanion, to give the redox product *rac*-[Li(DME)$_2$][{η^5:σ-$Me_2C(C_9H_6)(C_2B_{10}H_{10})$}$_2$Sm] [51] (Scheme 61).

Unlike the SmI_2 case, an equimolar reaction between the dianion and YbI_2 afforded the Yb(II) compound [η^5:σ-$Me_2C(C_9H_6)(C_2B_{10}H_{10})_2$]Yb(DME)$_2$. Reaction of

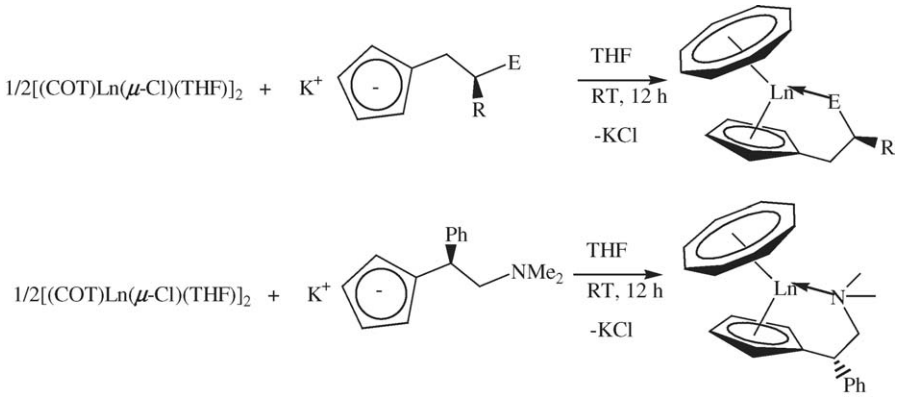

Scheme 58. Formation of the chiral cyclooctatetraenyl–cyclopentadienyl complexes.

$LnCl_3$ with 1 or 2 equiv. of the dianion yielded the organolanthanide dichloride and monochloride compounds, $[\eta^5\text{-}Me_2C(C_9H_6)(C_2B_{10}H_{11})]GdCl_2(THF)_2$ and $[\eta^5\text{-}Me_2C(C_9H_6)(C_2B_{10}H_{11})]_2LnCl(THF)(OEt_2)$ (Ln = Y, Yb), respectively [51].

Reaction of $LnCl_3$ with 2 equiv. of the dianion afforded ionic compounds *rac*-$[Li(DME)_2][\{\eta^5\text{:}\sigma\text{-}Me_2C(C_9H_6)(C_2B_{10}H_{10})\}_2Ln]$ (Ln = Yb, Nd, Er). All these compounds were fully characterized by various spectroscopic methods, single-crystal X-ray and elemental analysis [51].

Qian et al. [52] published the stereoselective synthesis and structural characterization of *rac*-planar chiral bis(2-methoxyethylindenyl)lanthanum and yttrium tetrahydroborate complexes. The complexes $(MeOCH_2CH_2C_9H_6)_2LnBH_4$ (Ln = Y, La) were synthesized in high yields by reaction of their chloride precursors $(MeOCH_2CH_2C_9H_6)_2LnCl$ with excess $NaBH_4$ in THF at room temperature (Scheme 62).

Both complexes are *rac*-planar chiral lanthanocenes with *trans* orientation of the η^5-indenyl planes as well as the coordinated side chains. The two molecular structures are essentially identical except for the coordination mode of BH_4^-. The Ln–O bond lengths are longer than those of the cyclopentadienyl analogues. The two bridging Y–H distances of Y–H(27) = 2.33(5) Å and Y–H(28) = 2.39(6) Å (see Fig. 74) are comparable to those of the cyclopentadienyl analogue of 2.26(6) and 2.27(5) Å. In contrast, the three hydrogen bridges between the lanthanum and the boron atoms have significantly different La–H distances La–H(27) = 2.38(5) Å, La–H(28) = 2.50(6) Å and La–H(29) = 2.60(6) Å (see Fig. 75). The two complexes have

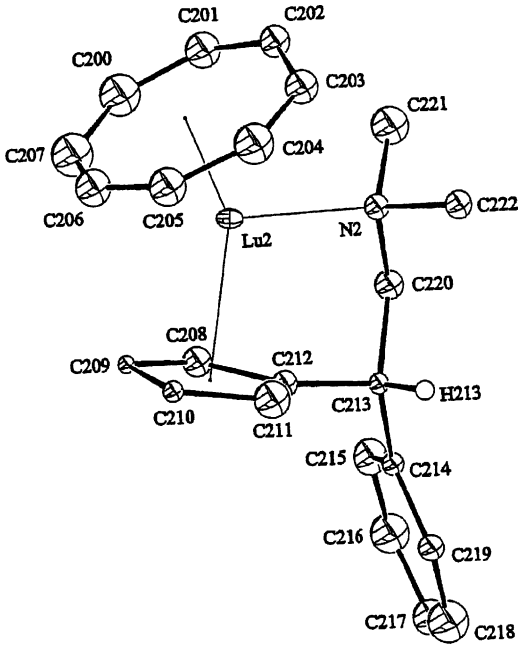

Fig. 72. ORTEP view of the complex [(COT)Lu{(*S*)-η^5:η^1-$C_5H_4CH(Ph)CH_2NMe_2$}].

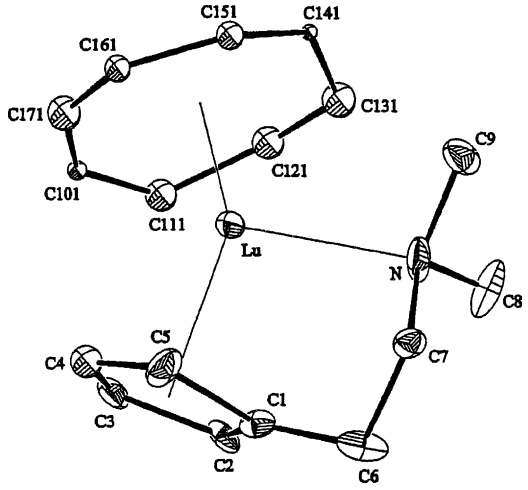

Fig. 73. ORTEP view of the complex [(COT)Lu{η^5:η^1-$C_5H_4CH_2CH_2NMe_2$}].

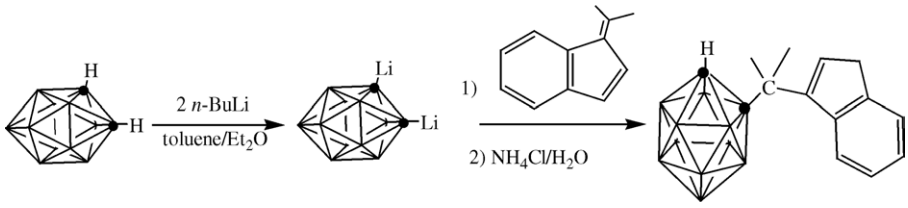

Scheme 59. Formation of the new ligand $Me_2C(C_9H_7)(C_2B_{10}H_{11})$.

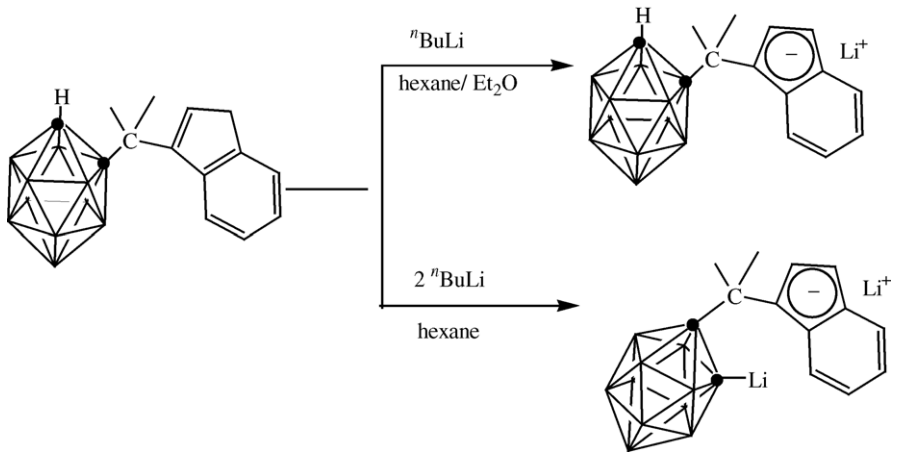

Scheme 60. Formation of the mono- and dianion $Li[Me_2C(C_9H_6)(C_2B_{10}H_{11})]$ and $Li_2[Me_2C(C_9H_7)(C_2B_{10}H_{10})]$.

been fully characterized by elemental analyses, MS, ^{1}H NMR and IR spectra. The tetrahydroborate ion has been identified as slipped bidentate $(\mu_2\text{-H})_2BH_2$ and tridentate $(\mu_2\text{-H})_3BH$ ligands in the complexes, respectively [52].

Anwander and co-workers [53] synthesized indenyl-derived ytterbocene(II) complexes $[1\text{-}(SiHR_2)\text{-}2\text{-}R'\text{-}C_9H_5]_2Yb(L)_2$ (R = Me, C_6H_5; R′ = H, Me; L = donor ligand) via silylamine elimination from $Yb[N(SiMe_3)_2]_2(THF)_2$ (Scheme 63).

The authors also investigated the fluxional behavior of the stereoisomers in solution, the ratio and interconversion of

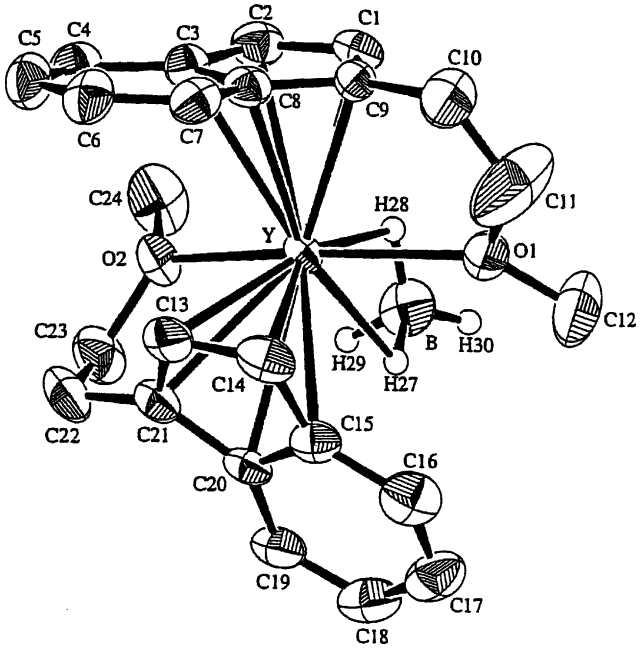

Fig. 74. ORTEP view of the complex $(MeOCH_2CH_2C_9H_6)_2YBH_4$.

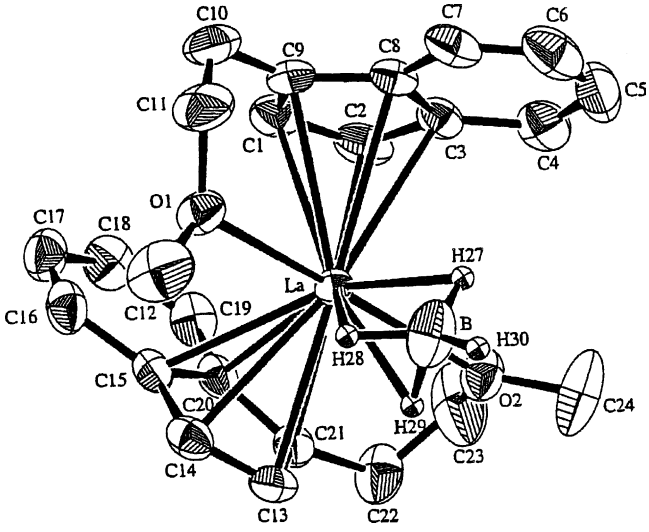

Fig. 75. ORTEP view of the complex $(MeOCH_2CH_2C_9H_6)_2LaBH_4$.

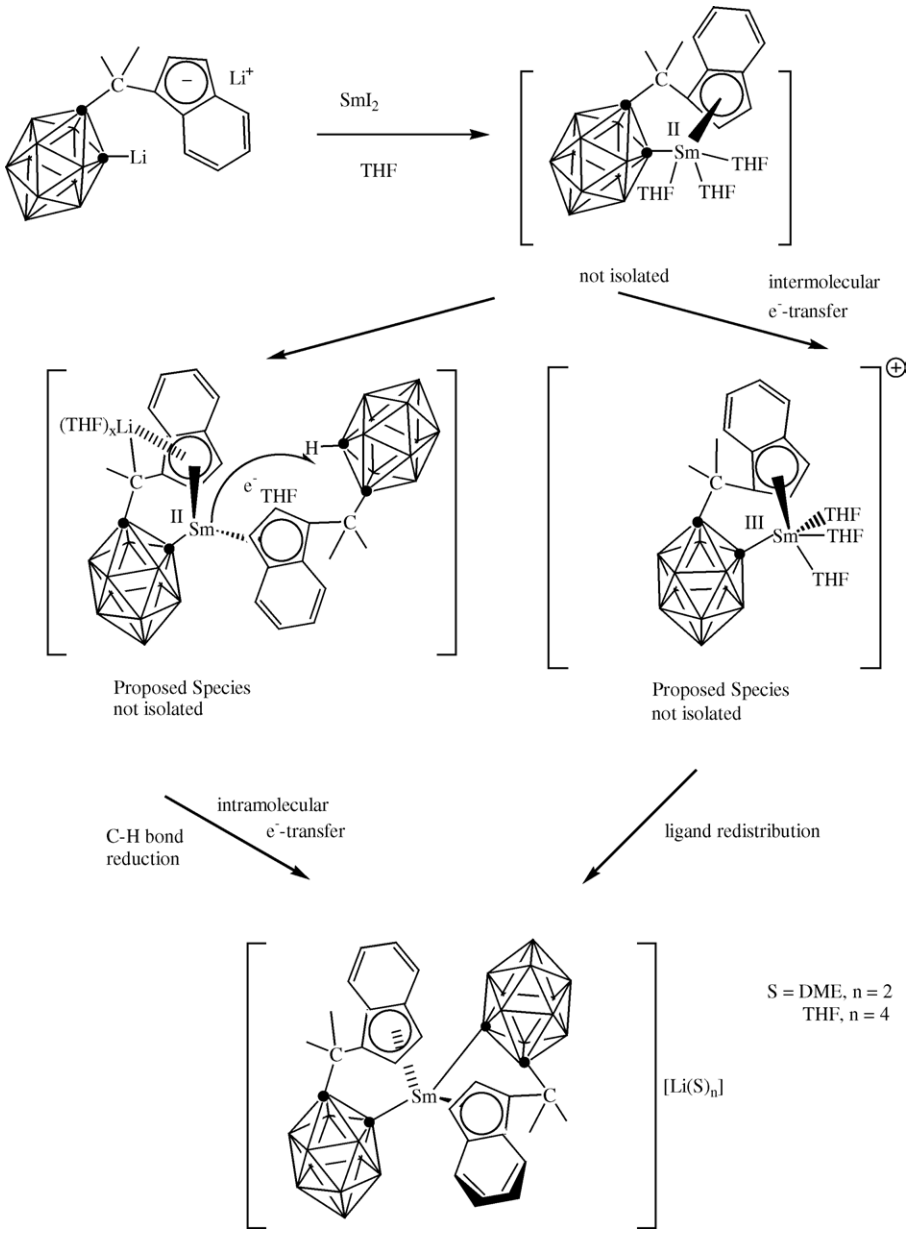

Scheme 61. Intramolecular and intermolecular electron-transfer pathways to form the Sm(III) complex *rac*-[Li(DME)$_2$][{η^5:σ-Me$_2$C(C$_9$H$_6$)-(C$_2$B$_{10}$H$_{10}$)}$_2$Sm].

which are affected by the size and ring position of substituents as well as the type of donor ligand, e.g. THF versus TMEDA [53].

Schumann et al. [54] published the synthesis and characterization of the first bis- and tris[1-(ω-alken-1-yl)indenyl]lanthanide complexes (Ln = Gd, Er, Y, Lu).

$$(MeOCH_2CH_2C_9H_6)_2LnCl \xrightarrow[\text{r.t./48 h}]{NaBH_4} (MeOCH_2CH_2C_9H_6)_2LnBH_4 + NaCl$$
$$Ln = Y,\ La$$

Scheme 62. Formation of the complexes (MeOCH$_2$CH$_2$C$_9$H$_6$)Ln(μ-H)$_n$BH$_{4-n}$, Ln = Y, La.

$$Yb[N(SiMe_3)_2]_2(THF)_2 \xrightarrow[\text{r.t., 3h}\ -\ 2\ HN(SiMe_3)_2]{2\ (R\text{-}Ind)H,\ n\text{-hexane}} (R\text{-}Ind)_2Yb(THF)_2$$

(R-Ind)H = 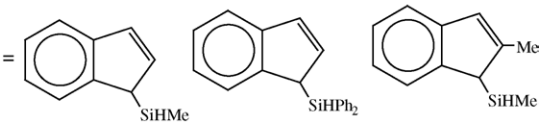

Scheme 63. Synthesis of ytterbium indenyl complexes via silylamine elimination.

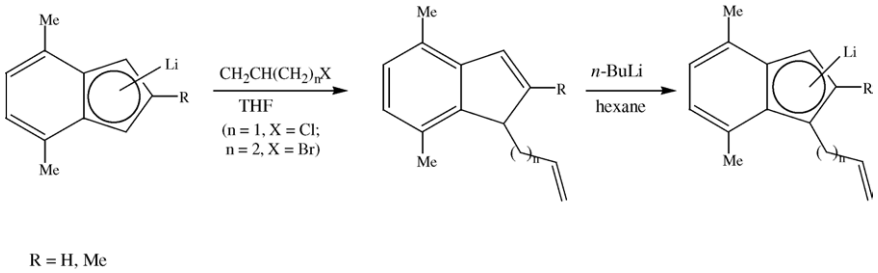

Scheme 64. Synthesis of the ligands.

1-Allyl-2,4,7-trimethyl-1*H*-indene and 1-(3-buten-1-yl)-4,7-dimethyl-1*H*-indene were prepared from (2,4,7-trimethylindenyl)lithium and allyl chloride or from (4,7-dimethylindenyl)lithium and 4-bromo-1-butene (Scheme 64).

Subsequent reactions with the trichlorides of gadolinium, erbium, yttrium, lutetium and ytterbium in THF gave the bis[(1-allyl-2,4,7-trimethylindenyl)]lanthanide chloride complexes $L_2LnCl(THF)$ (Ln = Gd, Er), bis[(1-buten-1-yl)-4,7-dimethylindenyl]lanthanide complexes (Ln = Y, Lu) or the hetero bimetallic *ate* complex bis[(1-buten-1-yl)-4,7-dimethylindenyl]Yb(μ-Cl)$_2$Li(THF)$_2$ [54] (Scheme 65 and Figs. 76 and 77).

The trichlorides of the comparatively large samarium and lanthanum ions react with different molar amounts of bis[(1-buten-1-yl)-4,7-dimethylindenyl]lithium in THF exclusively to give the tris(indenyl) complexes tris[(1-buten-1-yl)-4,7-dimethylindenyl]samarium or tris[(1-buten-1-yl)-4,7-dimethylindenyl]lanthanum(μ-Cl)Li(Et$_2$O)$_3$ (Scheme 66 and Figs. 78 and 79).

Yasuda and co-workers [55] realized a novel type of metallotropic tautomerism: reversible and equilibrium isomerization of bis(η^5-Me$_3$Si-fluorenyl) rare-earth metal complexes to bis(η^6-Me$_3$Si-fluorene-AlR$_3$) rare-earth metal complexes. This metallotropic tautomerism was effected by the addition of aluminum trialkyls to the bimetallic complexes. Bis(η^5-Me$_3$Si-fluorenyl)Sm(THF)$_2$ was synthesized from (Me$_3$Si-fluorenyl) potassium and SmI$_2$(THF)$_2$, and its molecular structure was analyzed by X-ray diffraction (Scheme 67 and Fig. 80).

Bis(η^6-Me$_3$Si-fluorenyl-AlMe$_3$)Sm was synthesized by the reaction of bis(η^5-Me$_3$Si-fluorenyl)Sm(THF)$_2$ with excess AlMe$_3$. The corresponding reaction of excess AlEt$_3$ with bis(η^5-Me$_3$Si-fluorenyl)Sm(THF)$_2$ gave bis(η^6-Me$_3$Si-fluorenyl-AlEt$_3$)Sm (Scheme 68 and Figs. 81 and 82).

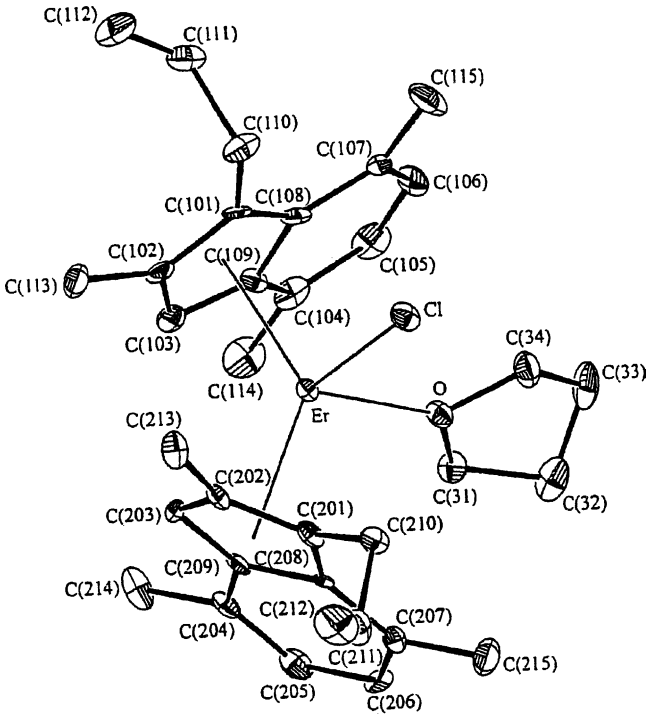

Fig. 76. ORTEP view of bis[(1-allyl-2,4,7-trimethylindenyl)]erbium chloride.

2.4. Complexes with cyclooctatetraenyl ligands

Ephritikhine and co-workers [18] synthesized the mono(cyclooctatetraenyl)neodymium complex (COT)-Nd(BH$_4$)(THF). This complex was obtained by the reaction of Nd(BH$_4$)$_3$(THF)$_3$ with K$_2$COT. Treatment with [NEt$_3$H]BPh$_4$ afforded the cationic complex [(COT)Nd-(THF)$_4$][BPh$_4$]. The heteroleptic compound (COT)Nd-(Cp*)(THF), the alkoxide [(COT)Nd(OEt)(THF)]$_2$, and the thiolates Na[(COT)Nd(S^{t}Bu)$_2$] and [Na(THF)$_2$]-[{(COT)Nd}$_2$(μ-S^{t}Bu)$_3$] were synthesized by treating (COT)Nd(BH$_4$)(THF) or [(COT)Nd(THF)$_4$][BPh$_4$] with the alkali metal salts of the corresponding anionic reagents (Scheme 69).

The X-ray crystal structures of [(COT)Nd(OEt)(THF)]$_2$ and [Na(THF)$_2$][{(COT)Nd}$_2$(μ-S^{t}Bu)$_3$] have been determined (Fig. 83).

The structure of the alkoxide comprises two monomeric units that are linked by two bridging alkoxide ligands. This geometry is similar to that of the other two crystallographically characterized [(COT)Ln(OR)(THF)]$_2$ compounds. The Nd–C distances range from 2.678(4) to 2.703(4) Å, and the average Nd–C(COT) length is 2.69(1) Å (which is identical

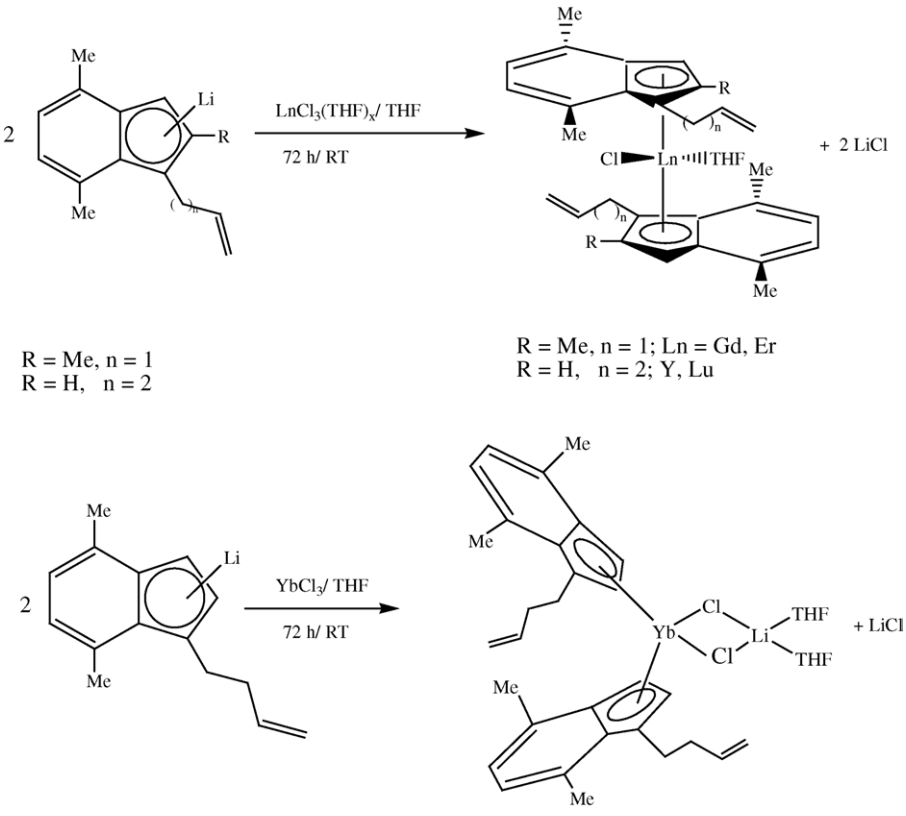

Scheme 65. Formation of the bis(indenyl)lanthanide complexes.

to that found in (COT)Nd($C_5H_4CH_2CH_2OMe$) 2.697(2) Å) [18] (Fig. 84).

In the crystal structure of toluene-solvated $[Na(THF)_2][\{(COT)Nd\}_2(\mu\text{-}S^tBu)_3]$, the two (COT)Nd fragments are bridged by three S^tBu groups. Each Nd atom has a pseudo-tetrahedral arrangement, if the cyclooctatetraenyl group is considered a monodentate ligand. The two tetrahedra share the common trigonal basis defined by the S atoms. This basal plane is parallel to the planar COT rings and perpendicular to the COT(centroid)–Nd–Nd–COT(centroid) axis. The COT ligation is quite similar to that found in the complex $[(COT)Nd(OEt)(THF)]_2$, with an average Nd–C

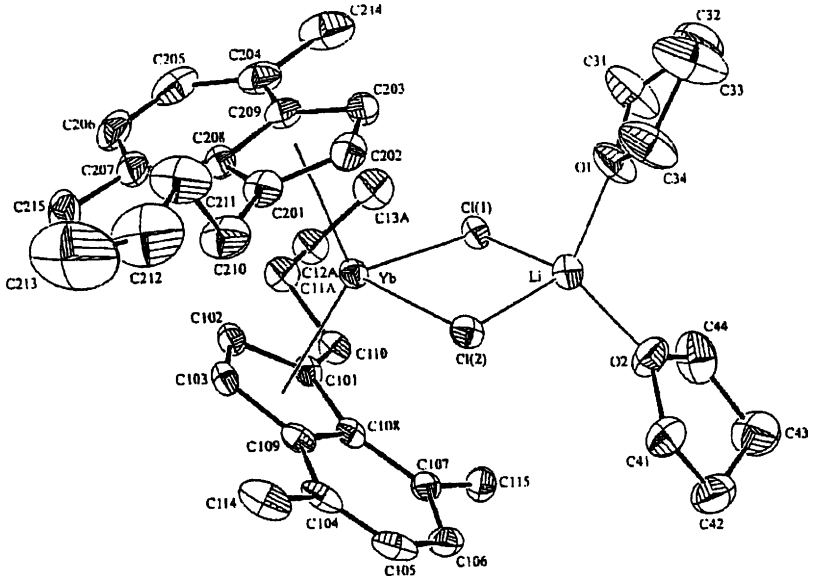

Fig. 77. ORTEP view of the heterometallic complex bis[(1-buten-1-yl)-4,7-dimethylindenyl]Yb(μ-Cl)$_2$Li(THF)$_2$.

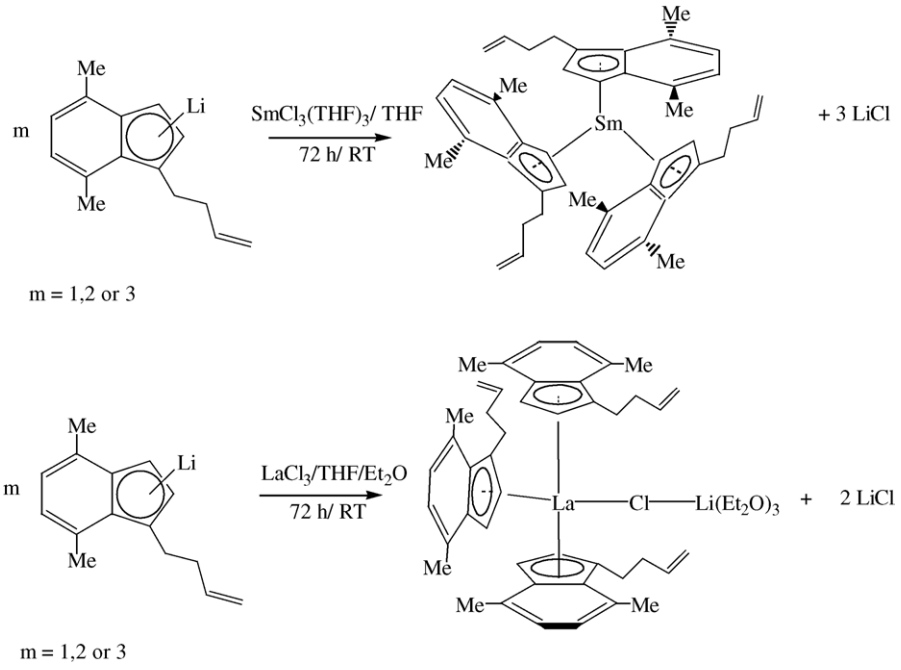

Scheme 66. Synthesis of tris(indenyl)complexes of samarium and lanthanum.

bond length of 2.67(3) Å. The Nd–S–Nd angles range from 88.50(5)° to 91.0(3)°; the S(1)–Nd–S(2) angles, which vary from 71.3(2)° to 87.0(2)°, due to coordination of S(1) and S(2) to the sodium ion [18].

Edelmann and co-workers [56] investigated the synthesis and characterization of half-sandwich complexes of the lanthanides containing cyclooctatetraenyl ligands. At first they successfully characterized the crystal structure of $[(COT)Ce(\mu\text{-}O_3SCF_3)(THF)_2]_2$. The compound crystallizes in the triclinic space group $P\bar{1}$. Together with the bridging triflate ligands the cerium atoms form an eight-membered $Ce_2O_4S_2$ ring (Fig. 85).

The complex $[(COT)Ce(\mu\text{-}O_3SCF_3)(THF)_2]_2$ reacts with 2 equiv. of $K[1,3\text{-}^tBu_2C_5H_3]$ to give the mixed-sandwich complex $(COT)Ce(\eta^5\text{-}1,3\text{-}^tBu_2C_5H_3)$ in 78% yield [56] (Scheme 70).

Also reported was the preparation of a series of new lanthanide half-sandwich complexes containing the 1,4-

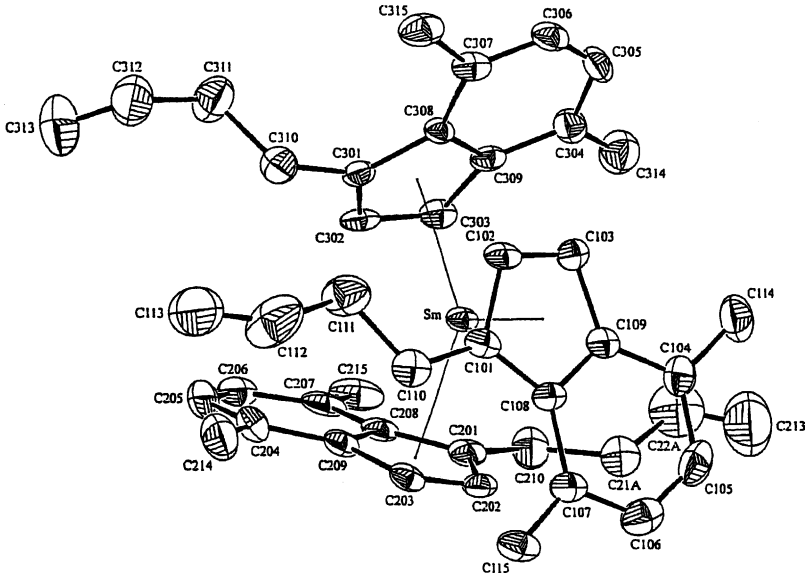

Fig. 78. ORTEP view of tris[(1-buten-1-yl)-4,7-dimethylindenyl]samarium.

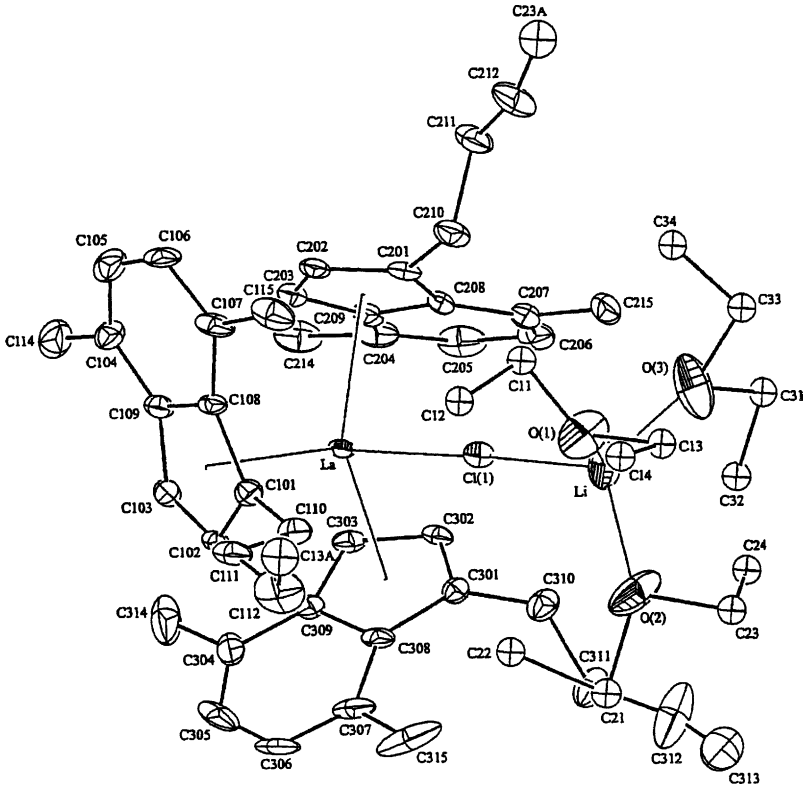

Fig. 79. ORTEP view of tris[(1-buten-1-yl)-4,7-dimethylindenyl]lanthanum(μ-Cl)Li(Et_2O)$_3$.

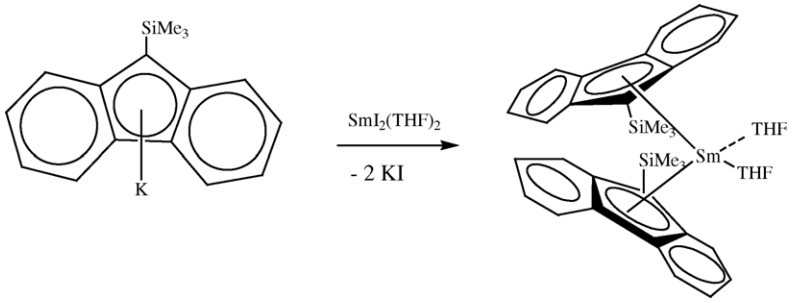

Scheme 67. Formation of bis(η^5-Me_3Si-fluorenyl)Sm(THF)$_2$.

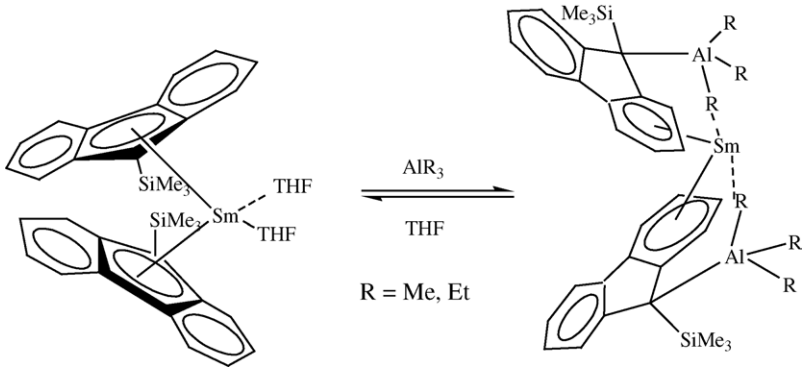

Scheme 68. A novel type of metallotropic tautomerism.

$$(COT)Nd(BH_4)(THF)_2 + NaOEt \xrightarrow{THF} 1/2[(COT)Nd(OEt)]_2 + NaBH_4$$

$$[(COT)Nd(THF)_4][BPh_4] + NaOEt \xrightarrow{THF} 1/2[(COT)Nd(OEt)]_2 + NaBH_4$$

$$(COT)Nd(BH_4)(THF)_2 + 2\,NaS^tBu \xrightarrow{THF} Na[(COT)Nd(S^tBu)_2] + NaBH_4$$

$$[(COT)Nd(THF)_4][BPh_4] + 2\,NaS^tBu \xrightarrow{THF} Na[(COT)Nd(S^tBu)_2] + NaBH_4$$

Scheme 69. Synthesis of mono(cyclooctatetraenyl)neodymium complexes.

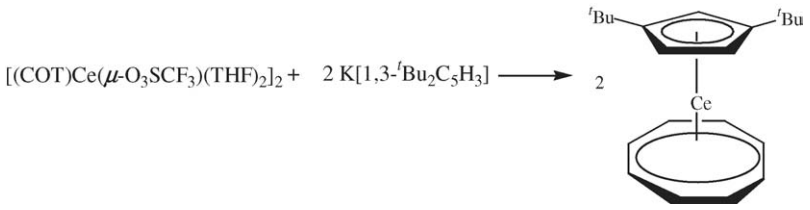

Scheme 70. Preparation of the mixed-sandwich complex (COT)Ce(η^5-1,3-^{t}Bu$_2$C$_5$H$_3$).

bis(trimethylsilyl)cyclooctatetraenyl ligand and additional heteroallylic, aryloxide and alkyl ligands [56].

Evans et al. [57] investigated the variability of (ring centroid)–Ln-(ring centroid) angles in the mixed ligand Cp*/COT complexes Cp*LnCOT and [Cp*Yb(THF)](μ-η^8:η^8-C$_8$H$_8$)[YbCp*]. The solid-state structures of Cp*Sm(COT), Cp*Dy(COT), Cp*Er(COT) and Cp*Yb(COT) were determined for comparison with that of Cp*Lu(COT) (Fig. 86).

The Ln–C(Cp*) and Ln–C(COT) distances decrease from Sm to Lu with changes that follows the differences in

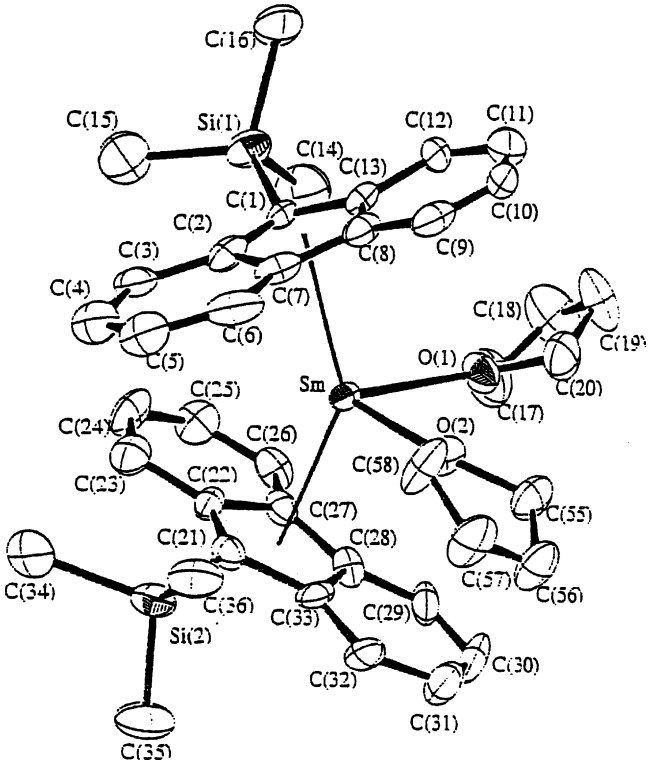

Fig. 80. ORTEP view of the complex bis(η^5-Me$_3$Si-fluorenyl)Sm(THF)$_2$.

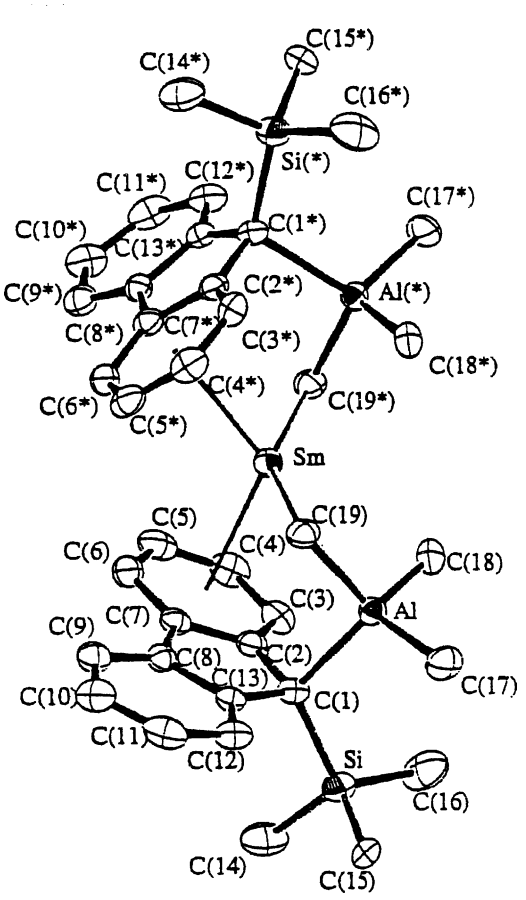

Fig. 81. ORTEP view of the complex bis(η^6-Me$_3$Si-fluorene-AlMe$_3$)Sm.

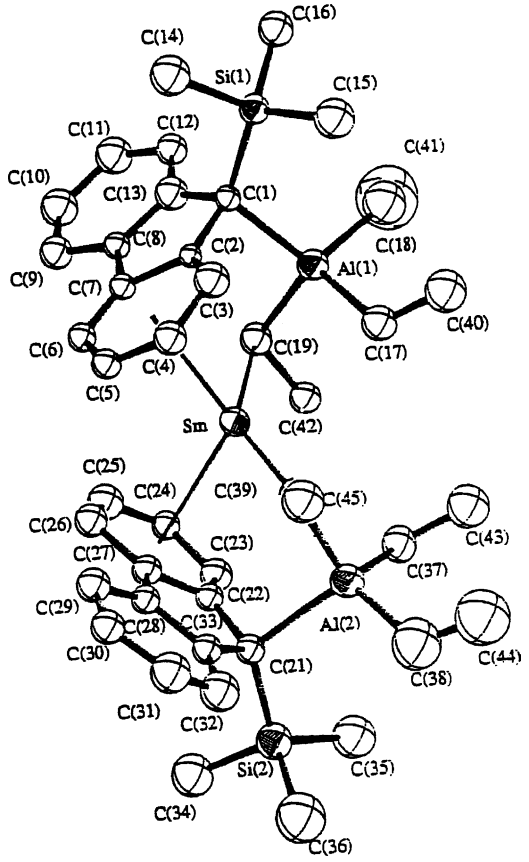

Fig. 82. ORTEP view of the complex bis(η^6-Me_3Si-fluorene-$AlEt_3$)Sm.

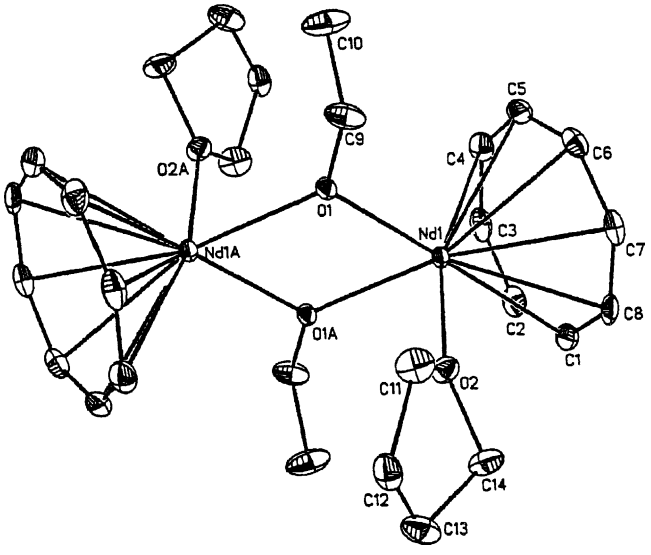

Fig. 83. ORTEP view of the complex $[(COT)Nd(OEt)(THF)]_2$.

eight-coordinate metal radii. The complex $[Cp^*Yb(THF)](\mu$-η^8:η^8-$C_8H_8)[YbCp^*]$ was obtained from a reaction of one-half equivalent of Al_2Et_6 with 1 equiv. of $Cp^*Yb(COT)(THF)$ [57] (Fig. 87).

The bond lengths and angles in this complex are significantly different on the solvated and unsolvated sides of the complex and are compared to the data of unsolvated $[Cp^*Yb]_2(COT)$. The Yb(1)–C(Cp^*) average distance is 2.683(3) Å on the solvated side versus 2.615(3) Å for the unsolvated Yb(2)–C(Cp^*) [57].

2.5. Organolanthanide complexes in organic synthesis

Ishii and co-workers [58] published the efficient synthesis of dinitrile derivatives by the reaction of oxime esters

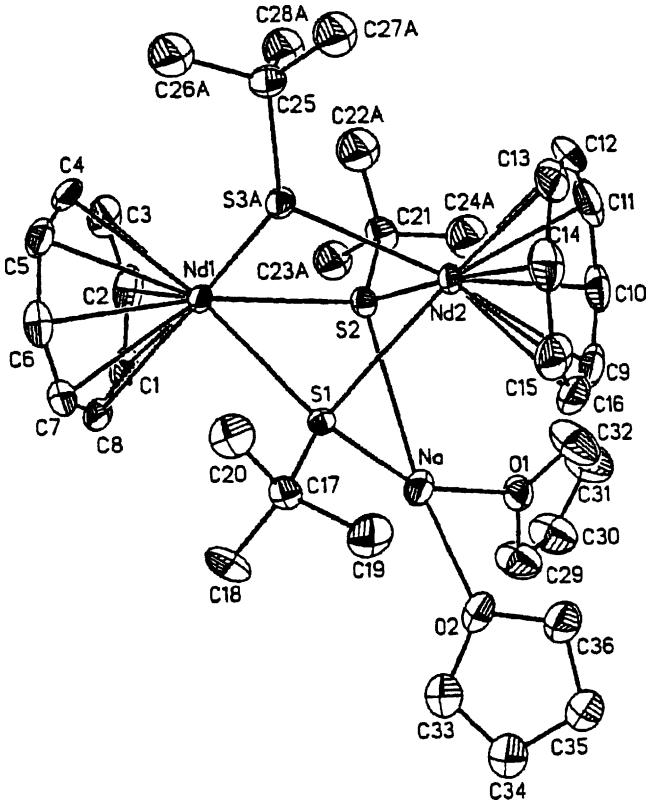

Fig. 84. ORTEP view of the complex $[Na(THF)_2][\{(COT)Nd\}_2(\mu$-$S^tBu)_3]$.

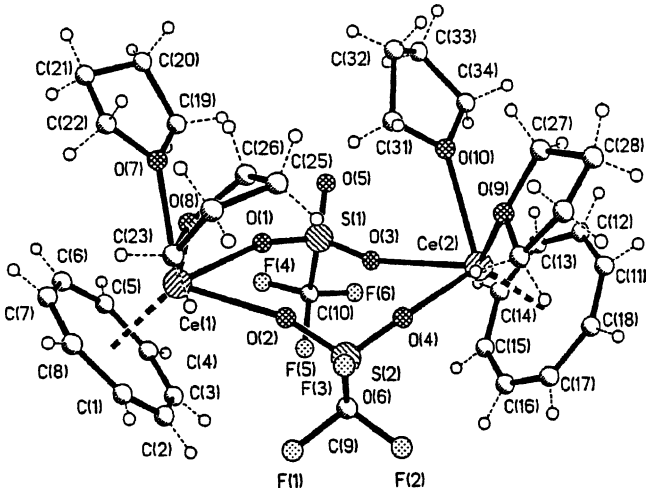

Fig. 85. ORTEP view of the molecular structure of the complex $[(COT)Ce(\mu$-$O_3SCF_3)(THF)_2]_2$.

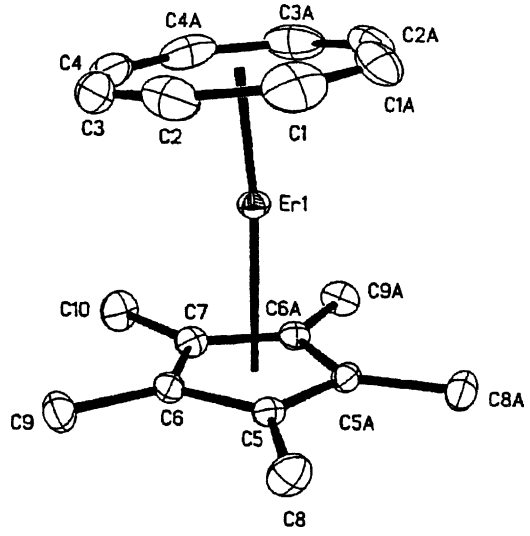

Fig. 86. ORTEP view of the molecular structure $Cp^*Er(COT)$.

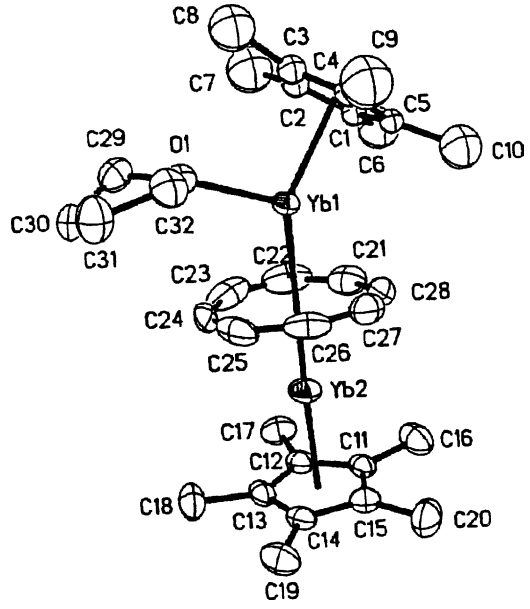

Fig. 87. ORTEP view of the complex $[Cp^*Yb(THF)](\mu\text{-}\eta^8\text{:}\eta^8\text{-}C_8H_8)[YbCp^*]$.

or acid anhydrides with cyanotrimethylsilane catalyzed by $La(O^iPr)_3$. The reaction seems to proceed through the formation of acyl cyanides as intermediate, followed by the addition of Me_3SiCN to acyl cyanides.

Kunishima et al. [59] developed three methods for generating alkynylsamarium complexes: (1) reduction of iodoalkynes with SmI_2 in the presence of HMPA, (2) deprotonation at the terminal position of 1-alkynes either by tetrahydrofurylsamarium intermediates generated from PhI and SmI_2 in THF, or (3) deprotonation by butyllithium followed by metal–metal exchange with SmI_2. Alkynylsamariums arising from iodoalkynes with SmI_2 undergo coupling with carbonyl compounds under both Barbier and Grignard conditions in benzene–HMPA or THF–HMPA as a solvent system. Tetrahydrofurylsamarium species generated from iodobenzene and SmI_2 in THF deprotonate terminal alkynes to yield the alkynylsamarium complex, whereas other alkylsamariums, such as ethyl-, isopropyl-, cyclohexyl- and cyclopentylsamarium intermediates, cannot be generated with this procedure. Metal–metal exchange between an alkynyllithium and SmI_3 is also effective to produce alkynylsamarium species. To reveal the properties of alkynylsamariums, the authors examined their stability and reactivity towards various electrophiles.

Molander and Rzasa [60] demonstrated the synthetic utility of the cationic lanthanide complex $[Cp^*_2Ce][BPh_4]$ as an effective Lewis acid catalyst for the hetero-Diels–Alder reaction between Danishefsky's diene and substituted benzaldehydes (Scheme 71).

Li and Zhang [61] reported a direct access to a quaternary carbon center utilizing an organosamarium reagent. They treated lactams and acyclic amides containing an N–H bond with allylsamarium bromide and obtained 2,2-diallylated nitrogen heterocycles and diallylated amides in good yields under mild conditions (Scheme 72).

2.6. Organolanthanide catalysis

Qian et al. [43] published the results of the stereospecific polymerization of methyl methacrylate using the new *ansa*-organolanthanides $Me_2Si(Flu)(Cp)DyN(SiMe_3)_2$, $Me_2Si(Flu)(Cp)DyCH(SiMe_3)_2$, $Me_2Si(Flu)(Cp)ErN(SiMe_3)_2$ and $Me_2Si(Flu)(Cp)ErCH(SiMe_3)_2$ as initiators for catalytic reactions. They showed that the stereochemistry of the product depends on the substitution of the lanthanide complexes, the temperature and on solvent effects. The polymerization rates in the reaction catalyzed by the amide complexes increased when lowering the temperature, while those catalyzed by hydrocarbyls decreased. It was also shown that erbium complexes display a higher stereoselectivity than the dysprosium species.

Douglass and Marks [62] investigated the catalytic intramolecular hydrophosphination/cyclization of phosphinoalkenes and phosphinalkynes using organolanthanide precatalysts of the type $Cp^*_2LnCH(SiMe_3)_2$ (Ln = La, Sm, Y) and $Me_2Si(Me_4C_5)(^tBuN)SmN(SiMe_3)_2$ (Scheme 73 and Table 2).

Boisson and co-workers [63] were successful generating poly(ethane-*co*-1,3-butadiene) using the neodymocene catalysts $Cp^*_2Nd(\mu\text{-}Cl)_2Li(OEt_2)_2$, $(^tBuC_5Me_4)_2NdCl$, $(Me_3SiC_5Me_4)_2NdCl$ and $[Me_2Si(3\text{-}Me_3SiC_5Me_3)_2]NdCl$. Polymers with molecular masses of 2000 up to 15 000 were produced with polymerization times of 30–60 min.

Yasuda and co-workers [64] synthesized the alkyl complex $Me_2Si(C_5H_3\text{-}3\text{-}R)_2SmCH(SiMe_3)_2$ and the corresponding lanthanide hydride, $[Me_2Si(C_5H_3\text{-}3\text{-}R)_2SmH]_2$, which was structurally characterized by single-crystal X-ray analysis. Detailed studies were performed to explain the catalytic activity of this complex in the process of block copolymerization of ethylene with polar monomers. The first step is the re-

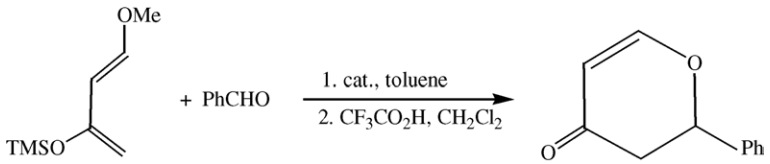

Scheme 71. Hetero-Diels–Alder reaction between Danishefsky's diene and substituted benzaldehydes.

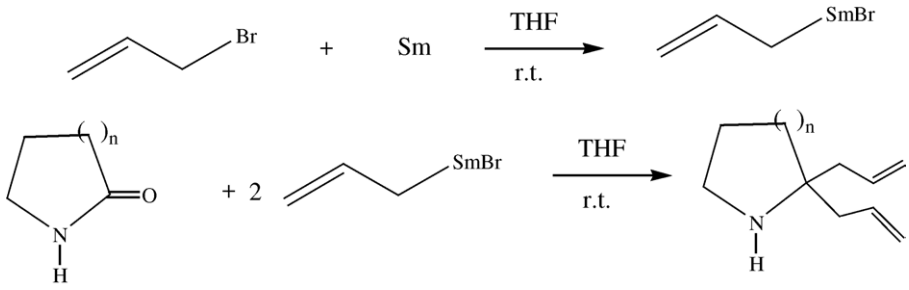

Scheme 72. Formation of 2,2-diallylated nitrogen heterocyles in the presence of allylsamarium bromide.

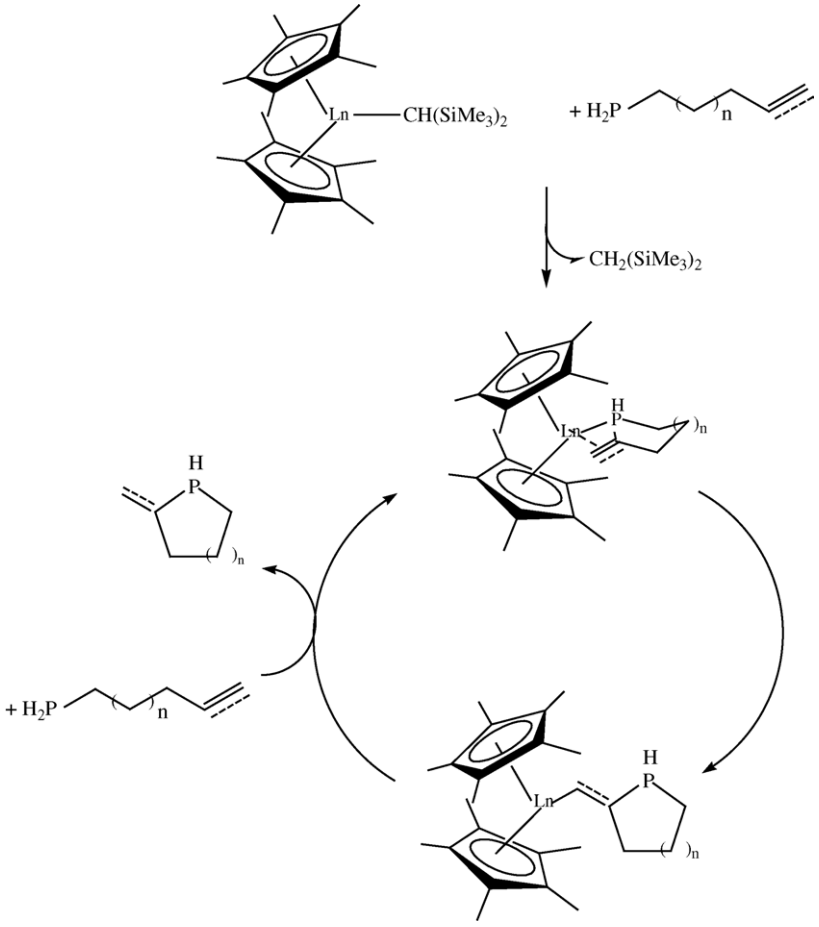

Scheme 73. Proposed catalytic cycle for organolanthanide-mediated hydrophosphination/cyclization of phosphinoalkenes and phosphinoalkynes.

Table 2
Results of the organolanthanide-catalyzed hydrophosphination/cyclization of phosphinoalkenes and phosphinoalkynes

Substrate	Product	Precatalyst
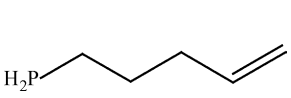	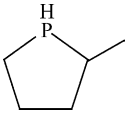	$Cp^*_2SmCH(SiMe_3)_2$
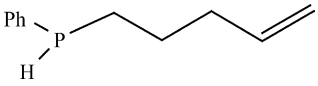	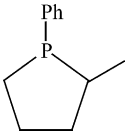	$Cp^*_2LaCH(SiMe_3)_2$
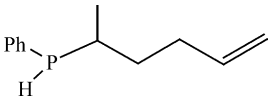	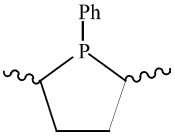	$Cp^*_2LaCH(SiMe_3)_2$
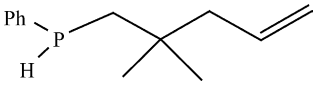	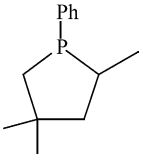	$Cp^*_2LaCH(SiMe_3)_2$
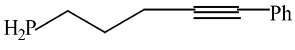	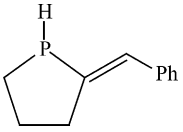	$Cp^*_2SmCH(SiMe_3)_2$, $Cp^*_2LaCH(SiMe_3)_2$, $Cp^*_2YCH(SiMe_3)_2$, $Me_2Si(Me_4C_5)(^tBuN)Sm(SiMe_3)_2$
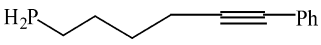	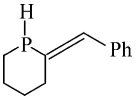	$Cp^*_2LaCH(SiMe_3)_2$
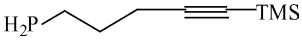	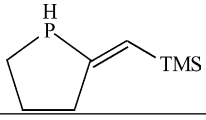	$Cp^*_2LaCH(SiMe_3)_2$

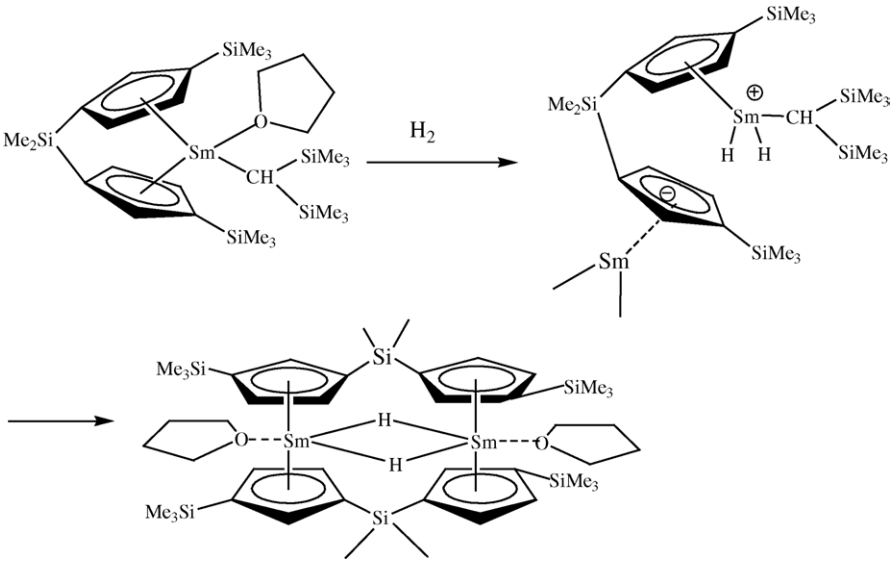

Scheme 74. Formation of the binuclear samarocene hydride.

action of the monomeric $Me_2Si(C_5H_3$-3-R$)_2SmCH(SiMe_3)_2$ with H_2 under formation of the dimeric hydride (Scheme 74 and Fig. 88).

Bonnaffé and co-workers [65] published L-iduronyl synthons catalyzed by a vinyl cerium reagent opening a way to an efficient preparation of 1,2,4-tri-*O*-acetyl-3-*O*-benzyl-L-iduronyl.

Bianconi and co-workers [66] reported surface functionalization with polymer and block copolymer films using organometallic catalysts. A layer of 5-hexenylsilane was generated on a silicon surface by reaction of a 5-hexenyltrichlorosilane precursor with pretreated surfaces. These functionalized silicon substrates were exposed to a THF solution of $Cp^*_2Sm(THF)_2$.

Junquan et al. [67] studied the behavior of the polymerization of methyl methacrylate initiated by single-component catalysts of the type $[O(C_2H_4C_5H_3CH_3)_2]LnCl$ (Ln = Y, Nd, Sm). The effects of temperature, time and molar ratio (MMA/catalyst) on the polymerization behavior were studied in detail. The results showed that higher temperature and longer time increased the catalytic activities. Kinetic studies indicated that the polymerization rate has a first-order dependence on the concentration of MMA and catalyst, respectively. The overall activation energy of polymerization is 33.9 kJ/mol.

Yasuda and co-workers [68] synthesized block copolymers catalyzed by the organosamarium complex $Cp^*_2SmMe(THF)$. Block copolymerizations of methyl methacrylate (MMA) with butyl acrylate (BuA), trimethylsilyl methacrylate (TMSMA) with MMA, and TMSMA with BuA were performed. All copolymerizations proceeded quantitatively in a short period of time, and the resulting polymers exhibited a high molecular weight ($M_n > 200\,000$) with narrow molecular weight distributions ($M_w/M_n < 1.5$). The viscoelastic and adhesive properties of these block copolymers proved to be very useful, especially in the high temperature range, compared with those obtained using conventional radical initiators.

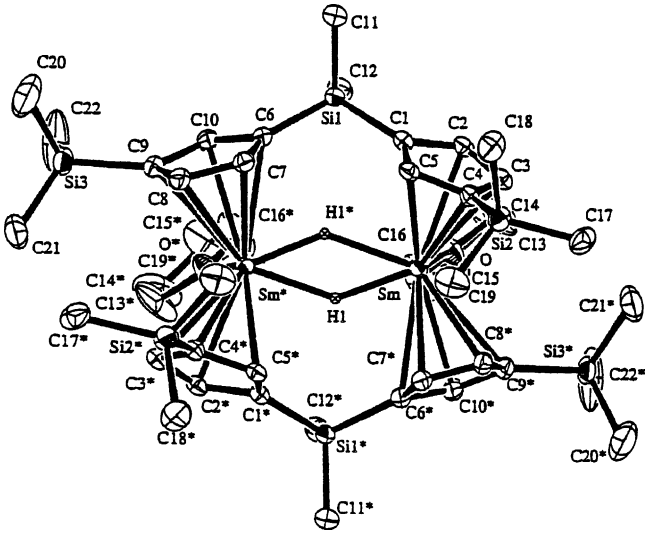

Fig. 88. ORTEP view of the binuclear samarocene hydride complex.

Hou et al. [45] published the results of the polymerization of styrene in the presence of samarium(II) complexes with mixed Cp^*/ER ligands (see Tables 3 and 4).

Carpentier and co-workers [69] investigated the polymerization of styrene in the presence of dialkylmagnesium or a combination of a chlorolanthanocene complex and dialkylmagnesium. In the presence of butylethylmagnesium or *n*,*s*-dibutylmagnesium, the styrene polymerization proceeds via thermal self-initiation, but is accompanied by a reversible transfer to dialkylmagnesium compounds giving oligostyrylmagnesium species. When the dialkylmagnesium is combined with a lanthanocene such as $Cp^*_2Nd(\mu\text{-}Cl)_2Li(OEt_2)_2$, an increase in activity is observed which is ascribed to additional styrene polymerization initiated by in situ generated alkyl(hydride)lanthanocene species. The influence of various reaction parameters on the performance of this system has been investigated. The oligostyrenes have a relatively narrow molecular mass distribution which can be explained by an efficient transfer between the chain-growing lanthanide and the oligostyrylmagnesium species. Finally, the combination of butylethylmagnesium and $Cp^*_2Nd(\mu\text{-}Cl)_2Li(OEt_2)_2$ has been used to produce (styrene-co-ethylene)block copolymers.

Yasuda and co-workers [70] described the first example of well-controlled block copolymerization of 1-olefins with methyl methacrylate or ε-caprolactone using the unique dual catalytic function of organolanthanide complexes to be active towards polymerization reactions of polar and non-polar monomers. The authors used bridged $Me_2Si(C_5R_4)_2LnH$ (Ln = Y, Sm) type complexes. These initiators are highly active in copolymerization processes without the presence of any cocatalyst (Scheme 75).

The dimeric structure of the yttrium and samarium hydride complexes is converted into a monomeric structure in the first step of the reaction. Subsequent reactions lead to a chain elongation. The authors report the preparation of block copolymers of hexene or pentene with methyl methacrylate and ε-caprolactone, respectively. The molecular masses of the polymers are in the range of 5000–15 000 with molecular mass distributions of 1.4–2.1. Detailed studies were carried out on the copolymerization of ethylene with methyl methacrylate, ε-caprolactone and 2,2-dimethyltrimethylene carbonate [71]. *Racemic* $Me_2Si(C_5H_2$-2-Me_3Si-4-^{t}Bu$)_2Sm(THF)_2$ or *meso* $Me_2Si(Me_2SiOSiMe_2)(C_5H_2$-3-^{t}Bu)Sm(THF) catalyzed the ABA-type triblock copolymerization.

Nodono et al. [72] presented a novel chain transfer polymerization mediated by $Cp^*_2Sm(III)$ species and organic compounds. The studied chain polymerization involves the reaction of organic compounds such as thiols or ketones with an active bond between samarium(III) and the enolate at the living end of poly(methyl methacrylate). This chain transfer reaction resulted in termination of the living chain end and the regeneration of the active initiator which would consist of $Cp^*_2Sm(III)$ and deprotonated organic compounds.

Table 3
Polymerization of styrene catalyzed by lanthanide(II) complexes

Run	Catalyst	Run time	Yield (%)	M_n ($\times 10^{-4}$)[a]	M_w/M_n[a]
1	$Cp^*_2Sm(THF)_{0\,or\,2}$	1 day	0	–	–
2	$Sm(OAr)_2(THF)_3$	1 day	0	–	–
3	$Sm(N(SiMe_3)_2)_2(THF)_2$	1 day	0	–	–
4	**1a**	30 min	89	34.7	1.73
5	**1b**	30 min	100	24.5	1.93
6	**1c**	150 min	79	17.1	1.45
7	**1d**	20 min	100	14.4	2.16
8	**1e**	10 min	100	8.2	2.45
9	**1f**	1 day	0	–	–
10	$Cp^*_2Sm(OAr)_2$	1 day	0	–	–
11	$Cp^*_2Sm(OC_6H_2{}^tBu_2\text{-}2,6\text{-}Me\text{-}4)$(HMPA)	1 day	0	–	–

Conditions: Sm(II) compound, 0.05 mmol; styrene, 4 ml; toluene, 10 ml; room temperature.
[a] Determined at 135 °C against polystyrene standard by GPC.

Table 4
Block copolymerization of ethylene and styrene by samarium(II) complexes bearing mixed Cp^*/ER ligands

Run	Catalyst	Styrene (ml)	Yield (g)			PS content (mol%)[a]	M_n ($\times 10^{-4}$)[b]	M_w/M_n[b]
			THF–sol (PS)[c]	Tol–sol (<108 °C) (PES)[c]	Tol–insol (108 °C) (PE)[c]			
1	**1a**	5	0.10	1.60	Trace	38	7.8	2.36
2	**1b**	3	0.46	2.14	Trace	34	15.9	1.97
3	**1b**	5	1.29	2.83	Trace	48	14.6	1.82
4	**1b**	7	1.37	2.94	Trace	68	15.1	1.92
5	**1b**	10	2.40	3.99	Trace	81	13.1	1.84
6	**1c**	3	0.06	1.31	Trace	13	11.3	2.21
7	**1c**	5	0.23	2.55	Trace	37	10.7	2.01
8	**1c**	7	0.27	2.74	Trace	43	13.7	1.73
9	**1c**	10	0.34	2.82	Trace	60	14.6	1.66
10	**1d**	3	1.89	1.21	Trace	36	5.7	3.75
11	**1e**	5	4.55	Trace	Trace	–	–	–

Conditions: a precatalyst, 0.05 mmol; ethylene, 1 atm; total volume of styrene and toluene, 25 ml; room temperature, 30 min, unless otherwise noted.
[a] Polystyrene content in the copolymers determined by ^{13}C NMR in *ortho*-dichlorobenzene/$CDCl_2CDCl_2$ at 125 °C.
[b] Determined at 135 °C against polystyrene standard by GPC.
[c] PS, atatic polystyrene; PES, block ethylene–styrene copolymer; PE, polyethylene.

Qian and co-workers [73] presented polymerization reactions of methyl methacrylate catalyzed by different mixed ligand lanthanocenes CpLnCl Schiff-base (Ln = Sm, Dy, Y and Er) complexes, were the Schiff-base is deprotonated *N*-(2-methoxyphenyl)salicylideneamine ($C_{14}H_{13}NO_2$). These complexes were used for the polymerization of methyl methacrylate along with $Al(^iBu)_3$ yielding poly-MMA with narrow molecular weight distribution.

2.7. Theoretical calculations, electronic structure determinations and gas-phase reactions

Nakajima and Kaya [74] published detailed studies of organometallic clusters in the gas phase containing scandium or lanthanide metals and aromatic ligand systems such as benzene (Bz), C_{60} or cyclooctatetraene. Novel network structures were found in organometallic clusters between metal atoms

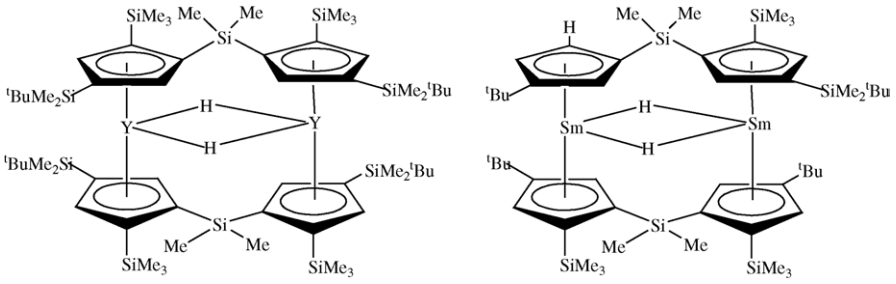

Scheme 75. Bridged organolanthanide hydrides of yttrium and samarium.

produced by laser ablation and organic ligand molecules. Size and structures of the clusters were determined using time of flight mass spectrometric techniques. For scandium–benzene clusters, Sc_nBz_m, a multiple-decker sandwich structure was found $(n, m) = (n, n + 1)$ in which the metal atoms and benzene are alternatingly piled up. A similar multiple-decker sandwich structure was formed between lanthanide metal atoms and the organic ligand cyclooctatetraene (COT) consisting of positively charged lanthanide ions and negatively charged COT.

Koch and co-workers [75] presented quantum chemical investigations of the initial steps of the yttrium-mediated polymerization of ethene and propene. The authors investigated the mechanistic details of the initial step of the polymerization brought about by a di(cyclopentadienyl)yttrium hydride catalyst using approximate density functional theory. In accord with the experimental information, the overall reaction sequences $Cp_2YH + C_2H_4 \rightarrow Cp_2Y{-}C_2H_5$ and $Cp_2YH + C_3H_6 \rightarrow Cp_2Y{-}C_3H_7$ were computed to be exothermic by approximately 22.2 and 20.8 kcal mol^{-1}, respectively.

3. Actinides

3.1. Cyclopentadienyl complexes

3.1.1. Mono(cyclopentadienyl) complexes

Barbier-Baudry et al. [12] successfully synthesized the new mono(cyclopentadienyl)uranium complex $(C_5H^iPr_4)U(BH_4)_3$ (Scheme 76).

Burns and co-workers [76] published the synthesis and characterization of mono(pentamethylcyclopentadienyl)uranium(III) complexes. The uranium(III) iodide precursor $UI_3(THF)_4$ reacts at ambient temperature with 1 equiv. of sodium or potassium pentamethylcyclopentadienide in THF to form the mono(cyclopentadienyl) complex(III) $Cp^*UI_2(THF)_3$ (Scheme 77).

In the solid state, the complex exhibits a pseudo-octahedral *mer*-, *trans*-geometry with the Cp^{*-} ligand occupying one axial position (Fig. 89).

This mono(cyclopentadienyl) complex also provides a convenient entry to a variety of other mono(cyclopentadienyl) complexes of uranium(III). In the presence of an excess of pyridine, the coordinated THF ligands of $Cp^*UI_2(THF)_3$ are readily displaced to form the tris(pyridine) adduct $Cp^*UI_2(py)_3$, which exhibits a *mer*-, *trans*-geometry in the solid state, similar to that of the THF adduct (Fig. 90).

The metathesis reaction of $Cp^*UI_2(THF)_3$ with 2 equiv. of $KN(SiMe_3)_2$ afforded the bis(amido) complex $Cp^*U[N(SiMe_3)_2]_2$ (Scheme 78 and Fig. 91).

Single-crystal X-ray diffraction studies of $Cp^*U[N(SiMe_3)_2]_2$ revealed that one methyl group of

$$(C_5H^iPr_4)Na \xrightarrow{U(BH_4)_4} (C_5H^iPr_4)U(BH_4)_3$$

Scheme 76. Synthesis of $(C_5H^iPr_4)U(BH_4)_3$.

$$UI_3(THF)_4 + Cp^*K \xrightarrow[25\ ^\circ C]{THF} Cp^*UI_2(THF)_3 + KI$$

Scheme 77. Formation of the mono(cyclopentadienyl) complex $Cp^*UI_2(THF)_3$.

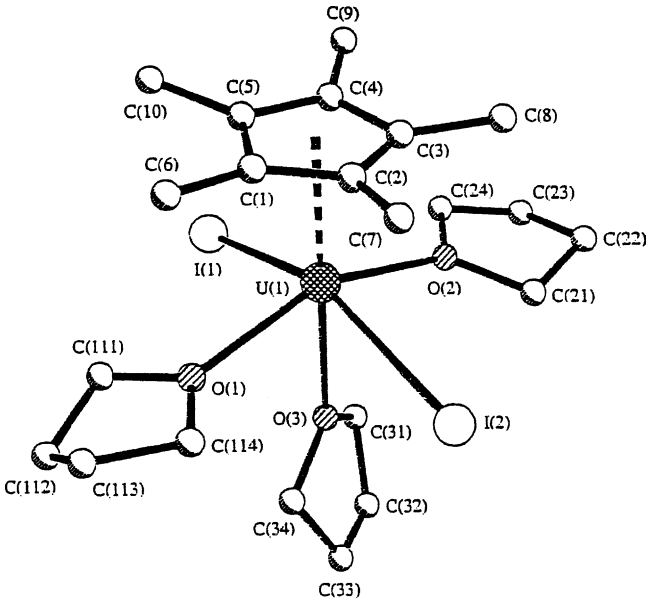

Fig. 89. ORTEP view of $Cp^*UI_2(THF)_3$.

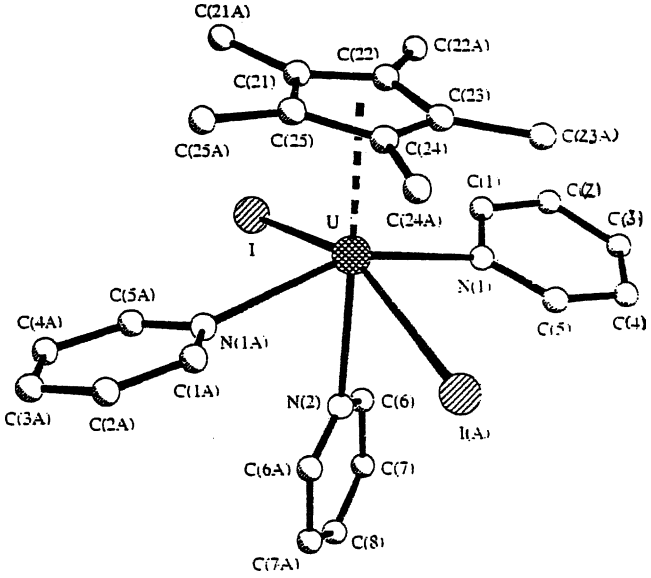

Fig. 90. ORTEP view of $Cp^*UI_2(py)_3$.

$$Cp^*UI_2(THF)_3 + 2\ K(SiMe_3)_2 \xrightarrow[25\ ^\circ C]{THF} Cp^*U[N(SiMe_3)_2]_2 + 2\ KI$$

Scheme 78. Formation of $Cp^*U[N(SiMe_3)_2]_2$.

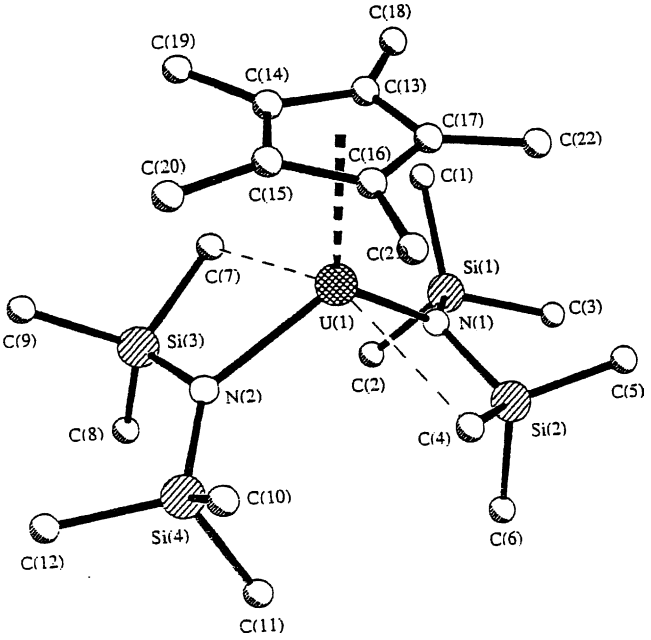

Fig. 91. ORTEP view of $Cp^*U[N(SiMe_3)_2]_2$.

$$Cp^*_2UCl_2 \xrightarrow[-\ LiCl]{Li(Bu^tNSPh)} Cp^*_2U(Bu^tNSPh)Cl$$

Scheme 79. Synthesis of $Cp^*_2U(\eta^2\text{-}Bu^tNSPh)Cl$.

each amido ligand is involved in an agostic interaction with the uranium(III) center.

3.1.2. Bis(cyclopentadienyl) complexes

Danopoulos et al. [77] published the synthesis of η^2-sulfenamido complexes of uranium. Thermally stable η^2-sulfenamido complexes of uranium, $U(\eta^2\text{-}Bu^tNSPh)_4$ and $Cp^*_2U(\eta^2\text{-}Bu^tNSPh)X$, X = Cl, Br, have been prepared by metathetical reactions of $Li^tN(Bu)SPh$ with UCl_4/PMe_3 and $Cp^*_2UCl_2$, respectively (Scheme 79 and Fig. 92).

Ephritikhine and co-workers [78] published the synthesis and characterization of the first dithiolene complexes of uranium. Treatment of $Cp^*_2UCl_2$ and $U(COT)X_2(THF)_n$ ($X = BH_4$, $n = 0$, $X = I$, $n = 2$) with Na_2dddt (dddt = 5,6-dihydro-1,4-dithiin-2,3-dithiolate) afforded the (dithiolene)uranium(IV) compounds Cp^*_2U(dddt) and after addition of 18-crown-6 $[Na(18\text{-crown-}6)]_2[U(COT)(dddt)_2]$ (Section 3.2) (Scheme 80).

3.1.3. Tris(cyclopentadienyl) complexes

Evans et al. [79] studied the steric influence of the pentamethylcyclopentadienyl ligand on the structural properties of tris(η^5-pentamethylcyclopentadienyl)actinides and synthesized Cp^*_3UCl and Cp^*_3UF. Starting from Cp^*_3U they performed the reaction with 1 equiv. of PhCl and obtained Cp^*_3UCl. Addition of another equivalent of PhCl led to $Cp^*_2UCl_2$ which was also isolated from the direct reaction of Cp^*_3UCl with 2 equiv. of PhCl (Scheme 81 and Fig. 93).

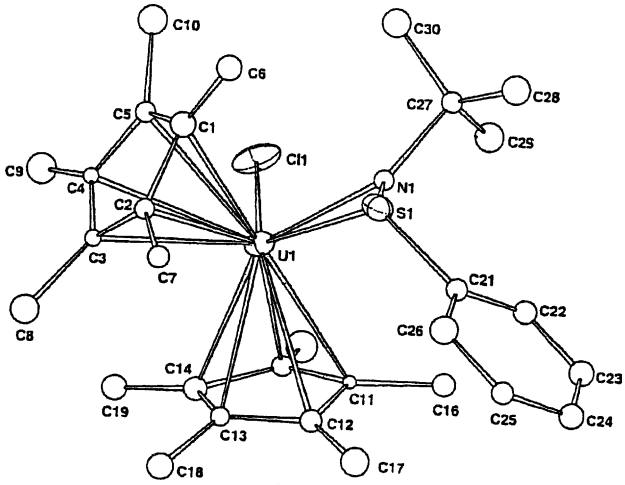

Fig. 92. Molecular structure of $Cp^*_2U(\eta^2\text{-}Bu^tNSPh)Cl$.

The complex crystallizes in the same space group as Cp^*_3U and both have similar unit cell constants. The U–C(Cp^*) distances are equivalent to those of Cp^*_3U. Thus the chloride ligand in Cp^*_3UCl does not appear to perturb the U–C(Cp^*) parameters, however, an exceptionally long U–Cl bond of 2.90(1) Å was observed. The homologous Cp^*_3UF could be synthesized from HgF_2 (Scheme 82).

3.2. Complexes with cyclooctatetraenyl ligands

Ephritikhine and co-workers [80] synthesized the first cationic borohydride and the first dicationic uranium complexes by protonolysis of borohydride precursors. The monocationic compound $[(COT)U(BH_4)(THF)_2][BPh_4]$ was prepared from $(COT)U(BH_4)_2(THF)$ and 0.87 equiv. of $[NEt_3H]BPh_4$ in THF (Scheme 83).

The reaction of the monocationic uranium complex and $[NEt_3H]BPh_4$ in refluxing THF afforded the dication $[(COT)U(THF)_x]^{2-}$. However, an excess of the ammonium salt was necessary to observe the complete formation of the complex, which could not be isolated purely from the reaction mixture. Protonation of $[(COT)U(BH_4)L_3][BPh_4]$

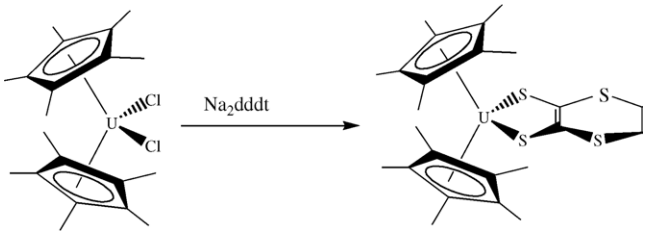

Scheme 80. Formation of Cp^*_2U(dddt).

$$Cp^*_3U + 2\ PhCl \xrightarrow[-Ph\text{-}Ph]{-1/2\ Cp^*_2} Cp^*_2UCl_2$$

Scheme 81. Formation of $Cp^*_2UCl_2$.

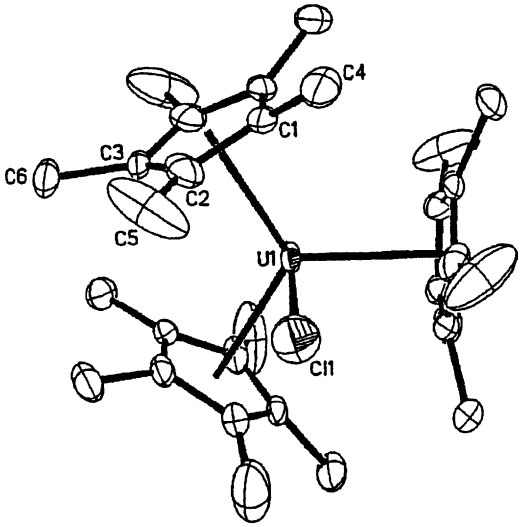

Fig. 93. ORTEP plot of Cp^*_3UCl.

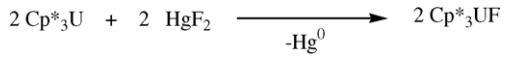

Scheme 82. Formation of Cp^*_3UF.

($L = OPPh_3$ and HMPA) was much more rapid, giving the dication $[(COT)UL_3]^{2-}$ (Scheme 84 and Fig. 94).

Single-crystal X-ray determinations show a three-legged piano-stool configuration with O–U–O angles of 84.0° to 88.2° and COT–U–O angles between 127.2° and 128.7°. The uranium–cyclooctatetraene distance is 1.92(2) Å with U–C bond distances of 2.65 Å; these values compare well with those determined for the monocationic cyclooctatetraenyl complex $[(COT)U(NEt_2)(THF)_3]^+$.

Ephritikhine and co-workers [81] synthesized and characterized a dinuclear cyclooctatetraene uranium complex with a bridging tetra-amide ligand. The complex was prepared by the transamination reaction of $(COT)U[N(SiMe_3)_2]_2$ with $H_2N(CH_2)_3NH(CH_2)_2NH(CH_2)_3NH_2$. The crystal structure revealed the shortest U–U distance 3.3057(9) Å ever observed in a molecular compound (Scheme 85 and Fig. 95).

Ephritikhine and co-workers [78] also synthesized dithiolene complexes of uranium containing a cyclooctatetraenyl ligand. The reaction of $[(COT)UX_2(THF)_n]$ with Na_2dddt and subsequent reaction with 18-crown-6 afforded the (dithiolene)uranium(IV) compound [Na(18-crown-6)]$_2$[U(COT)(dddt)$_2$] (dddt = dddt = 5,6-dihydro-1,4-dithiin-2,3-dithiolate) (Scheme 86).

This complex could be oxidized with $AgBPh_4$ in THF to give the corresponding monoanionic uranium(V) complex [Na(18-crown-6)(THF)][(COT)U(dddt)$_2$] (Scheme 87 and Fig. 96).

The uranium atom is coordinated by four sulfur atoms and the η^8-bonded cyclooctatetraenyl ligand in a distorted-square-pyramidal arrangement [78].

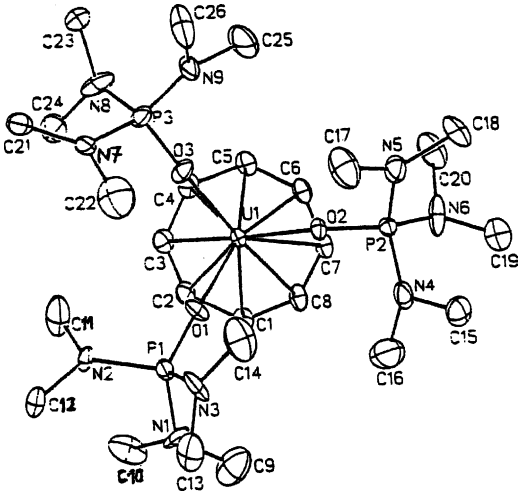

Fig. 94. ORTEP plot of the dicationic $[(COT)UL_3]^{2-}$.

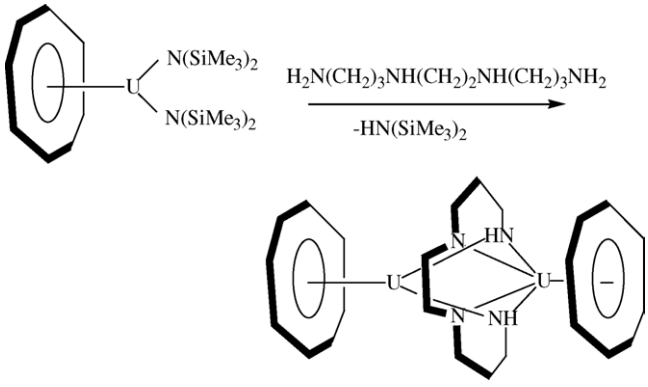

Scheme 85. Formation of the complex $[(COT)U]_2[\mu\text{-}\eta^4\text{:}\eta^4\text{-}HN(CH_2)_3N(CH_2)_2N(CH_2)_3NH]$.

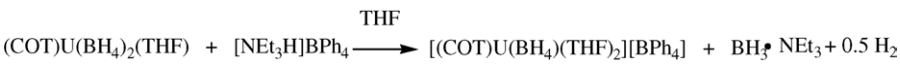

Scheme 83. Preparation of the monocationic complex $[(COT)U(BH_4)(THF)_2][BPh_4]$.

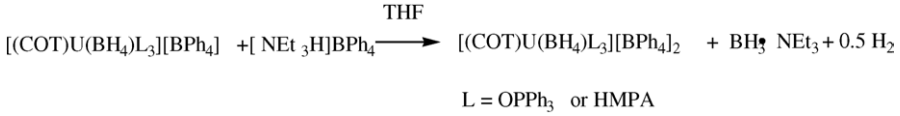

Scheme 84. Preparation of the dicationic complex $[(COT)U(BH_4)L_3][BPh_4]$.

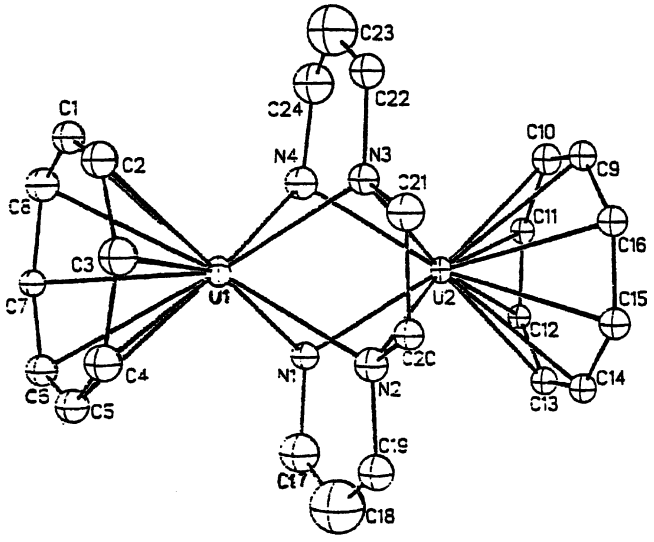

Fig. 95. ORTEP view of the complex $[(COT)U]_2[\mu\text{-}\eta^4{:}\eta^4\text{-}HN(CH_2)_3N(CH_2)_2N(CH_2)_3NH]$.

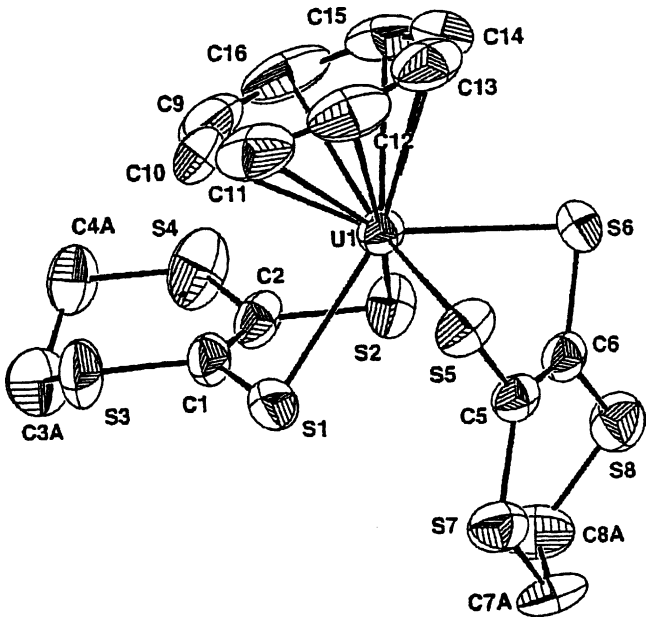

Fig. 96. ORTEP plot of the anion $[(COT)U(dddt)_2]^-$.

Evans et al. [82] published the synthesis of $[Cp^*(COT)U]_2[COT]$ from Cp^*_3U and cyclooctatetraene. Treatment of Cp^*_3U with C_8H_8 in a 2:3 ratio yielded the cyclooctatetraenyl-bridged dimer $[Cp^*(COT)U]_2[COT]$ and Cp^*_2(Scheme 88 and Fig. 97).

Ephritikhine and co-workers [83] synthesized and characterized the first urana [1]ferrocenophane complex. Reaction of UCl_4 with $Li_2fc\cdot tmeda$ (fc = 1,1′-ferrocenylene, tmeda = tetramethylendiamine) gave the tris(1,1′-ferrocenylene) uranium complex $[Li_2(py)_3U(fc)_3]$ (py = pyridine) (Fig. 98).

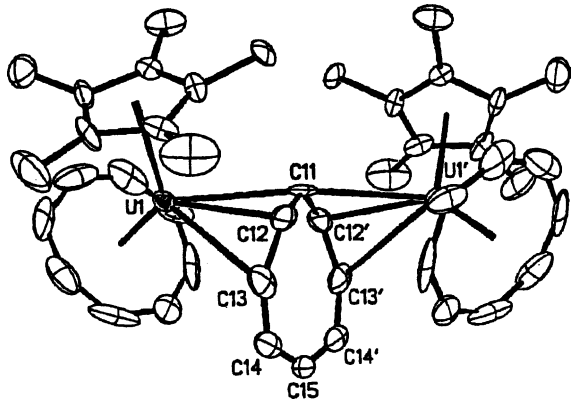

Fig. 97. ORTEP view of the complex $[Cp^*(COT)U]_2[COT]$.

3.3. Organoactinide catalysis

Ephritikhine and co-workers [84] investigated dehydrocoupling reactions of primary amines RNH_2 with $PhSiH_3$ catalyzed by $[(Et_2N)_3U][BPh_4]$. This reaction gave the cor-

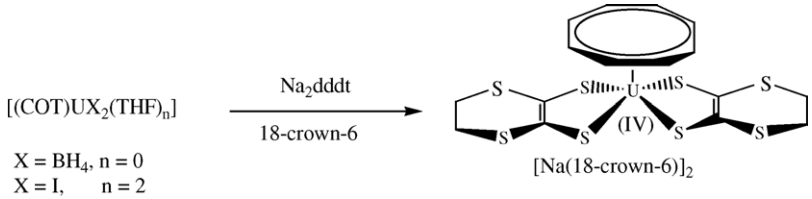

Scheme 86. Formation of $[Na(18\text{-crown-}6)]_2[U(COT)U(dddt)_2]$.

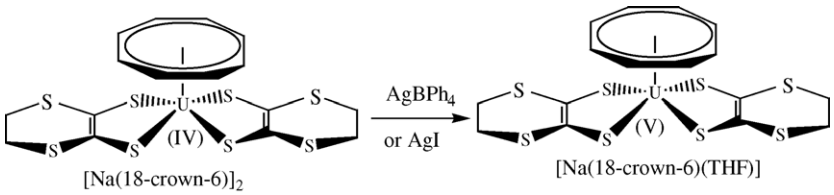

Scheme 87. Oxidation of $[Na(18\text{-crown-}6)]_2[(COT)U(dddt)_2]$ to $[Na(18\text{-crown-}6)(THF)][(COT)U(dddt)_2]$.

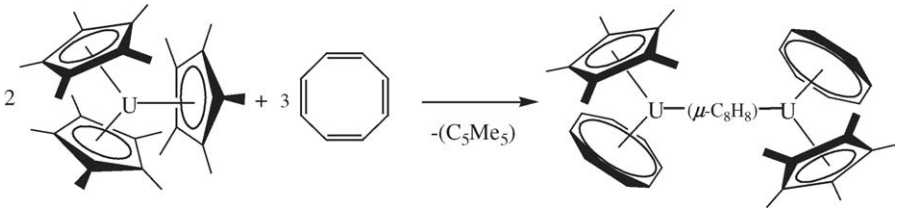

Scheme 88. Synthesis of the complex $[Cp^*(COT)U]_2[COT]$.

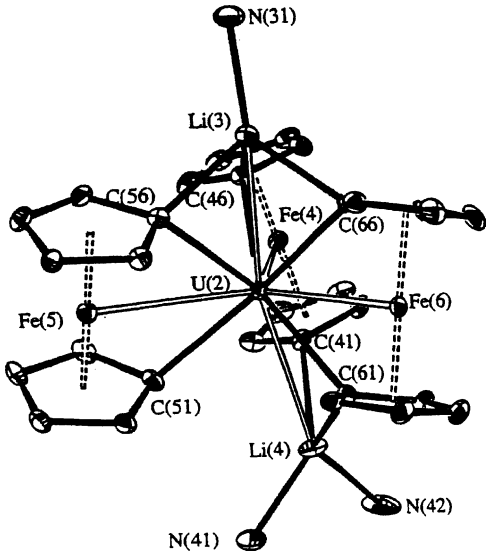

Fig. 98. ORTEP plot of $[Li_2(py)_3U(fc)_3]\cdot py$.

responding aminosilanes $PhSiH_{3-n}(NHR)_n$ ($n = 1$–3). The reactivity of RNH_2 for the reaction with a primary silane ($PhSiH_3$) follows the order: primary > secondary > tertiary. Similar dehydrocoupling reactions using secondary amines with secondary silanes were found to be less reactive. Homodehydrocoupling of the silane was found not to be a competing reaction at room temperature. The hydride $[(RNH)_2UH][BPh_4]$, which is plausibly formed in the reaction of $[(RNH)_3U][BPh_4]$ with $PhSiH_3$ is the likely intermediate complex in the catalytic cycle.

Eisen and co-workers [85] investigated the catalytic activity of the cationic actinide complex $[(Et_2N)_3U][BPh_4]$ for dimerization and hydrosilylation processes of alkynes. Furthermore they could characterize the first f-element alkyne π-complex $[(Et_2N)_2U(C{\equiv}C^tBu)(\eta^2\text{-}HC{\equiv}C^tBu)][BPh_4]$. Mechanistic studies showed that the first step in the catalytic cycle is the formation of the acetylide complex $[(Et_2N)_2U(C{\equiv}CR)][BPh_4]$ with the concomitant reversible elimination of Et_2NH, followed by the formation of the alkyne π-complex $[(Et_2N)_2U(C{\equiv}CR)(RC{\equiv}CH)][BPh_4]$ (Scheme 89).

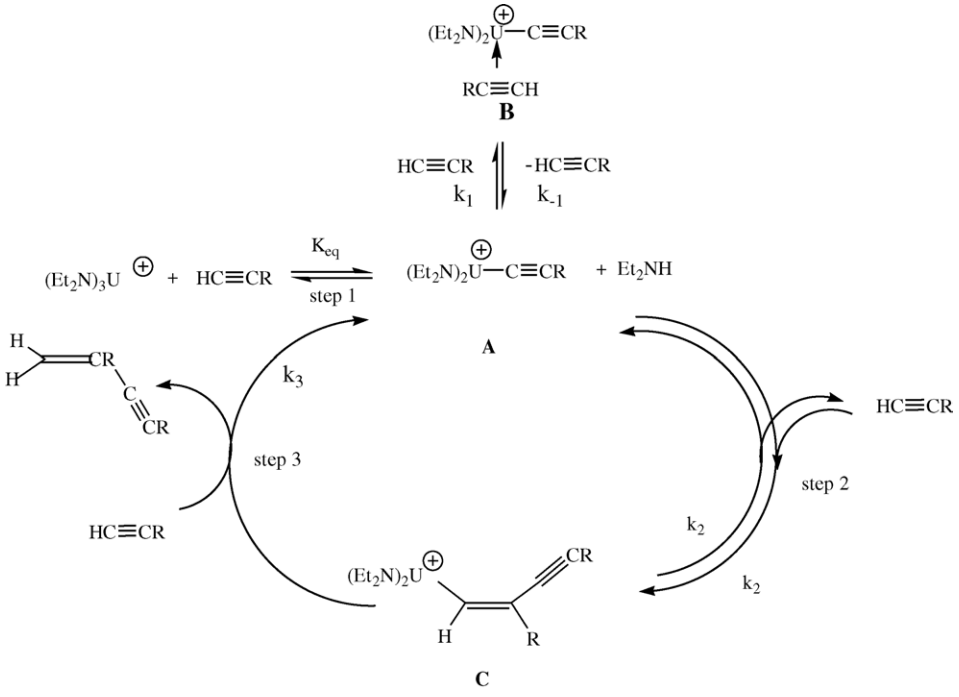

Scheme 89. Mechanism for the dimerization of terminal alkynes promoted by $[(Et_2N)_3U][BPh_4]$.

Acknowledgements

Financial support by the Deutsche Forschungsgemeinschaft, the Fonds der Chemischen Industrie and the Otto-von-Guericke-Universität Magdeburg is gratefully acknowledged.

References

[1] P.L. Stanghellini, E. Diana, E. Boccaleri, R. Rossetti, J. Organometall. Chem. 593/594 (2000) 36.
[2] M. Niemeyer, Z. Anorg. Allg. Chem. 626 (2000) 1027.
[3] H. Reddmann, C. Guttenberger, H.D. Amberger, J. Organometall. Chem. 602 (2000) 65.
[4] T. Dubé, S. Gambarotta, G.P.A. Yap, Organometallics 19 (2000) 121.
[5] T. Dubé, S. Gambarotta, G.P.A. Yap, Organometallics 19 (2000) 817.
[6] G. Lin, R. McDonald, J. Takats, Organometallics 19 (2000) 1814.
[7] P.W. Roesky, J. Organometall. Chem. 603 (2000) 161.
[8] T. Dubé, S. Cpnoci, S. Gambarotta, G.P.A. Yap, Organometallics 19 (2000) 1182.
[9] K.-Y. Chia, Z. Zhang, T.C.W. Mak, Z. Xie, J. Organometall. Chem. 614/615 (2000) 107.
[10] W.J. Evans, M.A. Johnston, C.H. Fujimoto, J. Greaves, Organometallics 19 (2000) 4258.
[11] G.M. Ferrence, R. McDonald, M. Morissette, J. Takats, J. Organometall. Chem. 596 (2000) 95.
[12] D. Barbier-Baudry, O. Blacque, A. Hafid, A. Nyassi, H. Sitzmann, M. Visseaux, Eur. J. Inorg. Chem. (2000) 2333.
[13] K. Chui, Q. Yang, Th.C.W. Mak, Z. Xie, Organometallics 19 (2000) 1391.
[14] Y. Wang, Q. Shen, F. Xue, K. Yu, J. Organometall. Chem. 598 (2000) 359.
[15] E. Ihara, M. Tanaka, H. Yasuda, N. Kanehisa, T. Maruo, Y. Kai, J. Organometall. Chem. 613 (2000) 26.
[16] I.L. Fedushkin, S. Dechert, H. Schumann, Organometallics 19 (2000) 4066.
[17] L. Zhang, X. Zhou, R. Cai, L. Weng, J. Organometall. Chem. 612 (2000) 176.
[18] S.M. Cendrowski-Guillaume, G. Le Gland, M. Nierlich, M. Ephritikhine, Organometallics 19 (2000) 5654.
[19] N.P. Alves, A. de Souza Maia, W. de Oliveira, J. Alloys Compd. 303/304 (2000) 178.
[20] A.A. Trifonov, E.N. Kirillov, Y.A. Kurskii, Ì.N. Bochkarev, Russ. Chem. Bull., Int. Ed. 4 (2000) 744.
[21] S. Arndt, P. Voth, T.P. Spaniol, J. Okuda, Organometallics 19 (2000) 4690.
[22] D. Barbier-Baudry, A. Dormond, M. Visseaux, J. Organometall. Chem. 609 (2000) 21.
[23] P.M. Gatti, M.A. da Luz, W. de Oliveira, Quimica Nova 23 (2000) 191.
[24] H.H. Karsch, V.W. Graf, W. Scherer, J. Organometall. Chem. 604 (2000) 72.
[25] P.B. Hitchcock, M.F. Lappert, S. Prashar, J. Organometall. Chem. 613 (2000) 105.
[26] H.S. Chan, Q. Yang, T.C.W. Mak, Z. Xie, J. Organometall. Chem. 601 (2000) 160.
[27] P.B. Hitchcock, M.F. Lappert, S. Tian, Organometallics 19 (2000) 3420.
[28] M. Visseaux, D. Barbier-Baudry, O. Blacque, A. Hafid, P. Richard, F. Weber, New J. Chem. 24 (2000) 939.
[29] G.B. Deacon, E.E. Delbridge, G.D. Fallon, Organometallics 19 (2000) 1713.
[30] I. Castillo, T.D. Tilley, Organometallics 19 (2000) 4733.
[31] M. Glanz, S. Dechert, H. Schumann, D. Wolff, J. Springer, Z. Anorg. Allg. Chem. 626 (2000) 2467.
[32] M. Schultz, C.J. Burns, D.J. Schwartz, R.A. Andersen, Organometallics 19 (2000) 781.
[33] Y. Wang, Q. Shen, F. Xue, K. Yu, Organometallics 19 (2000) 357.
[34] G.B. Deacon, D. Stellfeldt, G. Meyer, Z. Anorg. Allg. Chem. 626 (2000) 623.
[35] G.B. Deacon, G. Meyer, D. Stellfeldt, Eur. J. Inorg. Chem. (2000) 1061.
[36] H. Sitzmann, T. Dezember, O. Schmitt, F. Weber, G. Wolmershäuser, Z. Anorg. Allg. Chem. 626 (2000) 2241.
[37] M. Yousaf, Q. Liu, J. Huang, Y. Qian, A.S.C. Chan, Inorg. Chem. Commun. 3 (2000) 105.
[38] H. Schumann, M.R. Keitsch, S.H. Mühle, Acta Crystallogr. C 56 (2000) 48.
[39] C.G. Pernin, J.A. Ibers, Inorg. Chem. 39 (2000) 1216.
[40] A.A. Trifonov, E.A. Fedorova, E.N. Kirillov, M.N. Bochkarev, F. Girgsdies, H. Schumann, Russ. Chem. Bull. Int. Ed. 49 (2000) 1436.
[41] W.J. Evans, J.T. Leman, R.D. Clark, J.W. Ziller, Main Group Metal. Chem. 23 (2000) 163.
[42] R.L. Haltermann, H. Schumann, F. Dübner, J. Organometall. Chem. 604 (2000) 12.
[43] C. Qian, W. Nie, J. Sun, Organometallics 19 (2000) 4134.
[44] J. Eppiger, M. Spiegler, W. Hierlinger, W.A. Hermann, R. Anwander, J. Am. Chem. Soc. 122 (2000) 3080.
[45] Z. Hou, Y. Zhang, H. Tezuka, P. Xie, O. Tardif, T.A. Koizumi, H. Yamazaki, Y. Wakatsuki, J. Am. Chem. Soc. 122 (2000) 10533; Z. Hou, Y. Wakatsuki, J. Alloys Compd. 303/304 (2000) 75.
[46] Y.K. Gun'ko, P.B. Hitchckock, M.F. Lappert, Organometallics 19 (2000) 2832.
[47] W. Hierlinger, J. Eppinger, R. Anwander, W.A. Herrmann, J. Am. Chem. Soc. 122 (2000) 11983.
[48] H. Reddmann, H. Schultze, H.D. Amberger, N.M. Edelstein, J. Organometall. Chem. 604 (2000) 296.
[49] Q. Liu, X. Shen, J. Huang, Y. Qian, A.S.C. Chan, W.T. Wong, Polyhedron 19 (2000) 453.
[50] H. Schumann, E.C.E. Rosenthal, J. Demtschuk, S. Mühle, Z. Anorg. Allg. Chem. 626 (2000) 2161.
[51] S. Wang, Q. Yang, T.C.W. Mak, Z. Xie, Organometallics 19 (2000) 334.
[52] C.T. Qian, G. Zou, W.L. Nie, J. Sun, D.A. Lemenovskii, M.V. Bozov, Polyhedron 19 (2000) 1955.
[53] M.G. Klimpel, W.A. Herrmann, R. Anwander, Organometallics 19 (2000) 4666.
[54] H. Schumann, D.F. Karasiak, S.H. Mühle, Z. Anorg. Allg. Chem. 626 (2000) 1434.
[55] H. Nakamura, Y. Nakayama, H. Yasuda, T. Maruo, N. Kanehisa, Y. Kai, Organometallics 19 (2000) 5392.
[56] U. Reißmann, P. Poremba, M. Noltemeyer, H.G. Schmidt, F.T. Edelmann, Inorg. Chim. Acta 303 (2000) 156.
[57] W.J. Evans, M.A. Johnsten, R.D. Clark, J.W. Ziller, J. Chem. Soc., Dalton Trans. (2000) 1609.
[58] A. Fujii, S. Sakaguchi, Y. Ishii, J. Org. Chem. 65 (2000) 6209.
[59] M. Kunishima, D. Nakata, S. Tanaka, K. Hioki, S. Tani, Tetrahedron 56 (2000) 9927.
[60] G.A. Molander, R.M. Rzasa, J. Org. Chem. 65 (2000) 1215.
[61] Z. Li, Y. Zhang, Tetrahedron Lett. 42 (2000) 8507.
[62] M.R. Douglass, T.J. Marks, J. Am. Chem. Soc. 122 (2000) 1824.
[63] F. Barbotin, V. Monteil, M.F. Llauro, Ch. Boisson, R. Spitz, Macromolecules 33 (2000) 8521.
[64] G. Desurmont, Y. Li, H. Yasuda, T. Maruo, N. Kanehisa, Y. Kai, Organometallics 19 (2000) 1811.
[65] A. Lubineau, O. Gavard, J. Alais, D. Bonnaffé, Tetrahedron Lett. 41 (2000) 307.
[66] M.D.K. Ingall, S.J. Joray, D.J. Duffy, D.P. Long, P.A. Bianconi, J. Am. Chem. Soc. 122 (2000) 7845.

[67] S. Junquan, P. Zhida, Z. Yu, H. Weiqiu, Y. Shilin, Eur. Polym. J. 36 (2000) 2375.
[68] T. Kakehi, M. Yamashita, H. Yasuda, React. Funct. Polym. 46 (2000) 81.
[69] S. Bogaert, J.F. Carpentier, T. Chenal, A. Mortreux, G. Ricart, Macromol. Chem. Phys. 201 (2000) 1813.
[70] G. Desurmont, T. Tokimitsu, H. Yasuda, Macromolecules 33 (2000) 7679.
[71] G. Desurmont, M. Tanaka, Y. Li, H. Yasuda, T. Tokimitsu, S. Tone, A. Yanagase, J. Polym. Sci., Part A 38 (2000) 4095.
[72] M. Nodono, T. Tokimitsu, S. Tone, T. Makino, A. Yanagase, Macromol. Chem. Phys. 201 (2000) 2282.
[73] M. Yousaf, J.-L. Huang, Z.-F. Feng, Y.-L. Qian, J.-Q. Sun, Z.-D. Pan, Chinese J. Chem. 18 (2000) 759.
[74] A. Nakajima, K. Kaya, J. Phys. Chem. A 104 (2000) 176.
[75] N. Sändig, T.K. Dargel, W. Koch, Z. Anorg. Allg. Chem. 626 (2000) 392.
[76] L.R. Avens, C.J. Burns, R.J. Butcher, D.L. Clark, J.C. Gordon, A.R. Schake, B.L. Scott, J.G. Watkin, B.D. Zwick, Organometallics 19 (2000) 451.
[77] A.A. Danopoulos, D.M. Hankin, S.M. Cafferkey, M.B. Hursthouse, J. Chem. Soc., Dalton Trans. (2000) 1613.
[78] T. Arliguie, M. Fourmigué, M. Ephritikhine, Organometallics 19 (2000) 109.
[79] W.J. Evans, G.W. Nyce, M.A. Johnston, J.W. Ziller, J. Am. Chem. Soc. 122 (2000) 12019.
[80] S.M. Cendrowski-Guillaume, M. Lance, M. Nierlich, M. Ephritikhine, Organometallics 19 (2000) 3257.
[81] T.L. Borgne, M. Lance, M. Nierlich, M. Ephritikhine, J. Organometall. Chem. 598 (2000) 313.
[82] W.J. Evans, G.W. Nyce, J.W. Ziller, Angew. Chem. 112 (2000) 246;
W.J. Evans, G.W. Nyce, J.W. Ziller, Angew. Chem. Int. Ed. 39 (2000) 240.
[83] A. Bucaille, T.L. Borgne, M. Ephritikhine, J.C. Daran, Organometallics 19 (2000) 4912.
[84] J.X. Wang, A.K. Dash, J.C. Berthet, M. Ephritikhine, M.S. Eisen, J. Organometall. Chem. 610 (2000) 49.
[85] A.K. Dash, J.X. Wang, J.C. Berthet, M. Ephritikhine, M.S. Eisen, J. Organometall. Chem. 604 (2000) 83.